CHAPTER 4

PROCESSING AND DEGRADATION OF AMELOBLASTIN

ABSTRACT

Mmp-20 and Klk4 are enzymes that cleave enamel proteins and are critical for proper dental enamel formation. Mmp-20 is expressed early, during the secretory stage. Its expression gradually diminishes and ceases early in the maturation stage. Klk4 is expressed late, starting in the transition stage and continuing throughout enamel maturation. We hypothesize that Mmp-20 cleaves ameloblastin (Ambn) to generate the full set of ameloblastin cleavage products that accumulate during the secretory stage. The objective was to cleave recombinant ameloblastin with Mmp-20 and Klk4 and characterize the sites cleaved. Known Ambn cleavage sites were incorporated in fluorescence resonance energy transfer (FRET) peptides to determine where Mmp-20 and Klk4 cleave. The rpAmbn was incubated with rpMmp-20 or Klk4 isolated from *in vivo*. The digestions were evaluated by SDS-PAGE and Western blotting, using Ambn antibodies raised against four different regions of Ambn. Three FRET-Ambn peptides (Abz-SLQGLNMLSQYS-Lys-Dnp; Abz-SGVLGGLLANPK-nitro-Tyr; Abz-PGLADAYETYGA-nitro-Tyr) were synthesized, incubated with Mmp-20 or Klk4, and the digestions were analyzed by RP-HPLC. Mmp-20 and Klk4 readily cleaved rpAmbn, but generated different digestion patterns. The exact sites cleaved by Mmp-20 and Klk4

within the FRET-Ambn peptides were determined by LC-MS/MS. Mmp-20 cleaves ameloblastin at the same sites that are cleaved *in vivo* to generate the Ambn cleavage products that accumulate during the secretory stage. Klk4 cleaves Ambn *in vitro* but at different sites than Mmp-20, which is consistent with its role as a late degradative enzyme.

INTRODUCTION

Enamel proteinases are necessary for enamel formation

The generation of cleavage products from enamel matrix proteins is important for the crystal elongation and crystal maturation. Failure in processing of the matrix by either Mmp-20 or Klk4 results in retained enamel proteins and delayed mineralization. These defects are manifested clinically as hypomaturation types of amelogenesis imperfecta (AI). Mutations in *MMP20* (Kim *et al.*, 2005b; Ozdemir *et al.*, 2005b; Papagerakis *et al.*, 2008) and *KLK4* (Hart *et al.*, 2004) have been identified that cause AI. In mouse models lacking either *Mmp20* or *Klk4* enamel is rapidly fractured and abraded. The enamel of the *Mmp20* null mouse is insufficient in thickness and lacks rods and interrod organization (Caterina *et al.*, 2002). In the absence of *Klk4,* the crystallites remained separately and failed to unite (Simmer *et al.*, 2009).

Enamel proteinases have different expression patterns, different functions

Mmp-20 and Klk-4 are sequentially expressed by ameloblasts. Mmp-20 is expressed by secretory stage, transition, and early maturation stage ameloblasts. Klk4 is expressed by transition and maturation stage ameloblasts (Fig. 4.1) (Hu *et al.*, 2002).

As the early enzyme, Mmp-20 provides the initial cleavages of the enamel matrix proteins. These cleavage products are further degraded by Klk4, and virtually disappear from the matrix. Only about 1 % of the weight of dental enamel in erupted teeth is protein.

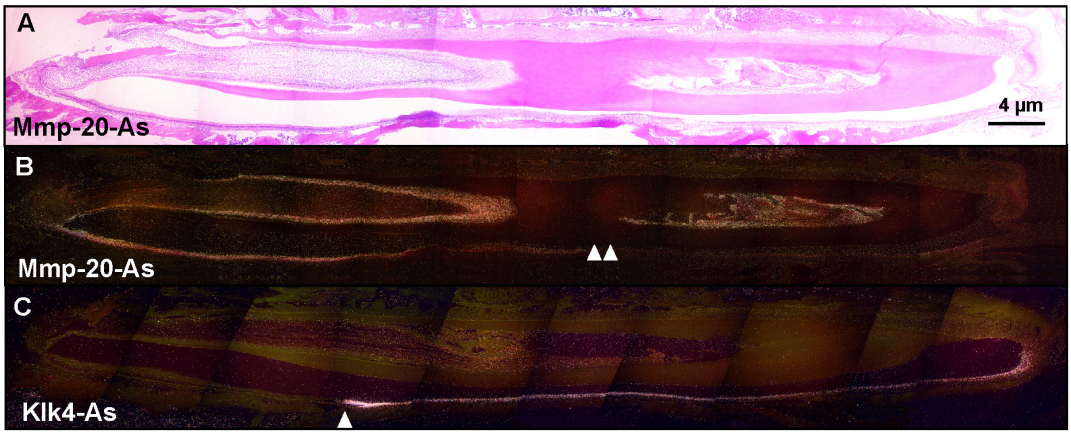

Figure 4.1: Mmp-20 and Klk4 mRNA detection in a day-28 mouse mandibular incisor.
A) Bright field view of an incisor section hybridized with an MMP-20 anti-sense riboprobe and H&E stained (Bar represents 4µm).
B) Dark field view of same section. Double arrowheads mark the limit of Mmp-20 mRNA detection in early maturation stage ameloblasts. Mmp-20 mRNA is detected strongly during secretory stage, transition stage and into early maturation stage.
C) Dark field view of an incisor section hybridized with a Klk4 anti-sense riboprobe. Klk4 mRNA is first observed in transition stage ameloblasts (single arrowhead) and continues into maturation stage. (Simmer *et al.,* 2003).

Enamel proteins as substrates

During mineralization, enamel proteins undergo enzymatic processing and endocytosis by ameloblasts. Three enamel proteins compose the bulk of the secretory stage enamel matrix: amelogenin, ameloblastin and enamelin. Amelogenin and ameloblastin give rise to variety through alternative splicing and through enzymatic processing. Each species is thought to have distinct function for mineralization as certain cleavage products remain in the mature enamel while others are reabsorbed. All enamel matrix proteins serve as substrate for Mmp-20 (Iwata *et al.*, 2007; Ryu *et al.*, 1999; Yamakoshi *et al.*, 2006a). The activity of Klk4 is complementary and resembles a degrading enzyme. It efficiently digests cleavage products generated by Mmp-20 regardless of glycosylations (Ryu *et al.*, 2002; Yamakoshi *et al.*, 2006a).

Ameloblastin cleavage products

A prominent characteristic of the ameloblastin structure is its susceptibility to cleavage. Ameloblastin is expressed in much lower quantities than amelogenin, and it is instantaneously cleaved. Ambn was discovered through purification of its cleavage products from immature enamel (Fukae and Tanabe, 1987a; Fukae and Tanabe, 1987b). Its composition was distinct from amelogenin, the major component of enamel. Anti-peptide antibodies against these cleavage products revealed the distinct localization of N-terminal ameloblastin cleavage products in the sheath space and C-terminal cleavage products in the rod (Uchida *et al.*, 1991; Uchida *et al.*, 1995; Uchida *et al.*, 1997; Uchida *et al.*, 1998). Subsequently, porcine ameloblastin was cloned (Hu *et al.*, 1997). Cleavage of ameloblastin separates N-and C-terminal pieces of opposite calculated pIs. The N-

terminus has a calculated basic pI of 10.8, while the Ambn C-terminus has an acidic pI of 4.5. A hypothetical, computer generated model of Ambn suggested that the secreted protein is comprised of two domains connected through an unstructured interfacing link that is susceptible to cleavage by Mmp-20 (Vymetal *et al.*, 2008).

Proteolysis starting in secretory stage generates sets of Ambn cleavage products from the N- and C-termini. As soon as the cleavages are made, the cleavage products localize to distinct compartments of the enamel. N-terminal Ambn is found in the sheath space throughout the thickness of the enamel. In contrast, C-terminal Ambn is found inside the rods, but only in the most superficial layers of enamel (Uchida *et al.*, 1997; Uchida *et al.*, 1998). C-terminal cleavage products are traced to lysosomes in ameloblasts, suggesting that they are removed from the matrix by endocytosis. How the cleavage products support the formation and mineralization of enamel is unknown. If and how the pI is related to the specific localization is unknown. In order to learn more about the relevance of Ambn cleavage products in enamel formation, their characterization is a prerequisite.

The aim of this study is the characterization of Ambn cleavage sites generated by Mmp-20 or Klk4 *in vitro*. Previous *in vitro* characterization of Ambn cleaved by rpMmp-20 identified some of the same cleavages that occur *in vivo*: after Pro^{2}, Gln^{130}, Gln^{139}, Arg^{170}, and Ala^{222} (Iwata *et al.*, 2007). However, comprehensive characterization of cleavage sites and their correlation to cleavage products isolated from pig enamel matrix is incomplete.

MATERIALS AND METHODS

For the characterization of the cleavage sites of porcine Ambn *in vitro*, two approaches were used, recombinant Ambn in full-length and synthetic Ambn peptides. To investigate the early and late effects of Ambn processing, Mmp-20 was produced in *E. coli* (Ryu *et al.*, 1999) and active porcine Klk4 was purified from the enamel matrix of developing teeth (Yamakoshi *et al.*, 2006a).

Synthetic Ambn peptides

Fluorescence resonance energy transfer (FRET) peptides containing 10 to 12 amino acid porcine ameloblastin sequences centering on known Ambn cleavage sites were synthesized and purified (JPT Peptide Technologies, Berlin, Germany). One FRET peptide (N-Ambn1: Ser^{26}-Ser^{37}, Abz-SLQGLNMLSQYS-Lys-Dnp) simulated an Ambn N-terminal cleavage site. Two sequences simulated Ambn cleavage sites from its C-terminal end (C-Ambn2: Ser^{295}-Lys^{306}, Abz-SGVLGGLLANPK-nitroTyr-NH_2 and C-Ambn3: Gly^{338}-Ala^{348}, Abz-GLADAYETYGA-nitroTyr-NH_2) (Fig. 4.2). The N-terminus of each FRET peptide contained a 2-aminobenzoyl (Abz) fluorescence signal. The C-terminus of each FRET peptide contained a quencher: nitro-tyrosine-amide (nitroTyr) or lysine-dinitro-phenol (Lys-Dnp). Separation of the fluorescence emitter (Abz) from the quencher (nitroTyr or Lys-Dnp) by enzymatic cleavages induces fluorescence (excitation at 320 nm and emission at 420 nm) that is detected in the material eluting from a C18 RP-HPLC column. The FRET-Ambn peptides were stored at -20 ºC.

To test if the FRET peptides were cleaved by Mmp-20 or Klk4, each peptide (100 µg) was resuspended in 50 mM Tris, pH 7.4, 10 mM $CaCl_2$ and incubated with rpMmp-20 or native Klk4 (10 µl aliquot) for 36-48 h at 37 ºC. The total volume of the reaction was 100 µl. The reaction was stopped by adding sample buffer (Laemmli Sample Buffer, Bio-Rad, Hercules, CA, USA) and freezing at -80 ºC.

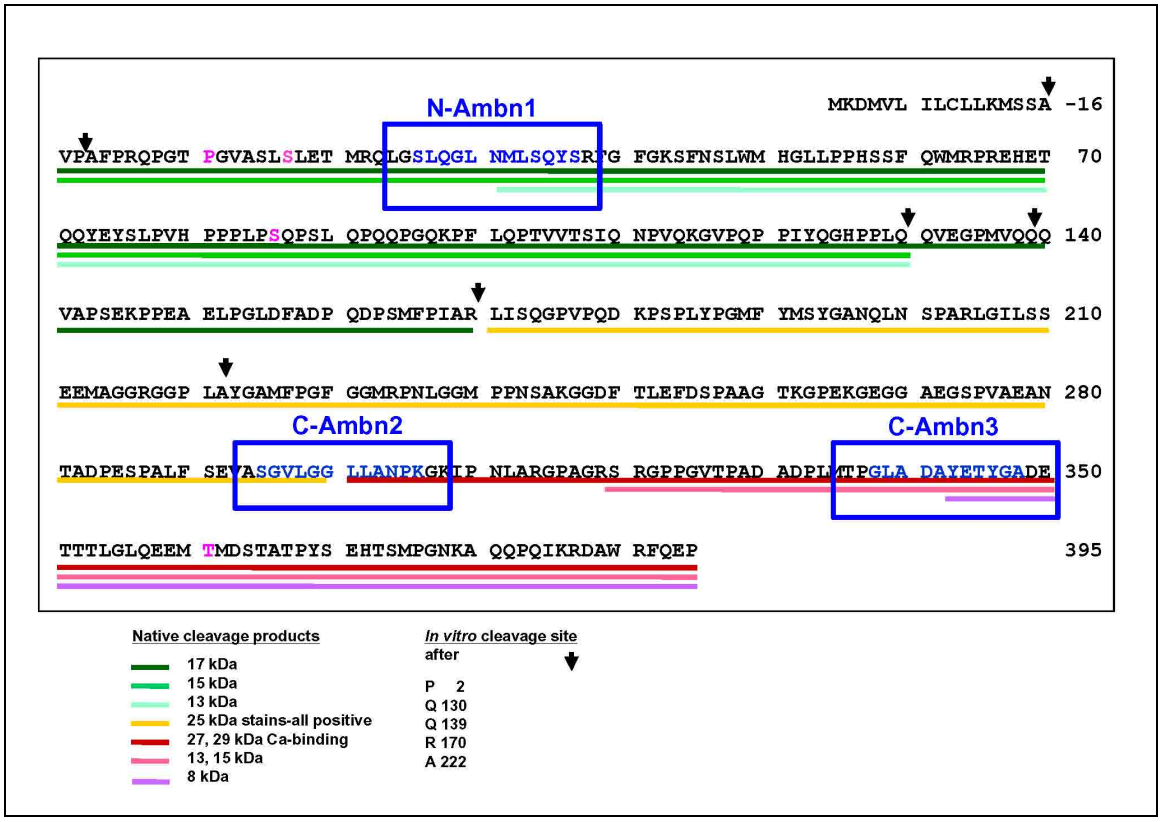

Figure 4.2: Sequences of synthetic peptides simulating *in vivo* Ambn cleavage sites. Synthetic peptides were designed to assay *in vitro* if sites within the Ambn sequence were cleaved by Mmp-20 and/or Klk4. Sequences underlined in different color indicate *in vivo* cleavage products that have been purified and identified in immature porcine enamel. Selected cleavage sites were synthesized as peptides with quenched fluorescence (N-Ambn1: Ser^{26}-Ser^{37}, C-Ambn2: Ser^{295}-Lys^{306}, and C-Ambn3: Gly^{338}-Ala^{348}).

Half of the digest was analyzed by RP-HPLC using a C18 column and the other half was submitted for LC-MS/MS analysis (NextGen Sciences, Ann Arbor, USA).

HPLC was carried out at a linear gradient of 2 % from 0-100 % with buffer A 0.05 % and buffer B 0.05 % TFA + 80 % acetonitrile. The flow rate was 1.0 ml per minute. Eluted material was continuously monitored by UV (230 nm) and fluorescence detectors (excitation 320 nm, emission 420 nm).

Production of recombinant pMmp-20 in *E. coli*

Full-length Mmp-20 has a highly conserved domain structure consisting of a signal peptide, propeptide domain, catalytic domain, linker region, and hemopexin domain (Fig. 4.3 B). Mmp-20 cDNA derived from a porcine dental library was cloned into pProEx1 (Life Technology, Gaithersburg, MD, USA) (Bartlett *et al.*, 1998). Previously, the construct was assembled by introducing restriction sites into the pMmp-20 cDNA by polymerase chain reaction (PCR) using primer 5'-CATATGGCCCCCTCCCTATTTGCA-3' resulting in a 5' NdeI site and primer 5'-AGATCTTCATTTCTCTGGAAAGACT-3' a 3' BglII. The 5' PCR primer was designed to eliminate the enamelysin signal peptide and the 3' PCR primer was designed to eliminate the majority of the 3' non-coding region. The amplification product was gel purified and ligated into the TA cloning vector pCR2.1 (Invitrogen, Carlsbad, CA, USA). From this construct, Mmp-20 cDNA was excised using NdeI and BamHI restriction enzymes, gel purified and ligated into the expression vector pProEx1 (Life Technology, Gaithersburg, MD, USA) using NdeI and BamHI restriction enzymes (Fig. 4.3 A). rpMmp-20 was expressed and purified with modifications according to Ryu *et al.* (1999).

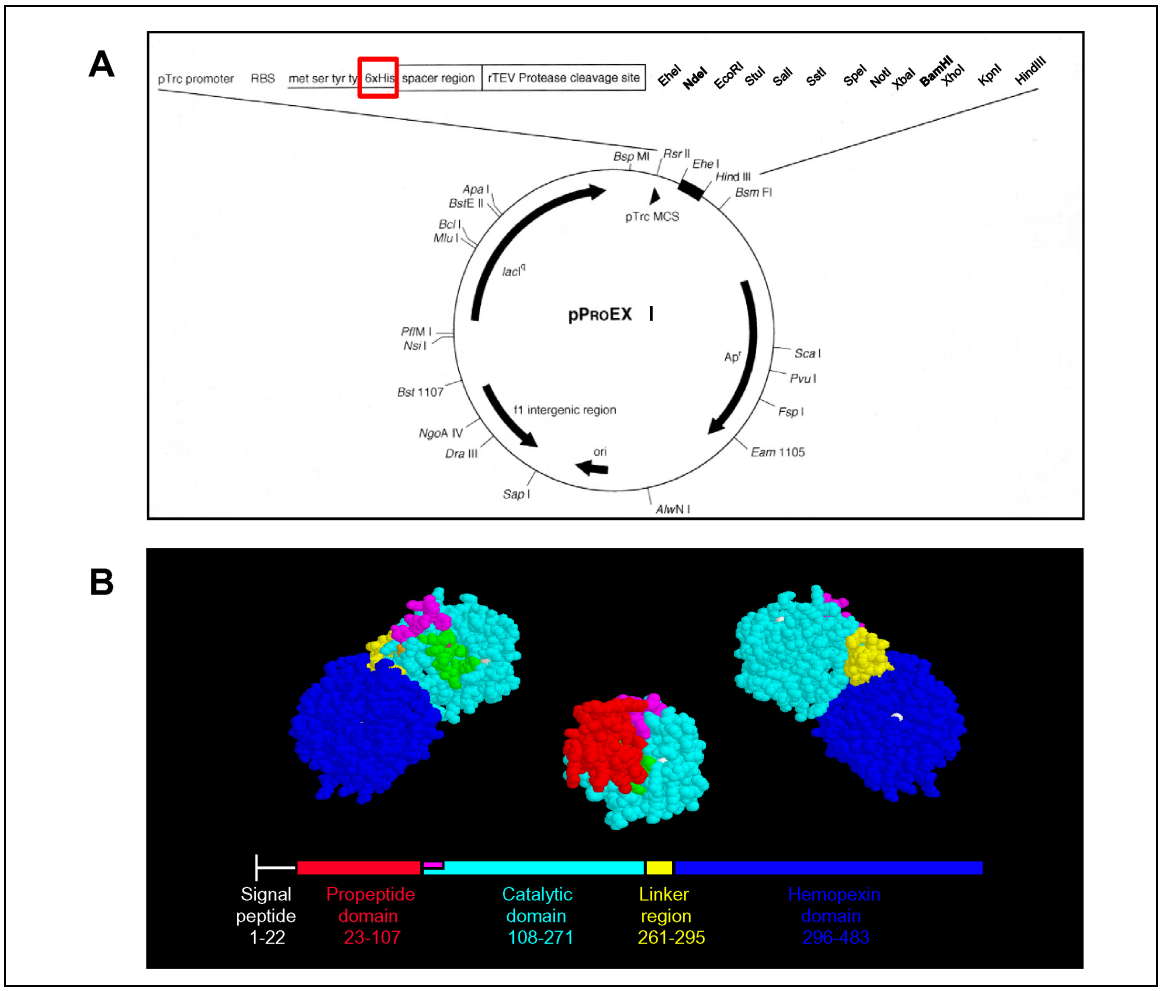

Figure 4.3: Expression vector for recombinant porcine Mmp-20 in *E. coli*.
A) The expression vector pProEx1 was used to express full-length rpMmp-20. In this vector, 6 histidine residues are attached N-terminal to the propeptide, which is exploited for IMAC. B) Molecular model of porcine Mmp-20. Full-length Mmp-20 has a highly conserved domain structure consisting of a signal peptide, propeptide domain, catalytic domain, linker region, and hemopexin domain. Upon self-activation the propeptide and hemopexin domains are cleaved off leaving the catalytic domain to carry out the enzymatic activity. (Bartlett and Simmer, 1999).

For recombinant Mmp-20 protein expression, *E. coli*, strain XL1-Blue (Stratagene, La Jolla, CA, USA) was transformed at 42 ºC for 45 seconds. Single colonies were grown in LB broth (Lennox L broth base, Invitrogen) at 37 ºC on an orbital shaker and screened for Mmp-20 protein expression by casein zymogram (Invitrogen). A colony was expanded first in 3 ml LB broth for 4 h and then added to 500 ml LB broth. When the optical density of the cells reached 0.6 at 600 nm, cells were induced to express

protein by adding isopropyl-β-D-thiogalacto-pyranoside (IPTG; Roche, Indianapolis, IN, USA) to a final concentration of 0.4 mM. The cells were grown for 3 more hours, centrifuged and resuspended in 4 M guanidine-HCl containing 50 mM Tris (pH 7.4), protease inhibitor cocktail (1 tablet of Mini-complete EDTA-free, Roche, Mannheim, Germany), PMSF 0.5 mM, DNase (Roche) 200 μg/g bacteria and sonicated. The sonicated lysate was pelleted and passed through a 0.45-μm syringe filter. Recombinant porcine Mmp-20 was extracted by IMAC using cobalt beads (Talon Metal Affinity Resin, Clontech, Mountain View, CA, USA). The beads were equilibrated with sodium phosphate buffer containing 8 M urea. rpMmp-20 was eluted with 200 mM imidazole in sodium phosphate buffer with 8 M urea, 0.5 mM beta-mercaptoethanol, pH 7.4. The elutant was desalted and concentrated using a centrifugal filter device with a 10-kDa molecular size cutoff (Amicon Ultra -15, Millipore, Billerica, MA, USA) against 50 mM Tris-HCl (pH 7.4), 150 mM sodium chloride, 0.05 % Brij 35. The rpMmp-20 pro-peptide containing the hemopexin domain was activated with 10 mM calcium for 12 h at 37 ºC. Activated catalytic domain cleaved contaminating substrates, which precipitated and were removed by centrifugation at 5,000 rpm. The expression and purification was monitored by SDS-PAGE on 4-20 % Tris-Glycine gels (Invitrogen) and casein gels (Invitrogen). Coomassie Brilliant Blue (CBB) staining and casein zymogram indicated that rpMmp-20 was expressed as a 50-kDa protein with enzymatic activity (Fig. 4.4, A, B, lane 6). Transblotted membranes were immunoblotted with an antibody against the N-terminal 6 x histidine-tag (BD, Franklin Lakes, NJ, USA) (Fig. 4.4, C, lane 6). Lower molecular weight species are due to Mmp-20 self-activation. After activation of Mmp-20 with calcium, the histidine-tag and the pro-peptide were removed by cleavage at the N-

terminus of the catalytic domain and the hemopexin like domain was removed by another cleavage at the C-terminus of the Mmp-20 catalytic domain (Fig. 4.4 B). The rpMmp-20 catalytic domain appeared as a 22-kDa band on zymograms (Fig. 4.4 B, lane 11).

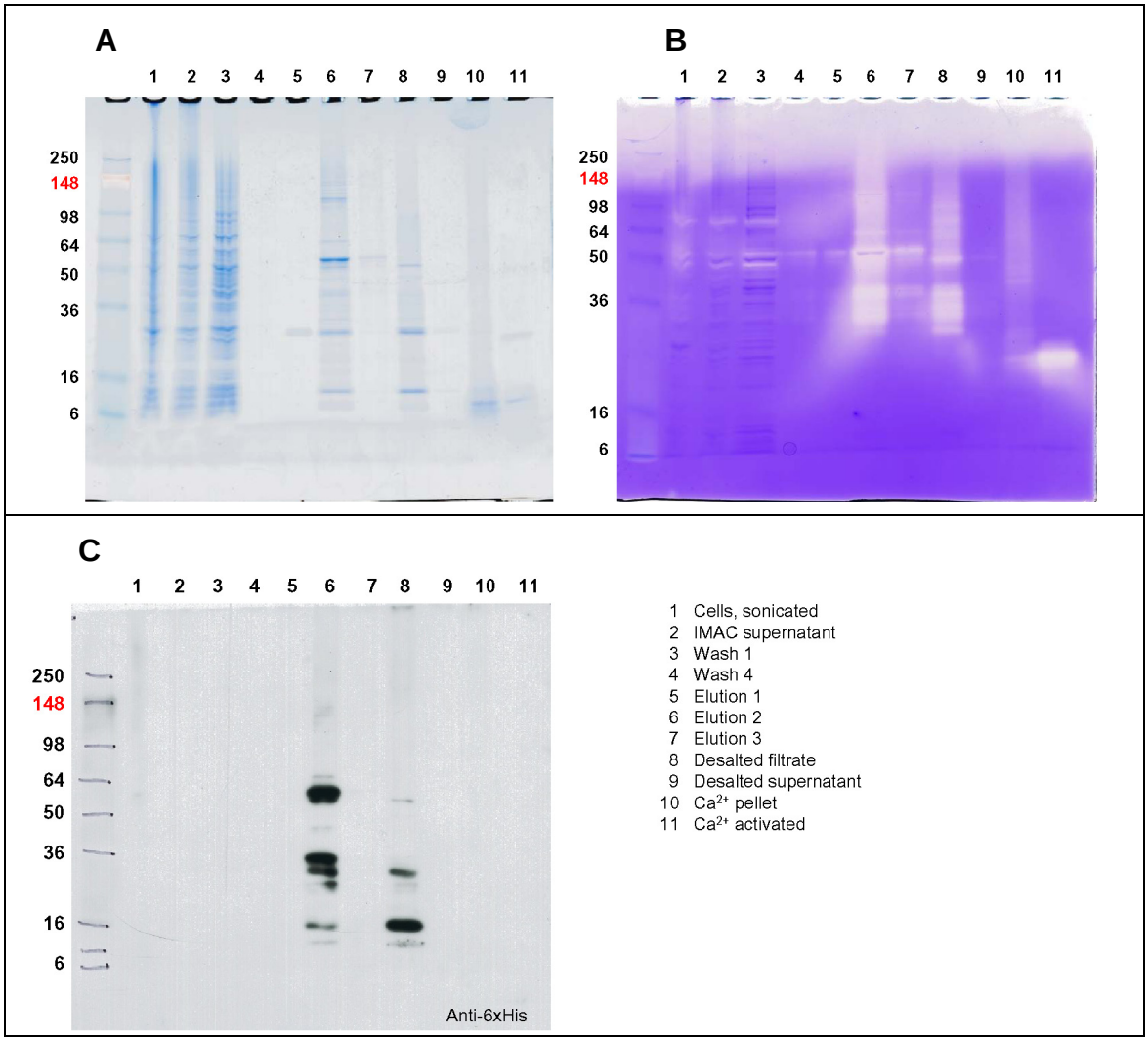

Figure 4.4: Expression and purification of rpMmp-20 in *E. coli*.
A) The CBB stained gel displays the total quantity of proteins during expression and purification of rpMmp-20. Lane 1 displays the starting material. During IMAC (lane 6), desalting (lane 8) and activation with Ca^{2+} (lane 11) Mmp-20 is purified and concentrated.
B) The casein zymogram demonstrates the enzymatic activity in fractions. Mmp-20 is expressed in full-length as 50 kDa protein (lane 1). The enzymatic activity increases as Mmp-20 is purified by IMAC (lane 6). The Ca^{2+} activation promotes self-activation of Mmp-20 resulting in a catalytic domain at 22 kDa (lane 11).
C) Western blot analysis of Mmp-20 expression and purification using an anti-6 x His antibody. Lane 6 contains the eluted protein; lane 8 contains the desalted and concentrated protein; lane 11 contains the catalytic domain lacking the antigenic N-terminal region.

The supernatant containing activated rpMmp-20 was fractionated on a heparin column (Heparin Sepharose 6 Fast Flow, GE Health Care Biosciences, Little Chalfont, UK) equilibrated with 20 mM sodium citrate, 20 mM citric acid, 6 M urea, pH 7.4. The protein was eluted with a linear gradient of 50 mM sodium chloride, 20 mM sodium citrate, 20 mM citric acid, 6 M urea, pH 7.4 using a peristaltic pump with a flow rate of 0.2 ml/min. Individual fraction were collected every 15 min. Fractions 1-29 were monitored by SDS-PAGE followed by zymography and silver stain on 4-20 % Tris-Glycine gel (Invitrogen) (Fig. 4.5). Fractions 8-14 contained the catalytic domain of rpMmp-20 with an apparent molecular weight of 25 kDa. The silver stained gel indicated purity and amount of rpMmp-20 in fractions 9 through 13. In total 20 ml rpMmp-20 were obtained. Aliquots of the fractions were stored at -80 ºC.

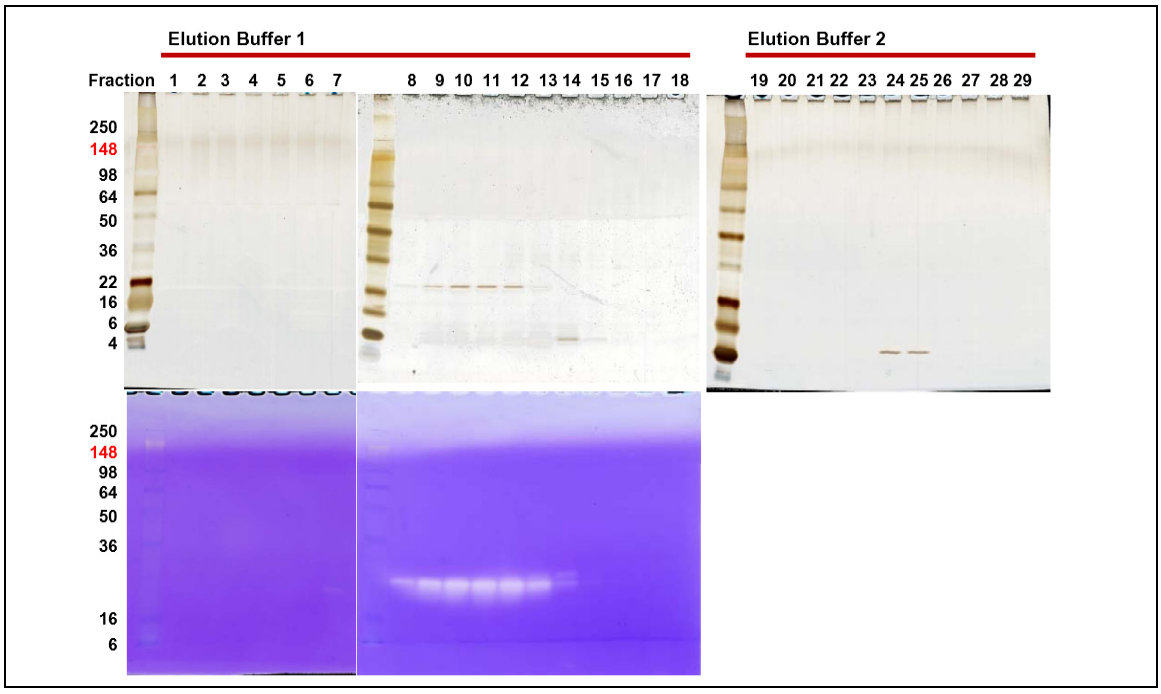

Figure 4.5: Fractionation of the rpMmp-20 catalytic domain on a heparin affinity column.
The protein was eluted with buffer 1 (20 mM NaCl, 20 mM citrate, 6 M urea, pH 7.4) (lanes 1-18). Residual proteins were eluted with a 10 times higher NaCl concentration (buffer 2) (lanes 19-29). Fractions 8-14 contained enzymatically active rpMmp-20 without apparent impurities in the silver stain SDS-PAGE.

Purification of Klk4 from mature porcine enamel matrix

Klk4 was purified from tooth germs of unerupted second molars of 6-month-old pigs obtained from the Michigan State University Meat Laboratory (East Lansing, MI, USA). The teeth were surgically extracted and the soft tissue including enamel organ epithelia (EOE) and dental pulp tissue were removed with tissue forceps. The soft, cheese-like enamel in the cervical area and the hard, early maturation-stage enamel in the coronal half of the crown were separately collected with a spatula and a dental curette. Klk4 was purified from the early maturation-stage enamel according to a purification strategy of a previous protocol (Yamakoshi *et al.*, 2006a). The hard-enamel shavings were homogenized in Sörensen buffer (Na_2HPO_4 and KH_2PO_4 with a final phosphate concentration of 50 mM; pH 7.4). The insoluble material was removed by centrifugation and the supernatant was saturated to 40 % with ammonium sulfate. The precipitate was removed by centrifugation and the supernant was saturated to 65 % with ammonium sulfate. The precipitate containing Klk4 was pelleted by centrifugation and was resuspended in 2 ml of resin buffer (0.05 M Tris-HCl, 0.5 M NaCl, pH 7.4). Klk4 was bound to benzamidine sepharose 4 Fast Flow (Amersham Biosciences, Uppsala, Sweden) of the same volume on a rotor at 4 °C overnight. After packing the beads into a column, the bound protein was eluted with 5 ml of 0.05 % TFA. The eluate was injected onto a C18 reverse-phase column (TSK-gel ODS-120T, 7.5 mm × 30 cm; TOSOH, Tokyo, Japan) and eluted with a linear gradient (20–80 % buffer B) at a flow rate of 1.0 ml per minute. Buffer A was 0.05 % TFA, and buffer B was 0.1 % TFA in 80 % aqueous acetonitrile. Protein was detected by absorbance at 230 nm. Using a cellulose membrane (Ultracel, NMWL: 3,000, Millipore Corporation) the buffer of the fraction containing Klk4 was changed to Tris (50 mM, pH 7.4). Klk4 aliquots were stored at -80 °C.

The quality of Klk4 was monitored by SDS-PAGE (4-20 % Tris Glycine) either stained with CBB or transblotted onto PVDF for Western blot analysis using a polyclonal antibody raised in rabbits against recombinant pig Klk4 (Hu *et al.*, 2000). The membrane was incubated in 5 % skim milk TBS-tween containing antibody in 1:1000 ratio for overnight, followed by HRP-rabbit IgG, 1:2000, for 2 h. The signal was detected colormetrically using diaminobenzidine (DAB) (Sigma, St. Louis, MO, USA). Gelatin zymograms were performed on 10 % SDS-PAGE gels containing 0.2 % gelatin (Invitrogen). The zymogram gel was incubated in 50 mM Tris, pH 7.4 for 24 h with $CaCl_2$ at 37 ºC.

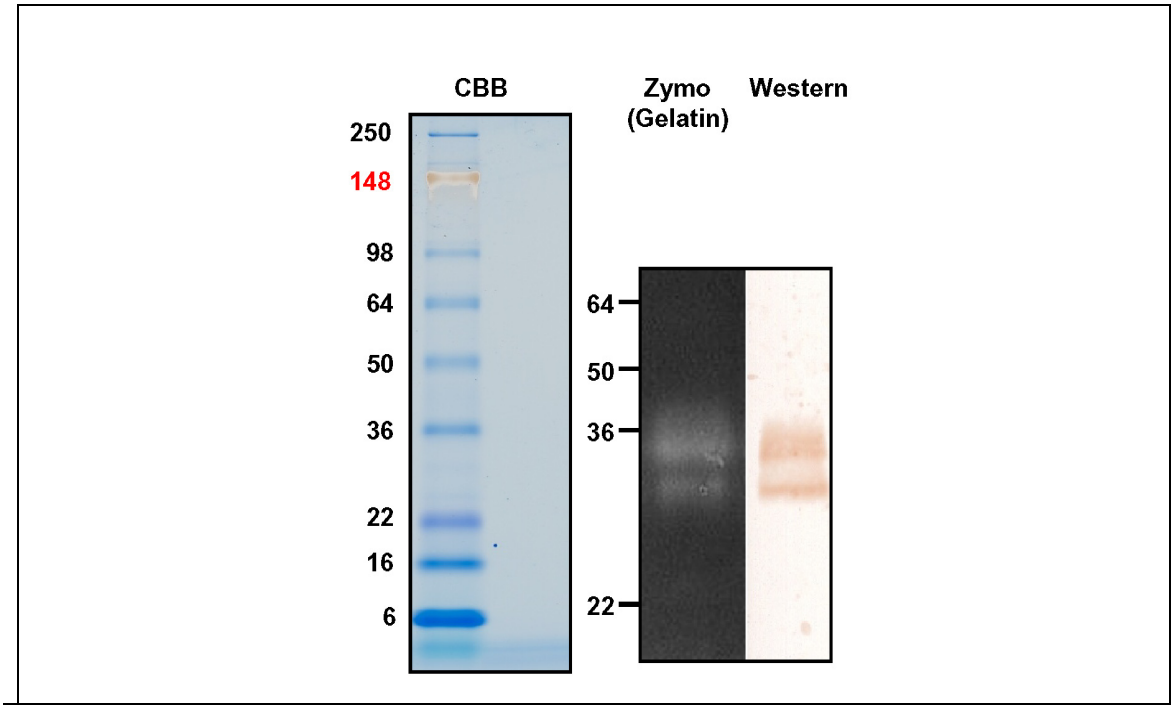

Figure 4.6: Klk4 purified from native maturation stage enamel.
The purified Klk4 was apparent as a doublet at around 30 kDa on gelatin zymogram and Western blot. The Klk4 antibody was used at 1:1000, and the membrane was incubated overnight. The secondary antibody (HRP-Rabbit IgG) was applied at 1:2000 for 2 hours. The membrane was developed using DAB. A standard aliquot did not reveal a band on a CBB stained gel. Therefore, contaminants were absent that could have interfered with the analysis of cleavage products.

Native Klk4 was isolated from hard enamel of porcine teeth. It migrated as a double band at above 30 kDa on SDS-PAGE and Western blots (Fig. 4.6). The positive bands on gelatin gels demonstrated an enzymatic protein. On CBB stained gels, it was not detectable.

Digestion of rpAmbn with either rpMmp-20 or pKlk4 *in vitro*

For the cleavage experiment, full-length rpAmbn was incubated *in vitro* with either rpMmp-20 or pKlk4. Proteinase (10 µl aliquot) and substrate (30-40 ug) were incubated in 50 mM Tris-HCl buffer (pH 7.4) with 10 mM Ca^{2+} at 37 °C. Reaction aliquots were quenched by the addition of sample buffer (Laemmli Sample Buffer, Bio-Rad) at 0, 2, 4, 8, 20 or 28 h and immediate freezing at -80 ºC. The digests were analyzed by SDS–PAGE on 4-12 % NuPAGE gels (Invitrogen). For total protein analysis, the gel was stained with silver stain and CBB. Stains-all staining was performed to evaluate the calcium-binding qualities of the cleavage products. For analysis of the cleavage products, duplicate gels were transblotted onto PVDF Hybond-P membranes (Amersham Biosciences). Western blot analysis was performed using 5 different antibodies against the N- and C-terminal regions of recombinant Ambn-his-V5. The PVDF membrane was stripped with Restore PLUS Western blot Stripping Buffer (Thermo Scientific, Rockford, IL, USA) between successive incubations with the various antibodies.

Identification of cleavage products by N-terminal sequencing

For N-terminal sequencing the cleavage products were separated on a SDS-PAGE gel, transferred onto a PVDF-membrane. The membrane was washed in water, stained with CBB, destained with 50 % methanol and dried. The bands of interest were excised with sharp scissors, and submitted for N-terminal sequencing. Automated N-terminal sequencing was performed on an Applied Biosystems Procise 494 cLC protein sequencer at the W.M. Keck Facility at Yale University.

Amino acid residues that carry post-translational modifications (PTM) resulted in a blank cycle. Since the porcine amino acid sequence of ameloblastin is known, the missing residue could be deduced and the context allowed predicting the type of PTM.

Comparison *in vitro* and *in vivo* Ambn cleavage sites

The identified cleavage products of the recombinant Ambn were compared with the cleavage products isolated from enamel matrix (Fukae *et al.*, 1993; Uchida *et al.*, 1991; Uchida *et al.*, 1995; Uchida *et al.*, 1997; Uchida *et al.*, 1998; Yamakoshi *et al.*, 2006b). The objective was to identify which protease (Mmp-20 or Klk4) catalyzes the cleavage of Ambn at the sites previously identified as occurring *in vivo*. A time-course for the *in vitro* cleavages was performed to gain information about the sequence of Ambn cleavages catalyzed by these enzymes.

RESULTS

Production of substrate and enzyme

For the *in vitro* characterization of porcine ameloblastin cleavages by early and late enamel proteinases, full-length rpAmbn was produced and 3 Ambn FRET peptides centering on known *in vivo* Ambn cleavage sites were synthesized. Recombinant porcine ameloblastin was expressed in HEK293 cells and isolated as a full-length protein (Chapter 3). Sufficient substrate quality and quantity were demonstrated. From medium collected during one week, 0.25 to 0.5 mg rpAmbn were purified. The synthetic peptides were located near the N-terminus (N-Ambn1: Ser^{26}-Ser^{37}, Abz-SLQGLNMLSQYS-Lys-Dnp) and from the C-terminal end (C-Ambn2: S^{295}-K^{306}, Abz-SGVLGGLLANPK-nitroTyr-NH_2; C-Ambn3: G^{338}-A^{348}, Abz-GLADAYETYGA-nitroTyr-NH_2) (Fig. 4.2).

Recombinant porcine Mmp-20 was expressed in *E. coli* as a full-length enzyme consisting of hemopexin domain, linker and catalytic domain. The N-terminus carried a 6 x histidine-tag for purification purposes, which was cleaved off during self-activation of Mmp-20 in the presence of $CaCl_2$. A standard aliquot of 10 µl of the catalytic domain of rpMmp-20 migrated at 25 kDa on SDS-PAGE with silver staining, but did not produce a visible band on a CBB stained gel (Fig. 4.7, lane 5). Casein zymogram demonstrated an enzymatically active catalytic domain (Fig. 4.5, fractions 8-14). Amelogenin is a known substrate for Mmp-20 (Ryu *et al.*, 1999). The activity level of rpMmp-20 was tested by incubation with recombinant porcine amelogenin (Fig. 4.7). Incubation at 37 ºC for 24 h gave the expected cleavage products at 23, 20, 13 and 6 kDa. The rpMmp-20 by itself did not produce a CBB visible band (lane 5). Thus, all new protein bands detected in a reaction are cleavage products.

Native Klk4 was purified from hard enamel of unerupted molars of 6-month-old pigs. Klk4 was active on gelatin zymogram and did not contain significant contamination.

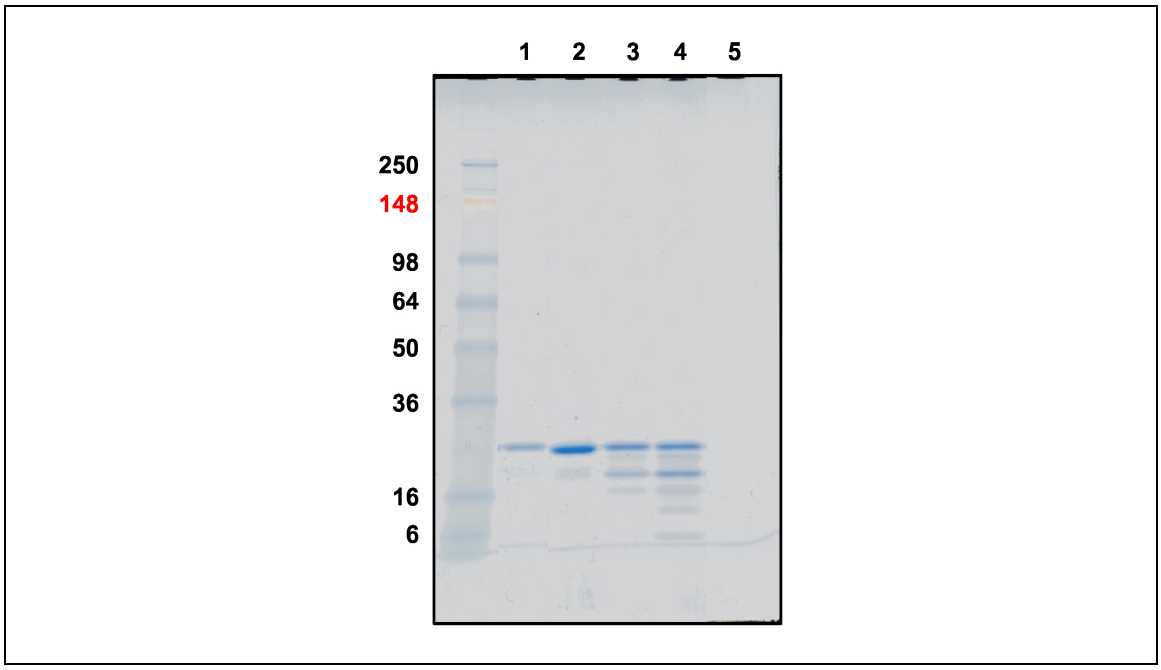

Figure 4.7: rpMmp-20 demonstrated enzymatic activity using rpAmel (P172) as substrate.
SDS-PAGE was performed on a 4-10 % Tris Glycine gel stained with CBB. Lane 1: P172 only, 24 h; lane 2: P172 + rpMmp-20 (10 µl), 0 h; lane 3: P172+rpMmp-20 (5 µl), 24 h; lane 4: P172+rpMmp-20 (10 µl), 24 h; lane 5: rpMmp-20 (10 µl), 24 h. rpMmp-20 cleaves P172 amelogenin and generates cleavage products that correspond to *in vivo* cleavage products.

Cleavage experiments

The rpAmbn was cleaved with single aliquots of rpMmp-20 and Klk4. The digestions were analyzed after 0, 2, 4, 8, 20 or 28 h at 37 ºC by SDS-PAGE gels stained with CBB, silver stain and Stains-all. Western blot analysis was performed using anti-Ambn antibodies reacting against the N- and C-terminal regions of the protein (Tab. 3.1). Discrete bands were generated by rpMmp-20 and Klk4 visible on transblotted PVDF membranes stained with CBB, which were submitted for N-terminal sequencing.

Processing of rpAmbn by rpMmp-20

The rpAmbn was incubated with rpMmp-20 for 0, 2, 4, and 20 h. After separation on SDS-PAGE gel, the cleavage products were apparent on CBB or silver stained gels as bands of 7, 22-25, 37 and 48-60 kDa (Fig. 4.8). The smears between 22-25 and 48-60 kDa were strongly stained. The immunoreactivity against anti-peptide antibodies identified N- and C-terminal species. The pattern of the C-terminal cleavage product was distinctly different from the N-terminal cleavage products. The sizes of the N-terminal bands ranged from 7 to 25 kDa. The sizes of the C-terminal cleavage products ranged from 40-50 and 48-60 kDa. Positive Stains-all staining identified the C-terminal cleavage products as being calcium-binding. The 13-, 15-, 27-, and 29-kDa C-terminal ameloblastin cleavage products isolated from *in vivo* are Stains-all positive proteins (Fukae and Tanabe, 1987a; Murakami *et al.*, 1997; Yamakoshi *et al.*, 2001). The calcium-binding properties are associated with the sulphation on the O-linked glycosylation of Thr^{361} (Yamakoshi *et al.*, 2001).

In total of eleven bands having apparent molecular weights of 7, 10, 22, 23, 24, 25, 37, 48, 49, 50, 57 kDa were selected from the CBB stained PVDF membranes and submitted for N-terminal sequencing degradation to W. M. Keck Foundation Biotechnology Resource Laboratory at Yale University (Fig. 4.8 C). N-terminal sequencing confirmed that sample contained Ambn. Bands of different molecular weights contained same N-terminal sequences. 1-VPAFPRQP was found in the 22-, 23-, 24-, 25- and 37-kDa bands. The sequence of 3-AFPXQPGT was also detected in bands of 22, 23 and 25 kDa. The 57-kDa band contained the sequence 131-QVEXPMVQ, and the 50-kDa band contained the sequence 171-LISQGPVP. The 48- and 49-kDa bands contained 223-YGAMFPGF. rpMmp-20 cleaved rpAmbn after Pro^{2}, Gln^{130}, Arg^{170}, and Ala^{222}. The

higher molecular weight bands (48 -57 kDa) all corresponded to C-terminal Western blot signals and were confirmed by N-terminal sequencing as C-terminal cleavage products. The lower molecular weight bands (22-37 kDa) were recognized by N-terminal antibodies and their sequences matched N-terminal cleavage products.

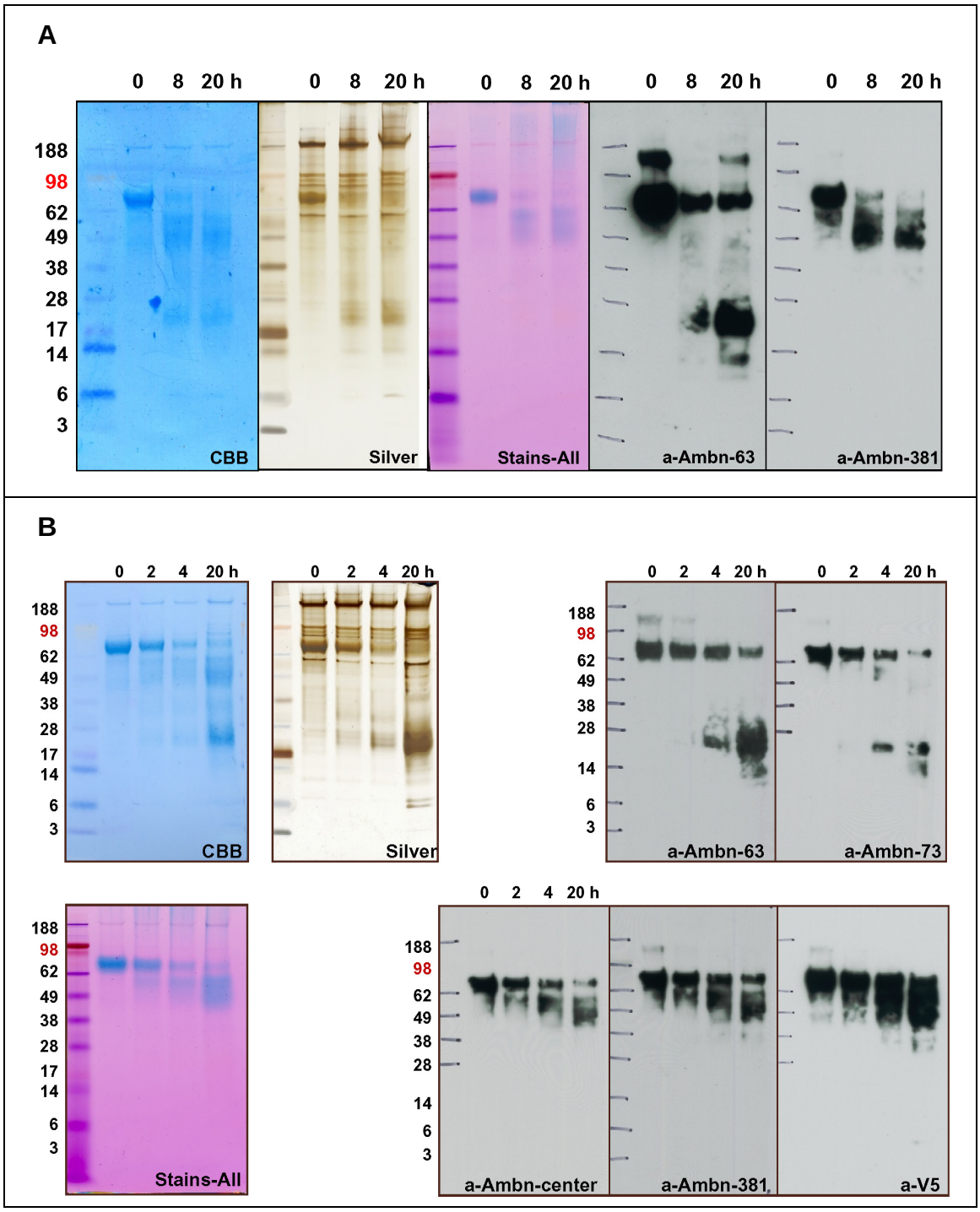

Figure 4.8: Digestion of rpAmbn by Mmp-20 analyzed by SDS-PAGE and N-terminal sequencing.

A) rpAmbn and rpMmp-20 were incubated for 0, 8, 20 h. Distinct cleavage products were generated noticeable on SDS-PAGE stained with CBB, silver and Stains-all. Western blot analysis using N-and C-terminal Ambn antibodies revealed clearly distinguishable cleavage products.

B) After incubations of 0, 2, 4 and 20 h N-terminal cleavage products migrated at 12 to 23 kDa, C-terminal products migrated at 40-50 and 48-60 kDa.

C

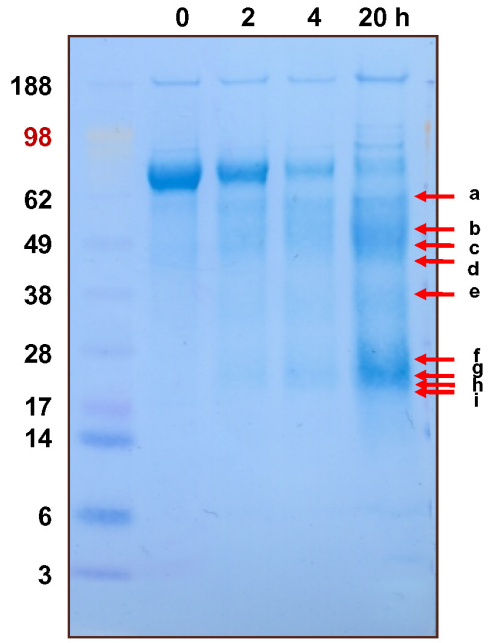

Band	Molecular weight (kDa)	Recognized by antibodies	Sequence
a	57	C-terminus, center	131-QVEXPMVQ
b	50	C-terminus, center	171-LISQGPVP
c	49	C-terminus, center	223-YGXMFPXF
d	48	C-terminus, center	223-YGAMFPGF
e	37		1-VPAFPXQP
f	25	N-terminus	1-VPAFPXQP 3-AFXXQPGT
g	24	N-terminus	1-VPAFPRQP
h	23	N-terminus	1-VPAFPXQX 3-AFXXQPGX
i	22	N-terminus	1-VPAFPXXP 3-AFPXQPGT

Figure 4.8: Digestion of rpAmbn by Mmp-20 analyzed by SDS-PAGE and N-terminal sequencing.
C) From the CBB stained membrane, bands 'a' through 'i' were selected for N-terminal sequencing. The table summarizes the size of the bands, their immunoreactivity and amino acid sequence.

Digestion of rpAmbn by native Klk4

Klk4 is the maturation stage proteinase in enamel. It digested rpAmbn producing specific cleavage products on SDS-PAGE stained with CBB, silver, Stains-all. Antibodies specifically recognizing the N- or C-terminal regions allowed the identification of rpAmbn cleavage products by Western blotting. With increasing incubation time the intensity of the original rpAmbn material decreased, indicating degradation. Cleaved species migrating at 17-25, 40-45, 40-55 and 60 kDa were observed (Fig. 4.9 A, B). Calcium binding cleavage products had an apparent molecular weight of 40-55 kDa and were antigenic for antibodies against the Ambn center and C-terminal regions. Distinct bands at around 5 and 6 kDa were recognized only by the V5 antibody and silver stain. As the C-terminus of rpAmbn carries six histidine residues and a V5 epitope with a calculated weight of 4.86 kDa, it is very likely that these bands represent the domain fused to the Ambn C-terminus. N-terminal cleavages generated low molecular species of 17-25 kDa in high abundance. In much lower abundance were N-terminal cleavage products of a 44-kDa product, which overlapped with C-terminal cleavage products at 48-50 kDa. Interestingly, at long incubation times of 20 or 28 h, this C-terminal species was no longer detected, and did not give rise to any detectable new cleavage products.

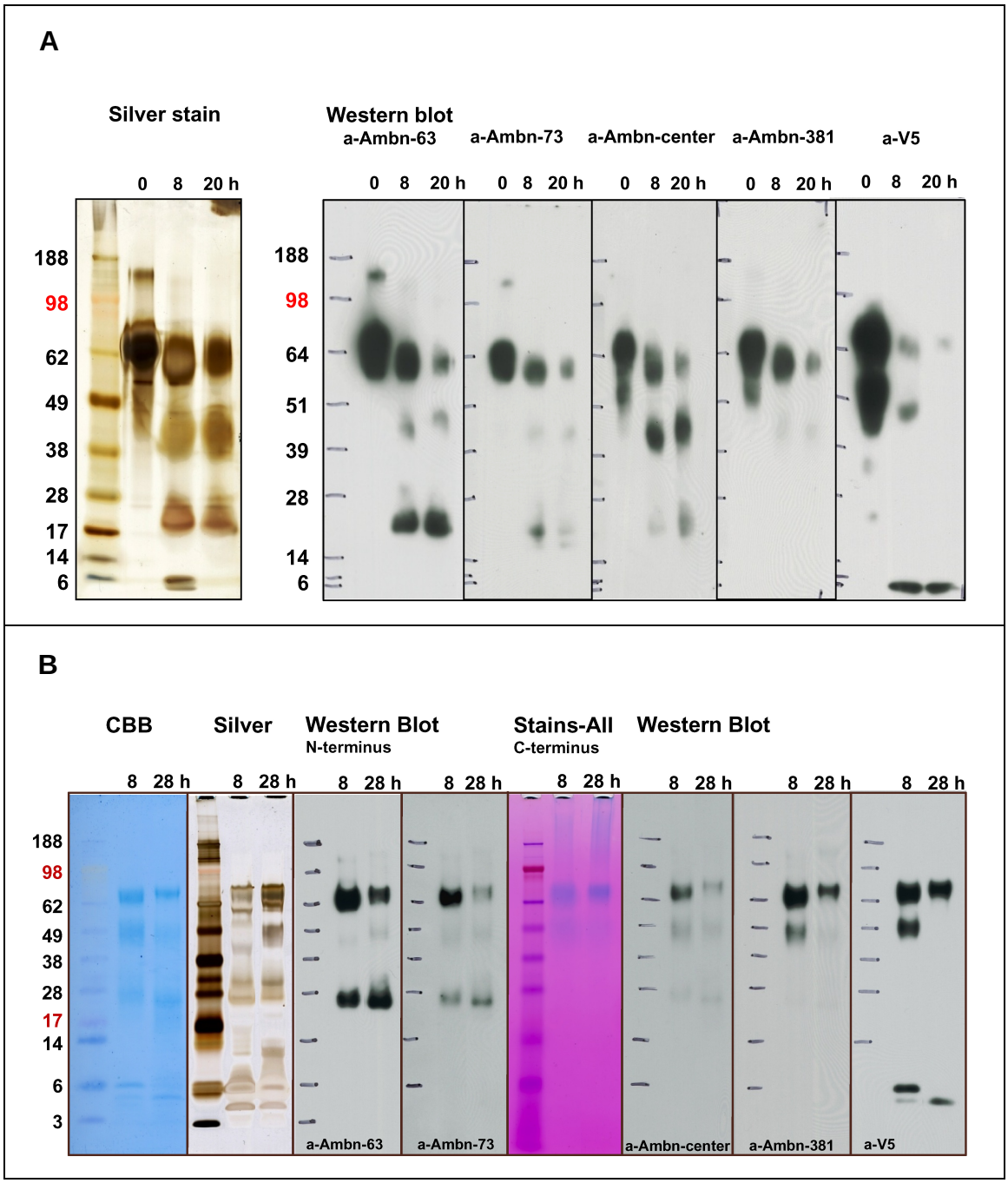

Figure 4.9: Digestion of rpAmbn by Klk4 analyzed by SDS-PAGE and N-terminal sequencing.

Digests of rpAmbn by native Klk4 were separated on 4-12 % NuPAGE using either MES or MOPS buffer.

A) rpAmbn was digested for 8 and 20 h at 37 ºC. The digests were analyzed by silver stain and Western blot using antibodies against Ambn specific for C- or N-terminal regions.

B) The digestion of rpAmbn by Klk4 was repeated with 8 and 28 h incubations at 37 ºC. The digests were analyzed by CBB, silver and stains-all staining and Western blot analysis.

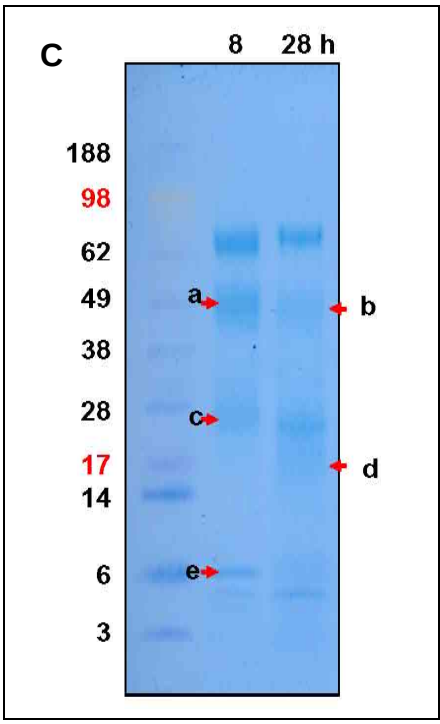

Band	Molecular weight (kDa)	Antibodies	Sequence
a	49	C-terminus center	171-LISQXPVP
b	48	C-terminus center	171-LISQGPVP 192-MXYXANQL
c	27	N-terminus center	29-GLNXLXXS 44-SFNSLWMX
d	17		171-LISQGPVP 192-MXYXANQL
e	6	V5	392-FQEPKGNSADIQ

Figure 4.9: Digestion of rpAmbn by Klk4 analyzed by SDS-PAGE and N-terminal sequencing.
Digests of rpAmbn by native Klk4 were separated on 4-12 % NuPAGE using either MES or MOPS buffer.
C) From the CBB stained PVDF membrane 5 bands (arrows, a-e) were determined for N-terminal sequencing. The table summarizes the size of the bands, their immunoreactivity and amino acid sequence.

Five bands selected from 8 h and 28 h digestions were sent for N-terminal sequencing at the W. M. Keck Foundation Biotechnology Resource Laboratory at Yale University to identify the cleavage sites that generated the 5, 6, 17, 25, 27, 44, 48, and 49 kDa products (Fig. 4.9 C). The sequence 171-LISQGPVP was present in bands of 17, 48 and 49 kDa generated from cleavages after Arg^{170}. 192-MXYXANQL was found in bands of 17 and 48 kDa. The band of 27 kDa contained 29-GLNXLXXS and 44-SFNSLWMX. The 6-kDa band contained 392-FQEPKGNSADIQ, which are the last 4 residues of pAmbn and 8 residues of the V5 epitope.

Digestion of FRET-Ambn peptides

The aliquots of enamel proteinases rpMmp-20 and Klk4 used in experiments by themselves did not generate significant chromatographic peaks when detected by UV absorbance at 230 nm (Fig. 4.13). Thus, they did not interfere with the chromatogram generated by the digested FRET-Ambn peptides.

The FRET-Ambn peptides were designed to cover cleavage sites previously identified from native porcine enamel. N-Ambn1 (Ser^{26}-Ser^{37}) simulates the cleavage that generates the 13-kDa from the 15-kDa N-terminal Ambn cleavage product (Fig. 4.10). Incubation of N-Ambn1 with rpMmp-20 resulted in multiple peptides recognizable as UV peaks at retention times of 46, 43, 49, 50.5, 51.5 min in lower abundance and distinct from the original material with a retention time of 58.5 min in high abundance. The peak at 46 min coincided with a fluorescent signal released as the N-terminal portion of the N-Ambn1 peptide Abz-SLQGLN identified by LC-MS/MS. Klk4 cleaved N-Ambn1 at a different site, after Gln^{28}. Peptides had retention times of 42, 47.5 and 52.5 min. The fluorescent N-terminal region of the cleaved peptide had a retention time of 52.5 min and was identified as the N-terminal portion Abz-SLQ. Mmp-20 cleaves the N-Ambn1 peptide after Asn^{31}, which correlates to an *in vivo* cleavage site. Klk4 cleaves N-Ambn1 after Gln^{28}.

The cleavage site covered by FRET-peptide C-Ambn2 (Ser^{295}-K^{306}) gives rise to major C-terminal cleavage products of 27 and 29 kDa *in vivo*. The digestion of C-Ambn2 by rpMmp-20 resulted in significant decrease of the original material and 3 new peaks at 38, 41.5 and 43.5 min retention times (Fig. 4.11). The peak at 41.5 min carried the N-terminal fluorescent region (Abz-SGVLGG) while the peak at 38 min represented the C-terminal aspect of C-Ambn2 (LLANPK). The peak at 43.5 min is likely to be an

unspecific cut unrelated to cleavages by enamel proteinases. The digestion of C-Ambn2 by Klk4 generated products of very low abundance indicating inefficient cleavages that are most likely unrelated to the normal processing of Ambn. LC-MS/MS analysis found the C-Ambn2 missing Abz- or nitro-Tyr-NH_2. The *in vivo* cleavage after Gly^{300} is reproduced *in vitro* by Mmp-20.

The native 8-kDa C-terminal cleavage product is covered by C-Ambn3 (Gly^{338}-Ala^{348}). The original material resulted in a peak at 47.5 min RP-HPLC retention time (Fig. 4.11). The rpMmp-20 cleaved it at low rate, but the peak at 41.5 min corresponds to Abz-GLADA and the peak at 40 min corresponds to YETYGA-nitroTyr. In contrast, Klk4 generated two new pronounced peaks at 44.5 min harboring the N-terminus and at 35.5, identified as cleavage after Tyr^{346}, which has not been identified as a cleavage site *in vivo*. Mmp-20 catalyzed the cleavage after Ala^{342}.

In summary, *in vitro* experiments confirmed cleavage sites of ameloblastin that have been identified from immature porcine enamel matrix. Mmp-20 catalyzed cleavages exclusively as expected from its expression by secretory stage ameloblasts. The FRET-Ambn peptides were useful to simulate the cleavages *in vitro*. The cleavage after Asn^{30} that generates the 13-kDa Ambn, the cleavage after Gly^{300} that generates the 27- and 29-kDa Ambn products, and the cleavage after Ala^{342} that releases the 8-kDa C-terminal product were all catalyzed by Mmp-20. Klk4 catalyzed cleavages after Gln^{28} and after Tyr^{346}, which are unknown cleavage sites *in vivo*.

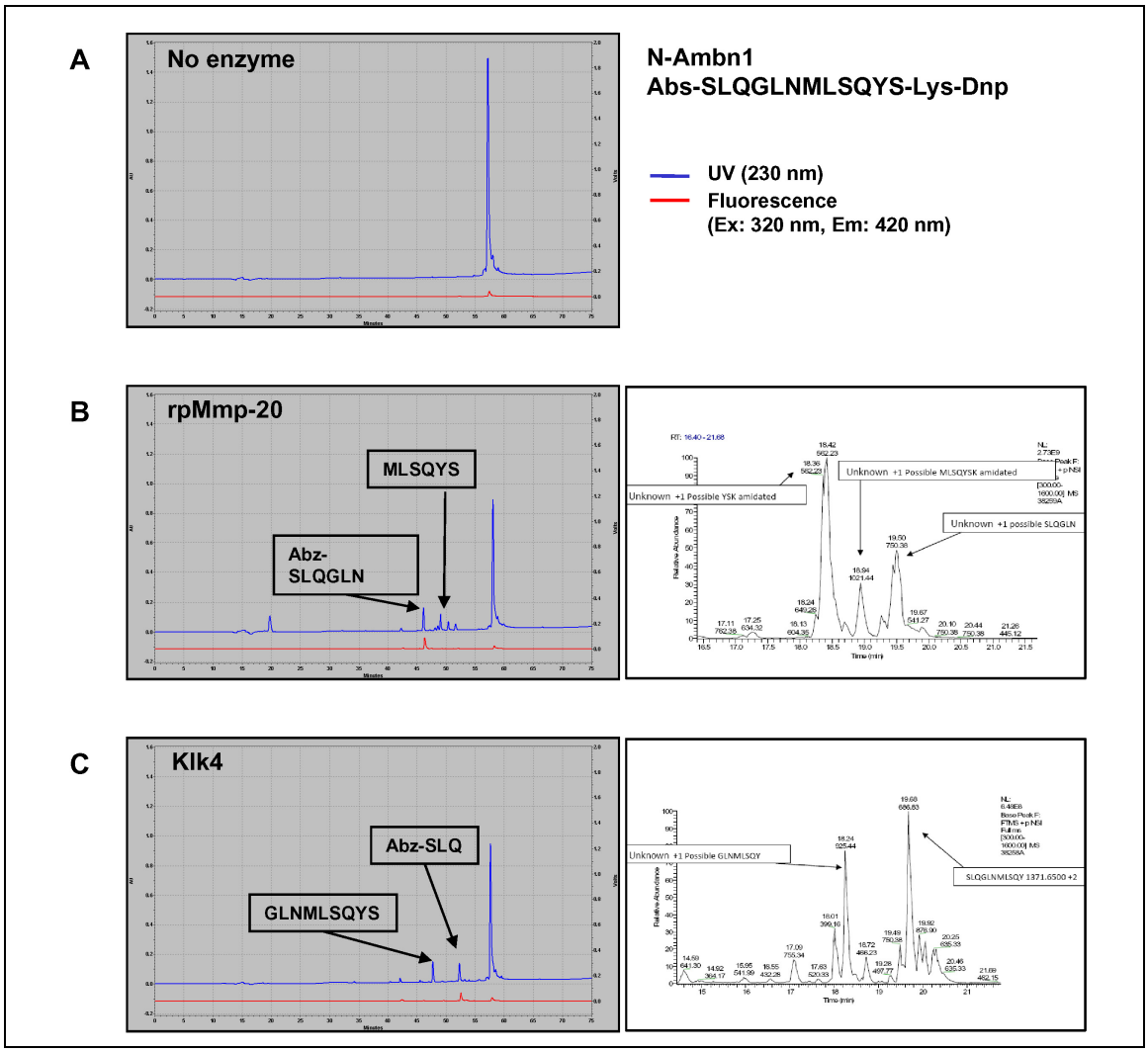

Figure 4.10: Analysis of processing of N-Ambn1 by enamel proteinases.
The Ambn *in vivo* cleavage site after Asn[31] was simulated in the peptide N-Ambn1 (Ser[26]-Ser[37]). While in the uncleaved peptide fluorescence is quenched, the signal is detectable upon cleavage after excitation at 320 nm and as emitted light at 420 nm (chromatogram in red). The digest is analyzed by RP-HPLC at 230 nm UV (chromatogram in blue), at 420 nm and by LC-MS/MS (right chromatogram).
A) Incubation of N-Ambn1 without enzyme. At 230 nm a single peak from the peptide was observed.
B) Incubation of N-Ambn1 with rpMmp-20. RP-HPLC displayed reduced quantity of the starting material and several new peaks. LC-MS/MS analysis identified two fragments (Abz-SLQGLN and MLSQYS) from the cleavage after Asn[31].
C) Incubation of N-Ambn1 with native Klk4. Two new peaks were detected in the UV chromatogram. The LC-MS/MS profile of these peaks identified cleavage products Abz-SLQ and GLNMLSQYS revealing a cleavage site after Gln[28].

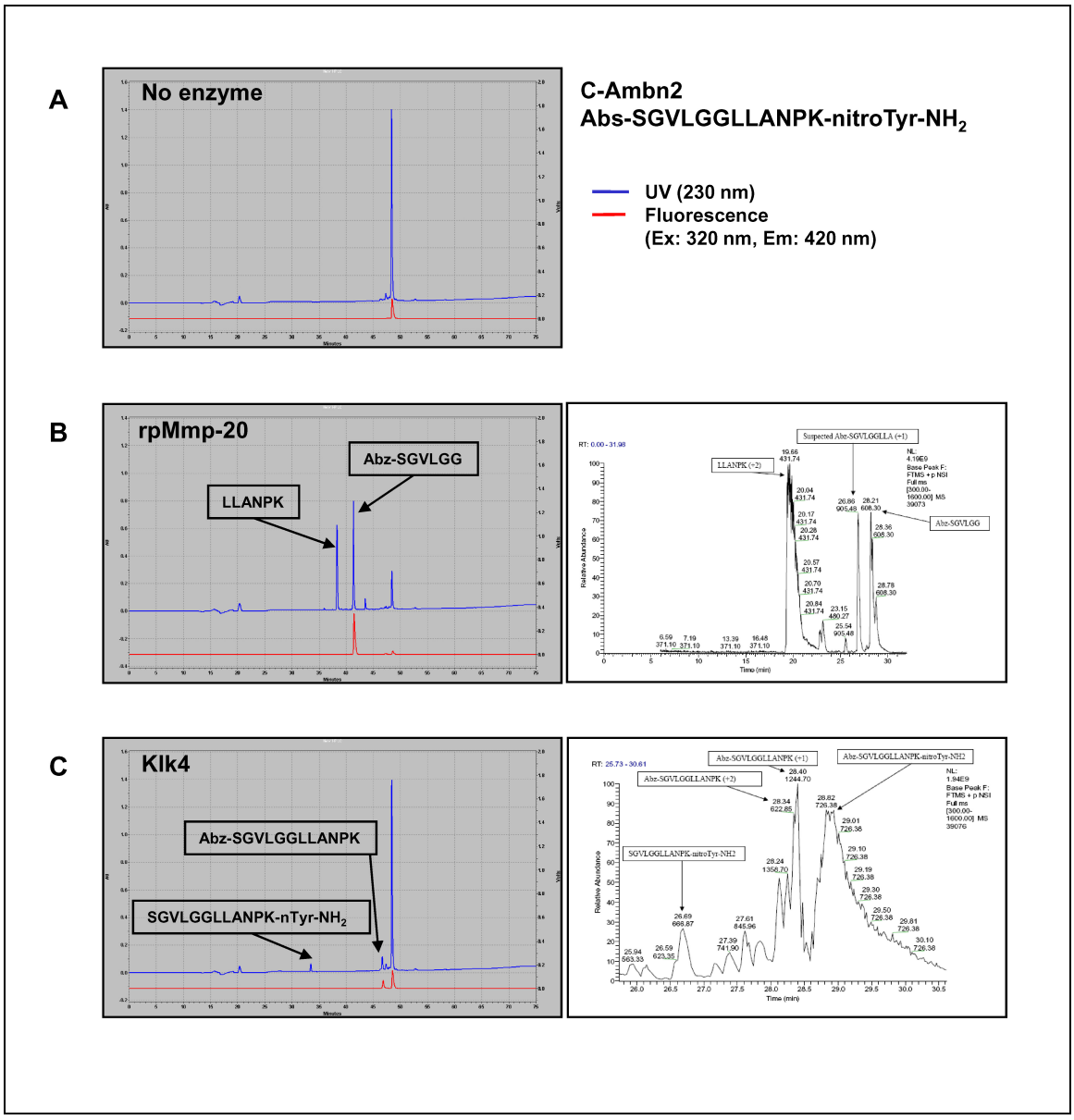

Figure 4.11: Analysis of processing of C-Ambn2 by enamel proteinases.
The Ambn *in vivo* cleavage site after Asn^{31} was simulated in the peptide C-Ambn2 (Ser^{295}-Lys^{306}).
A) C-Ambn2 was incubated without enzyme.
B) C-Ambn2 was incubated with rpMmp-20. The starting material was significantly reduced and two new peaks appeared representing accumulated cleavage products. LC-MS/MS data identified a cleavage site after Gly^{300} from peptides Abz-SGVLGG and LLANPK.
C) Incubation of C-Ambn2 with Klk4. LC-MS/MS analysis demonstrated that the peptide sequence itself was not cleaved by Klk4. The peptide was missing the either the N-terminal fluorescence or the C-terminal quencher.

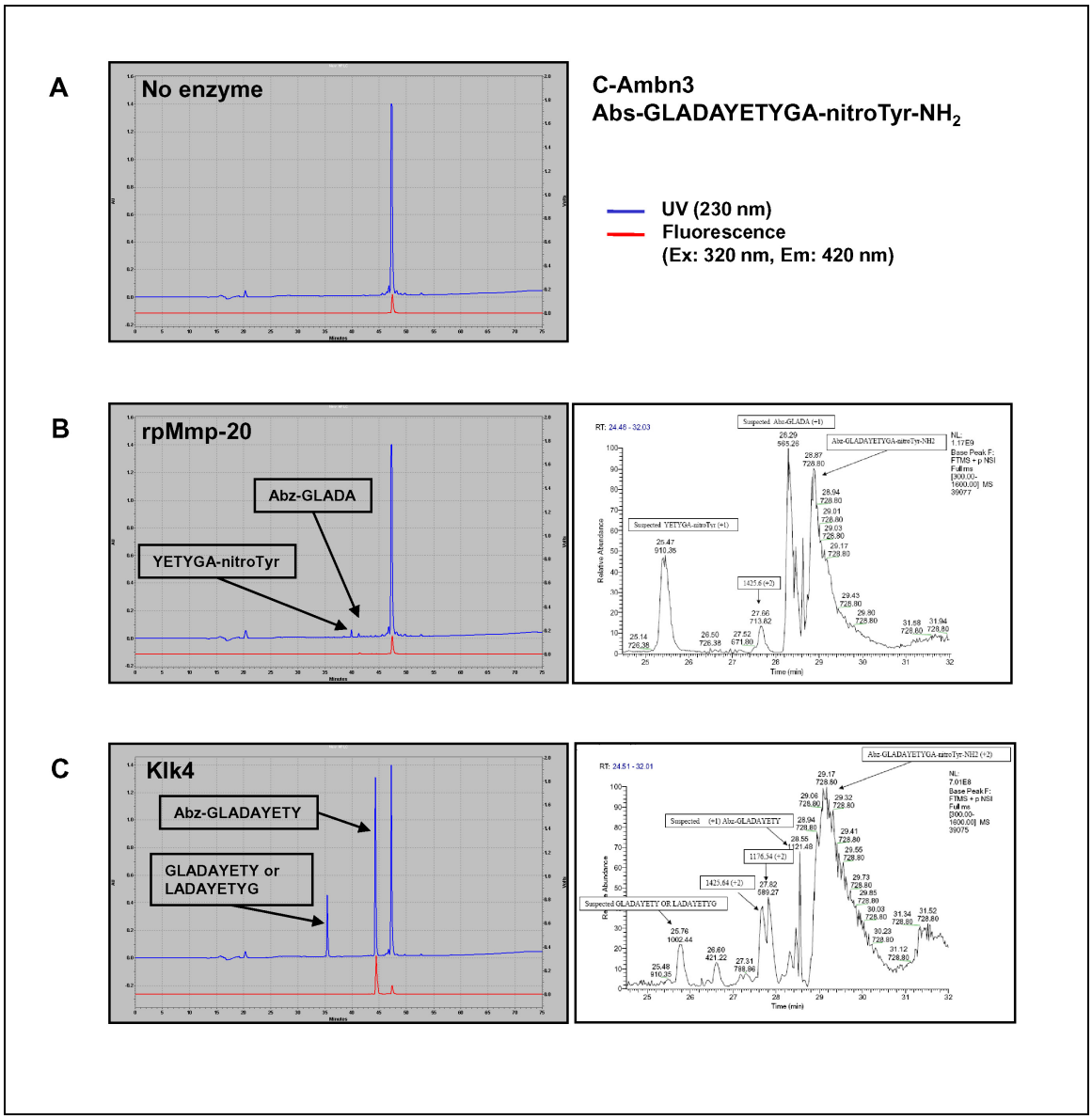

Figure 4.12: Analysis of processing of C-Ambn3 by enamel proteinases.
A) C-Ambn3 (Gly^{338}-Ala^{348}) was incubated without enzyme. The chromatogram displays the peptide as a single peak detected by UV.
B) C-Ambn3 was incubated with rpMmp-20. In the LC-MS/MS chromatogram the most significant peaks represent the uncleaved starting material, Abz-GLADA and YETYGA-nitroTyr. Two small new peaks were observed in the UV chromatogram that contained cleavage products separated after Ala^{342}. This cleavage site overlaps with an *in vivo* cleavage site in immature enamel.
C) After incubation of C-Ambn3 with Klk4, two cleavage products were generated. LC-MS/MS data identified fragments from cleavage after Tyr^{346}, which does not correlate to observed *in vivo* cleavage sites.

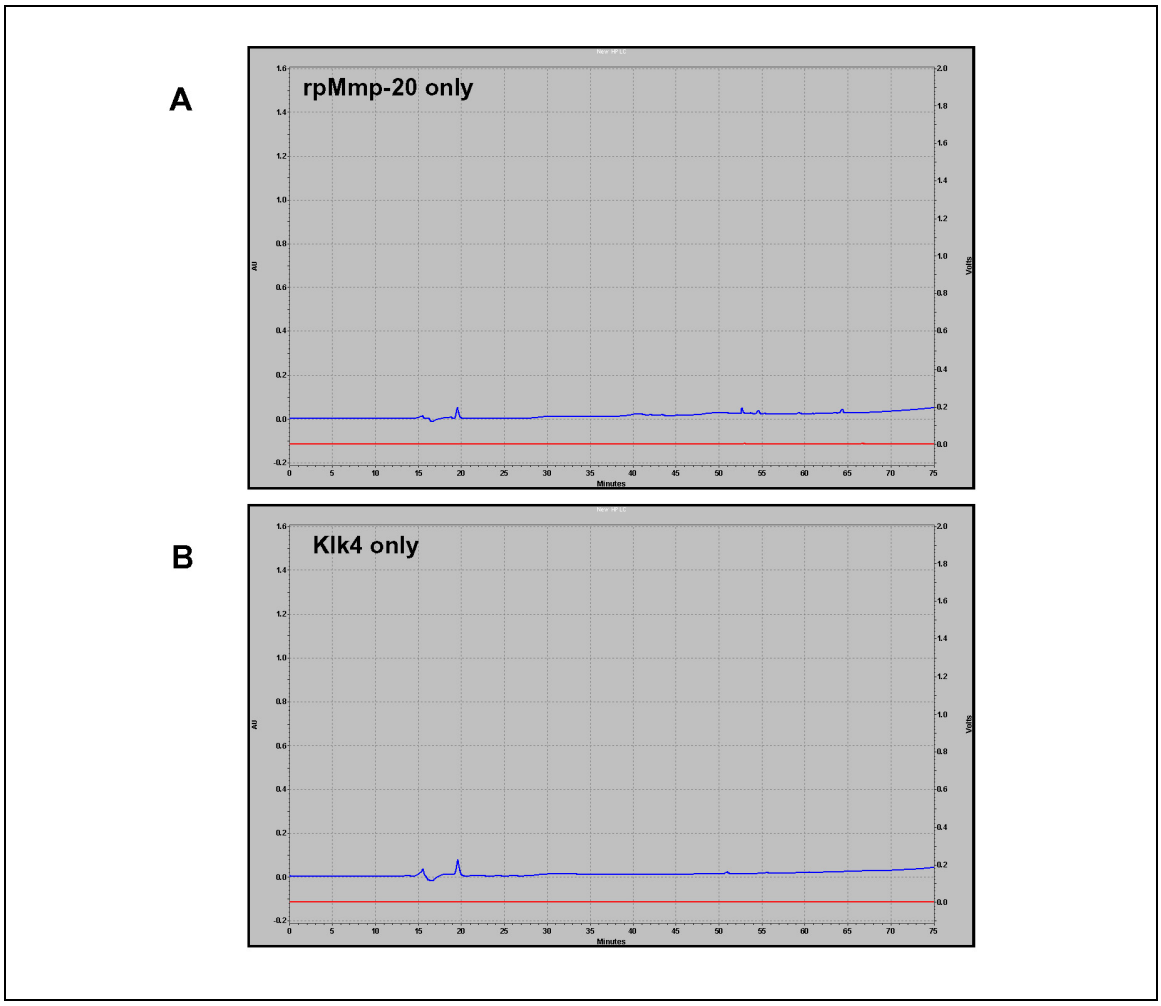

Figure 4.13: RP-HPLC chromatograms of rpMmp-20 and Klk4 without substrate. Neither rpMmp-20 (A) nor Klk4 (B) gave rise to a detectable peak in the RP-HPLC chromatogram.

Comparison of Ambn processing and degradation *in vivo* vs. *in vitro*

For the *in vitro* characterization of porcine ameloblastin processing by the enamel proteinases Mmp-20 and Klk4 two strategies were used: digestion of recombinant full-length ameloblastin and synthetic FRET-peptides of ameloblastin sequences. The *in vitro* incubations of Mmp-20 and Klk4 with rpAmbn and synthetic Ambn peptides demonstrated that both proteinases are able to cleave Ambn. Mmp-20 is able to catalyze

the cleavages *in vitro* after Pro^{2}, Asn^{31}, Gln^{130}, Arg^{170}, Ala^{222}, Gly^{300} and Ala^{342}. Klk4 cleaved after Gln^{28}, Lys^{43}, Arg^{170}, Tyr^{191}, Tyr^{346} and Arg^{391} (Fig. 4.14). Both enamel proteinases demonstrated distinct cleavage patterns, indicating complementary cleavage site specificity that is consistent with their temporally sequential expression in ameloblasts of developing teeth. Mmp-20 catalyzes the breakup of Ambn into center, N- and C-terminal cleavage products. Klk4 degrades these Ambn products into smaller pieces.

In general, the *in vitro* cleavage sites generated by Mmp-20 correspond to known cleavage sites from purified i*n vivo* cleavage products. The *in vitro* cleavage site after Pro^{2} does not correspond to a known *in vivo* site, but has been identified previously *in vitro* as a site recognized by Mmp-20 (Iwata et al., 2007). The cleavage site after Asn^{31} corresponds to the 13-kDa N-terminal Ambn and after Gln^{130} corresponds to the C-terminal end of 13-and 15-kDa N-terminal Ambn (Hu *et al.*, 1997). The cleavage site after Arg^{170} separates the N-terminus from the 25-kDa Ambn center (Uchida *et al.*, 1991). For the cleavage site after Ala^{222}, an *in vivo* cleavage product has been purified (Yamakoshi, unpublished data), and this site has been generated before *in vitro* (Iwata *et al.*, 2007). The cleavage site after Gly^{300} is known as the separation of the C-terminal Ambn cleavage products from the center (Yamakoshi *et al.*, 2001). The cleavage site after Ala^{342} generates the 8-kDa cleavage product (Yamakoshi *et al.*, 2006b).

Klk4 overlapped in cleavage site recognition with Mmp-20 after Arg^{170}. The remaining identified *in vitro* cleavage site after Gln^{28}, Lys^{43}, Tyr^{191}, Tyr^{346} and Arg^{391} are novel and are consistent with the degradative activity of Klk4. Mmp-20 and Klk4 activity are acting complementary in processing and degrading full-length ameloblastin.

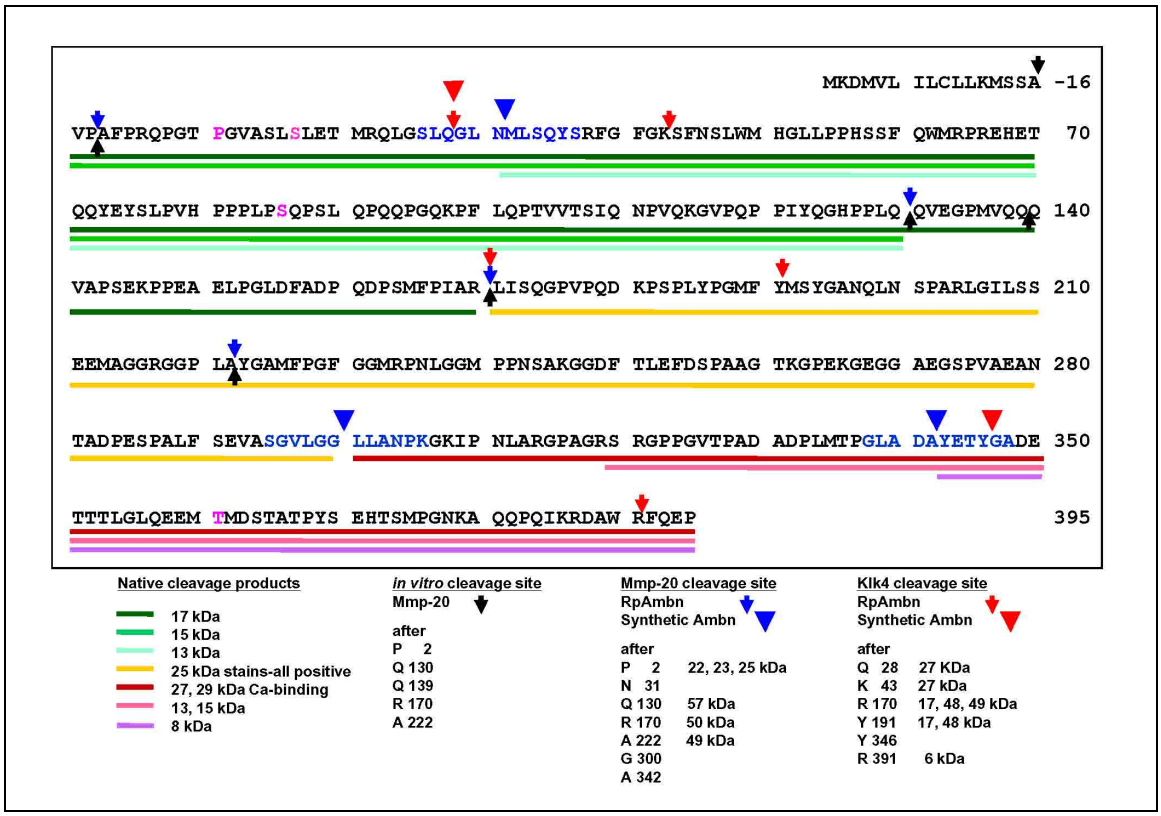

Figure 4.14: Summary of processing of ameloblastin.
Mmp-20 cleaved rpAmbn after Pro[2], Gln[130], Arg[170], and Ala[222] (blue arrow) and the synthetic peptides after Asn[31], Gly[300] and Ala[342] (blue arrowhead). All cleavage sites of rpAmbn recognized by Mmp-20 coincide with cleavage products purified from *in vivo* immature porcine enamel (underlined in different colors). Many of the cleavage sites overlap with cleavage sites identified *in vitro* using rpAmbn (black arrow) (Iwata *et al.*, 2007).
Klk4 cleaved rpAmbn and synthetic peptide after Gln[28], Lys[43], Arg[170], Tyr[191], Tyr[346] and Arg[391] (red arrow, red arrowhead).

DISCUSSION

In vitro strategies allow reducing the biological complexity to controllable conditions. Enamel proteins and their cleavages have been extensively characterized after being isolated from developing porcine teeth (Fukae and Tanabe, 1987b; Fukae and Tanabe, 1998; Tanabe, 1984; Tanabe *et al.*, 1992; Yamakoshi *et al.*, 2003). Similarly, the proteinases expressed and secreted by ameloblasts have been identified and their

importance to proper enamel formation has been proven (Bartlett *et al.*, 1996; Simmer *et al.*, 1998; Simmer *et al.*, 2003). The processing and degradation of enamel proteins is directly linked to mineralization events. The mineralization front and the Tomes' process are defective in the absence of substrates amelogenin, ameloblastin and enamelin (Fukumoto *et al.*, 2004; Gibson *et al.*, 2001; Hu *et al.*, 2008) and in the absence of Mmp-20 during secretory stage (Caterina *et al.*, 2002). As enamel proteins are secreted and processed by Mmp-20, the crystallites lengthen as long ribbons. Spaces between crystallites are filled with protein cleavage products, which are gradually replaced with mineral. During enamel formation, the task is to secrete protein that organize themselves and are removed such that mineral extends in a controlled manner. The rapid elongation of crystallites of 4 μm/day in humans indicate a rapid turnover at the mineralization front of protein secretion, processing and removal.

The enamel proteins amelogenin, enamelin and ameloblastin help to control initiation and growth of crystallites. Since they are secreted at a high rate, they need to be processed and specific cleavage products are removed from the tips of the crystallites to allow deposition of hydroxyapatite along the c-axis. During the secretory stage, Mmp-20 cleaves Amel, Ambn and Enam very rapidly. During the maturation stage, Mmp-20 generated cleavage products are degraded by Klk4 and removed through the sheath space as a channeling system back to ameloblasts. Degradation of cleavage products is necessary for their removal from the maturing matrix, which allows the crystal ribbons that were extended during the secretory stage, to grow in width and thickness. This maturation of the enamel crystals is necessary for hardening of the enamel layer.

Ameloblastin is essential for the formation of enamel. In its absence, the enamel layer is disrupted in a mouse model (Fukumoto *et al.*, 2004). Ambn sequences were first discovered through pH-based isolations of cleavage products from immature porcine enamel that were distinct from amelogenin (Fukae and Tanabe, 1987a; Fukae and Tanabe, 1987b). Full-length Ambn was never isolated because it is cleaved into multiple fragments shortly after its secretion. The N-terminal Ambn cleavage products, having apparent molecular weights of 13, 15, and 17 kDa, localize in the sheath space (Fukae *et al.*, 2006; Uchida *et al.*, 1995; Uchida *et al.*, 1997; Uchida *et al.*, 1998). The C-terminal Ambn cleavage products having apparent molecular weights of 8, 13-15, and 27-29 kDa (Fukae and Tanabe, 1987a; Murakami *et al.*, 1997; Yamakoshi *et al.*, 2006b) are found in the rod enamel near the surface, but are absent from the deeper secretory stage enamel (Yamakoshi *et al.*, 2006b). The rapid cleavage of Ambn seems to be a conserved feature. The principle Ambn pieces identified from rat secretory and transition stage enamel have products sizes of 13, 14, 15, 16, 17, 19, 37, 40, 52 kDa (Brookes *et al.*, 2001). Using anti-peptide antibodies the identity of rat cleavage products could be qualified as N-terminal 10-22 kDa with strong immunoreactivity, center cleavage products of 40-56 and 65 kDa as faint bands, and C-terminal distinct bands of 25, 33, 36, 41, 48, 65 kDa (Uchida *et al.*, 1997). The patterns of porcine cleavage products from our experiments are consistent with earlier *in vivo* experiments.

In this study, two types of substrate were utilized to determine how rpMmp-20 and pKlk4 cleave Ambn *in vitro*: recombinant full-length protein and synthesized peptide sequences. Ambn served as substrate for both enamel proteinases. Both enzymes generated

distinct cleavage products. Some of the *in vivo* cleavage sites from immature enamel had been previously recapitulated *in vitro* by Mmp-20 using recombinant Ambn: after Pro^{2}, Gln^{130}, Gln^{139}, Arg^{170}, and Ala^{222} resulting in cleavage products 23 kDa (Tyr^{223}), 17 kDa (Val^{1}-Arg^{170}), and 15 kDa (Val^{1}-Gln^{139}) (Iwata *et al.*, 2007).

The synthetic Ambn peptides complemented cleavage sites of rpAmbn. Previous experience has shown that it is difficult to recapitulate them to completeness *in vitro* (Iwata *et al.*, 2007). Limitations are the availability of recombinant protein, accumulation of cleaved material, a physiological enzyme – substrate ratio and the ability to detect all cleavage products by antibodies or stains.

In the present study, *in vitro* cleavages by Mmp-20 after Pro^{2}, Asn^{31}, Gln^{130}, Arg^{170}, Ala^{222}, Gly^{300} and Ala^{342} are reported that correspond to the cleavage sites used to generate important Ambn cleavage products in porcine secretory stage enamel (Fig. 4.14).

Initial cleavages are made in the center region of Ambn at different sites as high molecular bands ranging from 45-60 kDa rapidly accumulate (Fig. 4.8). These cleavage products starting with Gln^{131}, Leu^{171} and Tyr^{223} contain the C-terminus of Ambn as they immunoreact with C-terminal antibodies (Fig. 4.15). Later cleavages occur at cleavage products starting with Val^{1} or Ala^{3} differing in their molecular weight (22-37 kDa) due to cleavages from the C-terminus. Interestingly, the major cleavage site after Arg^{170} can be catalyzed by both Mmp-20 and Klk4.

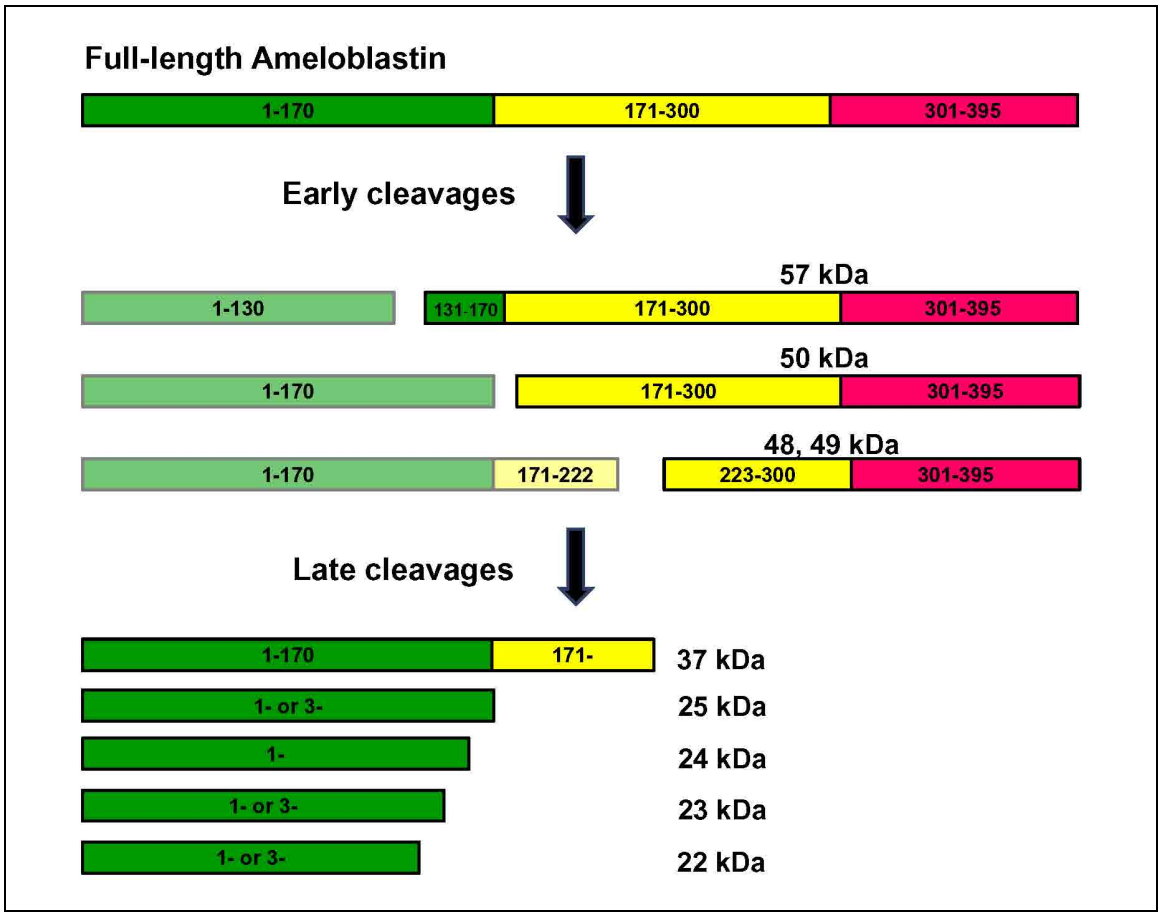

Figure 4.15: Schematic of ameloblastin processing by Mmp-20.
Initially, Mmp-20 cleaves Ambn in the middle region after Gln^{130}, Arg^{170}, Ala^{222} generating cleavage products of 48-50 kDa. Late cleavages occur at the N-terminus producing bands of 22-37 kDa. These cleavage products start with amino acid Val^{1} or Ala^{3}.

The Ambn cleavage sites catalyzed by Klk4 are distinct from Mmp-20 cleavage sites and generally do not correspond to the sites used to generate the Ambn cleavage products that accumulate during the secretory stage. The Klk4 cleavage sites are consistent with its degradative nature. In fact, its activity seems aggressive to the extent that it disrupts antigenic regions at the Ambn C-terminus.

Understanding of the mechanism that generates the cleavage products is important as the absence of either Mmp-20 or Klk4 results in severe defects in enamel mineralization

in humans and mice (Caterina *et al.*, 2002; Hart *et al.*, 2004; Kim *et al.*, 2005b; Ozdemir *et al.*, 2005b; Wright *et al.*, 2006). Mmp-20 is specifically co-secreted with enamel proteins during secretory-early maturation stage and is able to process *in vitro* recombinant amelogenin (Ryu *et al.*, 1999) at sites found *in vivo*. Klk4 expression starts in transition stage and has very little temporal overlap with Mmp-20 (Simmer *et al.*, 2003). *In vitro* Klk4 generates different and more cleavages in amelogenin than Mmp-20 (Ryu *et al.*, 2002). The enzymatic activities of Mmp-20 and Klk4 are complementary, with Mmp-20 processing proteins and Klk4 degrading them further. Organic matrix material is reabsorbed by ameloblasts. Klk4 can actively cleave sites that are protected by glycosylations and are not accessible for Mmp-20 as in 32-kDa enamelin (Yamakoshi *et al.*, 2006a).

The cleavage events separate the two different domains of Ambn (Vymetal *et al.*, 2008). The N-terminal domain has a predicted basic pI (10-11) and the C-terminal domain has a predicted acidic pI (4.5). They differ in their localization and their dynamics. Upon cleavage, N-terminal cleavage products are sorted into the sheath space. They are found throughout the enamel layer and accumulate in our *in vitro* experiment. N-terminal cleavage products could suppress mineralization of the sheath space to maintain access to deeper layers to remove proteins. Throughout enamel formation there is a need to remove degraded proteins from enamel. The sheath space at the junction of rods and interrods mineralizes last and N-terminal Ambn could be important in regulating the removal of cleavage products.

C-terminal cleavage products are only detectable on the surface on the enamel layer and inside the rod. They associate with the rods and may contribute to crystal growth along the c-axis. To accommodate the rapid elongation at the tips of the crystallites proteins need to be cleared rapidly. The dynamics of the processing of Ambn found in our experiments is consistent with this observation. Therefore, the rapid separation of the two domains of Ambn by cleavages at multiple sites in the center is important for this distinct task.

Ambn is secreted early during secretory stage when enamel crystallites are initiated at the DEJ. During the secretory stage, proteins are secreted and crystallites extend through the entire thickness of the enamel layer. The thin and long crystal ribbons are supported and arranged by all enamel proteins. The distinct biochemical properties of Ambn N- and C-terminal cleavage products could be related to their function. These domains may become functional only after separation by Mmp-20. During the maturation stage, mineral is deposited to widen crystallites. Cleavage products between crystallites and sheath space are finally degraded by Klk4 and removed by endocytosis to make room for crystals to interlock. The formation and growth of the enamel crystallites is controlled by ameloblasts through the secretion, processing and resorption of enamel proteins.

REFERENCES

Bartlett JD, Simmer JP (1999). Proteinases in developing dental enamel. Crit Rev Oral Biol Med 10:425-441.

Bartlett JD, Simmer JP, Xue J, Margolis HC, Moreno EC (1996). Molecular cloning and mRNA tissue distribution of a novel matrix metalloproteinase isolated from porcine enamel organ. *Gene* 183:123-128.

Bartlett JD, Ryu OH, Xue J, Simmer JP, Margolis HC (1998). Enamelysin mRNA displays a developmentally defined pattern of expression and encodes a protein which degrades amelogenin. *Connect Tissue Res* 39:101-109; discussion 141-149.

Brookes SJ, Kirkham J, Shore RC, Wood SR, Slaby I, Robinson C (2001). Amelin extracellular processing and aggregation during rat incisor amelogenesis. *Arch Oral Biol* 46:201-208.

Caterina JJ, Skobe Z, Shi J, Ding Y, Simmer JP, Birkedal-Hansen H, Bartlett JD (2002). Enamelysin (matrix metalloproteinase 20)-deficient mice display an amelogenesis imperfecta phenotype. *J Biol Chem* 277:49598-49604.

Fukae M, Tanabe T (1987a). Nonamelogenin components of porcine enamel in the protein fraction free from the enamel crystals. *Calcif Tissue Int* 40:286-293.

Fukae M, Tanabe T (1987b). ^{45}Ca-labeled proteins found in porcine developing dental enamel at an early stage of development. *Adv Dent Res* 1:261-266.

Fukae M, Tanabe T, Uchida T, Yamakoshi Y, Shimizu M (1993). Enamelins in the newly formed bovine enamel. *Calcif Tissue Int* 53:257-261.

Fukae M, Tanabe T (1998). Degradation of enamel matrix proteins in porcine secretory enamel. *Connect Tissue Res* 39:123-129; discussion 141-149.

Fukae M, Kanazashi M, Nagano T, Tanabe T, Oida S, Gomi K (2006). Porcine sheath proteins show periodontal ligament regeneration activity. *Eur J Oral Sci* 114 (Suppl 1) 212-218; discussion 254-6, 381-382.

Fukumoto S, Kiba T, Hall B, Iehara N, Nakamura T, Longenecker G, Krebsbach PH, Nanci A, Kulkarni AB, Yamada Y (2004). Ameloblastin is a cell adhesion molecule required for maintaining the differentiation state of ameloblasts. *J Cell Biol* 167:973-983.

Gibson CW, Yuan ZA, Hall B, Longenecker G, Chen E, Thyagarajan T, Sreenath T, Wright JT, Decker S, Piddington R, Harrison G, Kulkarni AB (2001). Amelogenin-deficient mice display an amelogenesis imperfecta phenotype. *J Biol Chem* 276:31871-31875.

Hart PS, Hart TC, Michalec MD, Ryu OH, Simmons D, Hong S, Wright JT (2004). Mutation in kallikrein 4 causes autosomal recessive hypomaturation amelogenesis imperfecta. *J Med Genet* 41:545-549.

Hu CC, Fukae M, Uchida T, Qian Q, Zhang CH, Ryu OH, Tanabe T, Yamakoshi Y, Murakami C, Dohi N, Shimizu M, Simmer JP (1997). Sheathlin: cloning, cDNA/polypeptide sequences, and immunolocalization of porcine enamel sheath proteins. *J Dent Res* 76:648-657.

Hu JC, Ryu OH, Chen JJ, Uchida T, Wakida K, Murakami C, Jiang H, Qian Q, Zhang C, Ottmers V, Bartlett JD, Simmer JP (2000). Localization of EMSP1 expression during tooth formation and cloning of mouse cDNA. *J Dent Res* 79:70-76.

Hu JC, Sun X, Zhang C, Liu S, Bartlett JD, Simmer JP (2002). Enamelysin and kallikrein-4 mRNA expression in developing mouse molars. *Eur J Oral Sci* 110:307-315.

Hu JC, Hu Y, Smith CE, McKee MD, Wright JT, Yamakoshi Y, Papagerakis P, Hunter GK, Feng JQ, Yamakoshi F, Simmer JP (2008). Enamel defects and ameloblast-specific expression in Enam knock-out/lacz knock-in mice. *J Biol Chem* 283:10858-10871.

Iwata T, Yamakoshi Y, Hu JC, Ishikawa I, Bartlett JD, Krebsbach PH, Simmer JP (2007). Processing of ameloblastin by MMP-20. *J Dent Res* 86:153-157.

Kim JW, Simmer JP, Hart TC, Hart PS, Ramaswami MD, Bartlett JD, Hu JC (2005). MMP-20 mutation in autosomal recessive pigmented hypomaturation amelogenesis imperfecta. *J Med Genet* 42:271-275.

Murakami C, Dohi N, Fukae M, Tanabe T, Yamakoshi Y, Wakida K, Satoda T, Takahashi O, Shimizu M, Ryu OH, Simmer JP, Uchida T (1997). Immunochemical and immunohistochemical study of the 27- and 29-kDa calcium-binding proteins and related proteins in the porcine tooth germ. *Histochem Cell Biol* 107:485-494.

Ozdemir D, Hart PS, Ryu OH, Choi SJ, Ozdemir-Karatas M, Firatli E, Piesco N, Hart TC (2005). MMP20 active-site mutation in hypomaturation amelogenesis imperfecta. *J Dent Res* 84:1031-1035.

Papagerakis P, Lin HK, Lee KY, Hu Y, Simmer JP, Bartlett JD, Hu JC (2008). Premature stop codon in MMP20 causing amelogenesis imperfecta. *J Dent Res* 87:56-59.

Ryu O, Hu JC, Yamakoshi Y, Villemain JL, Cao X, Zhang C, Bartlett JD, Simmer JP (2002). Porcine kallikrein-4 activation, glycosylation, activity, and expression in prokaryotic and eukaryotic hosts. *Eur J Oral Sci* 110:358-365.

Ryu OH, Fincham AG, Hu CC, Zhang C, Qian Q, Bartlett JD, Simmer JP (1999). Characterization of recombinant pig enamelysin activity and cleavage of recombinant pig and mouse amelogenins. *J Dent Res* 78:743-750.

Simmer JP, Fukae M, Tanabe T, Yamakoshi Y, Uchida T, Xue J, Margolis HC, Shimizu M, DeHart BC, Hu CC, Bartlett JD (1998). Purification, characterization, and cloning of enamel matrix serine proteinase 1. *J Dent Res* 77:377-386.

Simmer JP, Sun X, Yamada Y, Zhang C, Bartlett JD, Hu JC-C (2003). Enamelysin and kallikrein -4 expression in the mouse incisor. *Biomineralization (BIOMIN2001): formation, diversity, evolution and application.* 348-352.

Simmer JP, Sun X, Yamada Y, Zhang C, Bartlett JD, Hu J C-C (2003). Enamelysin and kallikrein -4 expression in the mouse incisor. *Biomineralization (BIOMIN2001): formation, diversity, evolution and application.* 348-352.

Simmer JP, Hu Y, Lertlam R, Yamakoshi Y, Hu J C-C (2009). Hypomaturation enamel defects in Klk4 knockout/LacZ knockin mice. *J Biol Chem* (in print).

Tanabe T (1984). Purification and characterization of proteolytic enzymes in porcine immature enamel. (in Japanese). *Tsurumi Univ Dent J* 10:443-452.

Tanabe T, Fukae M, Uchida T, Shimizu M (1992). The localization and characterization of proteinases for the initial cleavage of porcine amelogenin. *Calcif Tissue Int* 51:213-217.

Uchida T, Tanabe T, Fukae M, Shimizu M, Yamada M, Miake K, Kobayashi S (1991). Immunochemical and immunohistochemical studies, using antisera against porcine 25 kDa amelogenin, 89 kDa enamelin and the 13-17 kDa nonamelogenins, on immature enamel of the pig and rat. *Histochemistry* 96:129-138.

Uchida T, Fukae M, Tanabe T, Yamakoshi Y, Satoda T, Murakami C, Takahashi O, Shimizu M (1995). Immunological and immunocytochemical study of a 15 kDa non-amelogenin and related proteins in the porcine immature enamel: Proposal of a new group of enamel proteins 'sheath proteins'. *Biomedical Research* 16:131-140.

Uchida T, Murakami C, Dohi N, Wakida K, Satoda T, Takahashi O (1997). Synthesis, secretion, degradation, and fate of ameloblastin during the matrix formation stage of the rat incisor as shown by immunocytochemistry and immunochemistry using region-specific antibodies. *J Histochem Cytochem* 45:1329-1340.

Uchida T, Murakami C, Wakida K, Dohi N, Iwai Y, Simmer JP, Fukae M, Satoda T, Takahashi O (1998). Sheath proteins: synthesis, secretion, degradation and fate in forming enamel. *Eur J Oral Sci* 106 (Suppl 1) 308-314.

Vymetal J, Slaby I, Spahr A, Vondrasek J, Lyngstadaas SP (2008). Bioinformatic analysis and molecular modelling of human ameloblastin suggest a two-domain intrinsically unstructured calcium-binding protein. *Eur J Oral Sci* 116:124-134.

Wright JT, Daly B, Simmons D, Hong S, Hart SP, Hart TC, Atsawasuwan P, Yamauchi M (2006). Human enamel phenotype associated with amelogenesis imperfecta and a kallikrein-4 (g.2142G>A) proteinase mutation. *Eur J Oral Sci* 114 (Suppl 1) 13-17; discussion 39-41, 379.

Yamakoshi Y, Tanabe T, Oida S, Hu CC, Simmer JP, Fukae M (2001). Calcium binding of enamel proteins and their derivatives with emphasis on the calcium-binding domain of porcine sheathlin. *Arch Oral Biol* 46:1005-1014.

Yamakoshi Y, Hu JC-C, Ryu OH, Tanabe T, Oida S, Fukae M, Simmer JP (2003). A comprehensive strategy for purifying pig enamel proteins. *Biomineralization (BIOMIN2001): formation, diversity, evolution and application.* 326-332.

Yamakoshi Y, Hu JC, Fukae M, Yamakoshi F, Simmer JP (2006a). How do enamelysin and kallikrein 4 process the 32-kDa enamelin? *Eur J Oral Sci* 114 (Suppl 1) 45-51; discussion 93-95, 379-380.

Yamakoshi Y, Hu JC, Zhang H, Iwata T, Yamakoshi F, Simmer JP (2006b). Proteomic analysis of enamel matrix using a two-dimensional protein fractionation system. *Eur J Oral Sci* 114 (Suppl 1) 266-71; discussion 285-286, 382.

CHAPTER 5

AMELOBLASTIN FUNCTION *IN VIVO*

ABSTRACT

Ameloblastin is essential for enamel formation as ameloblastin null mice (*Ambn*$^{-/-}$) present with hypoplastic amelogenesis imperfecta. The amorphous matrix is characterized by a lack of enamel crystallites and a loss of rod and interrod organization. Heterozygous mice (*Ambn*$^{+/-}$) have enamel of regular thickness and appearance, suggesting a recessive pattern of inheritance. To create an *in vivo* assay to investigate the function of Ambn, an *Ambn* transgene was introduced into *Ambn*$^{-/-}$ mice through mating and the progeny studied for recovery of the enamel phenotype. The *Ambn* transgenic *(Ambn*^{Tg}*)* mice express Ambn in secretory stage ameloblasts at comparable levels as wild-type Ambn. The transgene construct expressed the coding region for the 395 amino acid Ambn from the ameloblast-specific amelogenin promoter and terminated from the amelogenin 3'UTR. This construct was injected in fertilized oocytes and 17 positive founders were generated. Germline transmission was evaluated by mating with C57BL/6 mice. To quantify transgene expression level, secretory stage molars from F1 offspring were collected at day 5 for real-time PCR of the Ambn transgene, Ambn wild-type and amelogenin. Of the 17 transgene positive founders, 13 transmitted to offspring. The ameloblastin Tg expression level in day 5 molars ranged between 5 times to less than 1 compared to Ambn^{WT} in founder offspring. The enamel phenotype was evaluated in

founders and offspring. The enamel of the incisors appeared to be opaque with variations in the severity of the phenotype. Transgene lines with similar Ambn expression level as wild-type and enamel were selected and crossed with *Ambn*$^{-/-}$ mice to recover the enamel phenotype. Preliminary SEM analysis of *Ambn*$^{+/-Tg}$ enamel demonstrated rescue of enamel thickness and rod spacing.

INTRODUCTION

Amelogenesis is regulated by secreted proteins that are proteolytically processed and then removed from the matrix. Inherited defects in the genes encoding enamel proteins cause amelogenesis imperfecta (AI) of either hypoplastic or hypomaturation types (Hu *et al.*, 2007; Wright, 2006). Non-syndromic hypoplastic AI is caused by genetic alterations in a secreted enamel protein or in its quantity. Hypomaturation AI is related to a defect in the removal of proteins from the matrix (Wright *et al.*, 1992). In hypoplastic AI the enamel layer is very thin and disorganized (Kim *et al.*, 2004; Mardh *et al.*, 2002). This phenotype has been linked to human mutations of amelogenin (*AMELX*, Xp22.3) or enamelin (*ENAM*, 4q13.2). To date, 15 different mutations in *AMELX* and 9 different mutations in *ENAM* have been identified in AI kindreds (Hu *et al.*, 2007). No human mutations of *AMBN* (4q13.3) have been reported to date. The severity of the hypoplastic AI correlates with the type of mutation (Wright *et al.*, 2009).

Mouse models lacking Amel, Ambn or Enam exhibit hypoplastic AI with severe chalky discolorations of the enamel. Only a thin, unstructured layer of calcospherites covered by a protein layer is found. As a consequence of the hypoplastic enamel, the teeth undergo faster than normal attrition. Amelogenin accounts for about 90 % of total

enamel protein, and Amel deficient mice display hypoplastic enamel lacking crystal organization (Gibson *et al.*, 2001). Although Enam is the least abundant enamel protein, it is critical for proper enamel organization and extension of crystallites at the mineralization front (Hu *et al.*, 2008).

In mice null for *Ambn*, the enamel lost the organization in rods and interrods, and the matrix secreted by ameloblasts mineralized into random calcospherites (Fig. 5.1) (Fukumoto *et al.*, 2004). Initially, ameloblasts of *Ambn* null mice were not different from wild-type cells with regular polarization. However, by postnatal day 3, the *Ambn* deficient ameloblasts lost their Tomes' Processes and detached from the enamel (Fukumoto *et al.*, 2004). This event seemed to be in response to the lack of onset of Ambn secretion, which usually starts on day 2 (Torres-Quintana *et al.*, 2005).

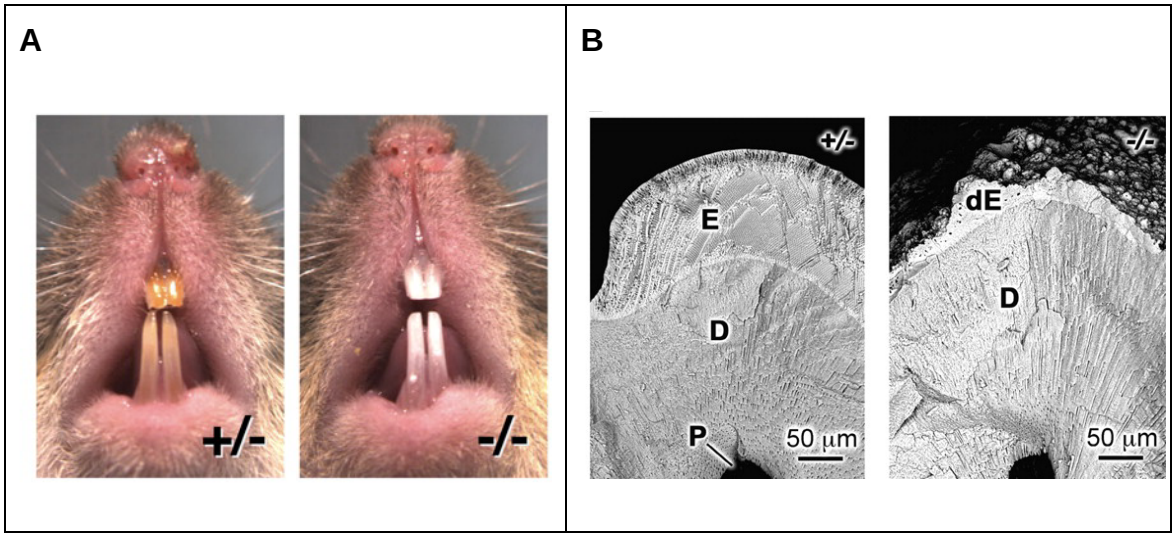

Figure 5.1: Enamel phenotype of the *Ambn* null mouse.
A) Frontal view of incisors of 8-week-old *Ambn* heterozygous and homozygous mice. Teeth in homozygous null mouse are chalky white display amelogenesis imperfecta.
B) Crossection of incisors of *Ambn* heterozygous and homozygous mice analyzed by Scanning electron microscopy (SEM). The enamel layer in the $Ambn^{-/-}$ mouse is hypoplastic and the enamel surface is very rough. The characteristic prism pattern is missing. E enamel, D dentin, P pulp, dE defective enamel. (Fukumoto *et al.*, 2004)

In the opposite event, when Ambn was overexpressed in mice, the enamel did not differ clinically from wild-type enamel. However, the organization of rod and interrod regions was disrupted with reduced rod areas and more dominant interrod areas (Paine *et al.*, 2003). The crystallites in the transgenic animals were twice in diameter as wild-type crystallites. For proper enamel formation, the correct dose of Ambn seems to be critical.

The goal of this study was to establish an *in vivo* assay system to probe ameloblastin structure/function relationships by site directed mutagenesis. Components of this system are the *Ambn* null mouse and transgenic mice that express wild-type or mutant Ambn. The *Ambn* transgene expression was driven by the *Amel* promoter, which targets secretory stage ameloblasts. The null and transgenic mice were mated and the degree of recovery of the enamel layer evaluated. To demonstrate feasibility of the system, wild-type *Ambn* was expressed as a transgene and introduced into the *Ambn* null background. The outcome was evaluated by SEM for enamel thickness and organization of enamel rods.

MATERIALS & METHODS

In the ameloblastin knockout mouse the tooth phenotype of lacking enamel matrix and mineralized enamel with rod organization (Fukumoto *et al.*, 2004) was investigated by reconstituting ameloblastin expression through introduction of full-length Ambn as a transgene. The fundamental question was, whether ameloblastin is able to recover the enamel phenotype in Ambn null mice. For the generation of the Ambn transgenic mouse, the tissue-specific expression of mouse ameloblastin was driven by the *AmelX* promoter. This promoter has been successfully utilized for enamel organ epithelial specific expression (Snead *et al.*, 1996; Snead *et al.*, 1998). The generation of the *Ambn*

transgenic mice involved cloning of the *Ambn* transgene plasmid construct, driven by the tissue-specific amelogenin promoter, microinjection of the DNA into fertilized eggs, identification of adequate founders and introduction of the transgene into *Ambn* null mice by mating.

Animal protocol

All procedures involving animals were reviewed and approved by the UACUC Committee at the University of Michigan.

Ameloblastin transgene construct

The mouse ameloblastin transgene was designed to consist of the mouse amelogenin promoter, the mouse ameloblastin coding region and the mouse amelogenin 3' end. Amelogenin is expressed from the X chromosome and is the highest expressed gene among the enamel proteins. Its temporal expression pattern is similar to ameloblastin with expression during secretory stage. The *AmelX* promoter of 2263 bp upstream of the translation initiation codon has been characterized as harboring information to regulate expression in ameloblasts during secretory stage (Snead et al., 1996). For this study, the *AmelX* promoter region was increased to 4.6 kb upstream and included *AmelX* exon 1, intron 1 and exon 2. The mouse genomic sequences for the amelogenin promoter (*AmelX5'*, 4.6 kb), (1744 bp) and amelogenin 3' end (*AmelX3'*, 1145 bp) were cloned using mouse genomic DNA as template. To clone the full-length mouse Ambn cDNA, RNA was extracted using Trizol (Invitrogen, Carlsbad, CA, USA) and chloroform. The cDNA was synthesized using SuperScript II reverse transcriptase (Invitrogen). The

components of the *Ambn* transgene construct were obtained by polymerase chain reaction (PCR) amplification using primer sets designed to introduce restriction sites and separately ligated into the vector pCR2.1-TOPO (3.9 kb) (Invitrogen) (Tab. 5.1).

A) AmelX5-AmelX3' **AmelX5'F(NotI): agcggccgcTGCACAAACAGATATTTGGAAT** **AmelX5'R(AscI): tggcgcgccCTTGATGGTTCTGAAATGTAAATC** **Sense: gatttacatttcagaaccatcaagGGCGCGCCA**
B) Ameloblastin Code: **Ambn5(AscI): tGGCGCGCCttcaaaatgaagggcctgatcc** **Ambn3(SgfI): aGCGATCGCtttatttaaaacaggccaattgccc** **Sense: gggcaattggcctgttttaaataaaGCGATCGCt** ***Insert oriented so its 5' end is on the *NotI* side of cloning site.**
C) *AmelX 3'* end: **AmelX3'F(SgfI): tGCGATCGCcgaagtggatactttggttg** **AmelX3'R(SrfI): aGCCCGGGCctaaggataaggaattactg** **Sense: cagtaattccttatccttagGCCCGGGCt**

Table 5.1: Generation of the transgene components by PCR: *AmelX* promoter, *Ambn* coding region, *AmelX3'*.
The three cassettes were individually cloned and ligated into pCR2.1-Topo. Unique restriction sites are introduced by primers to facilitate cloning and ligation into one transgene vector.
A) Primers to clone the *AmelX* promoter flanked by a NotI 5' and an AscI site 3'.
B) *Ambn* coding region is cloned with AscI 5' and SgfI 3' sites to provide correct orientation.
C) *AmelX 3'* end with transcription termination signals.

The *AmelX* promoter was amplified using Pfu turbo DNA polymerase (Stratagene, La Jolla, CA, USA) introducing a NotI site at the 5' and a AscI site at the 3' end. The *Ambn* coding region was amplified flanked by an AscI site at the 5' and a SgfI site at the 3' end. The *AmelX3'* UTR was amplified with a SgfI site at the 5' and a SrfI site at the 3'end. The cassettes were subcloned into pCR2.1-TOPO and the sequence was analyzed by sequencing. For the assembly of the three cassettes, first the *AmelX* promoter and *Ambn* cassettes were merged by double digesting the *AmelX* promoter with NotI and AscI. The *AmelX* promoter was purified from a gel (QIAquick gel extraction kit, Qiagen, Valencia, CA, USA) and ligated into the pCR2.1-TOPO containing *Ambn*. The *Ambn*

coding region was double digested with NotI and AscI and purified for a 4.6 kb region containing pCR2.1-TOPO. *AmelX* promoter and *Ambn* were joined at the AscI site resulting in the cassette *AmelX*-promoter-*Ambn*-Vector (~10.2 kb). The *AmelX*-promoter-*Ambn* cassette was double digested with NotI and SgfI. The *AmelX-Ambn* code (~6.3 kb) was gel purified and ligated into the *AmelX3'*-vector (~5.0 kb) using NotI and SgfI sites. The final *Ambn* transgene construct comprised ~11.3 kb (Fig. 5.2).

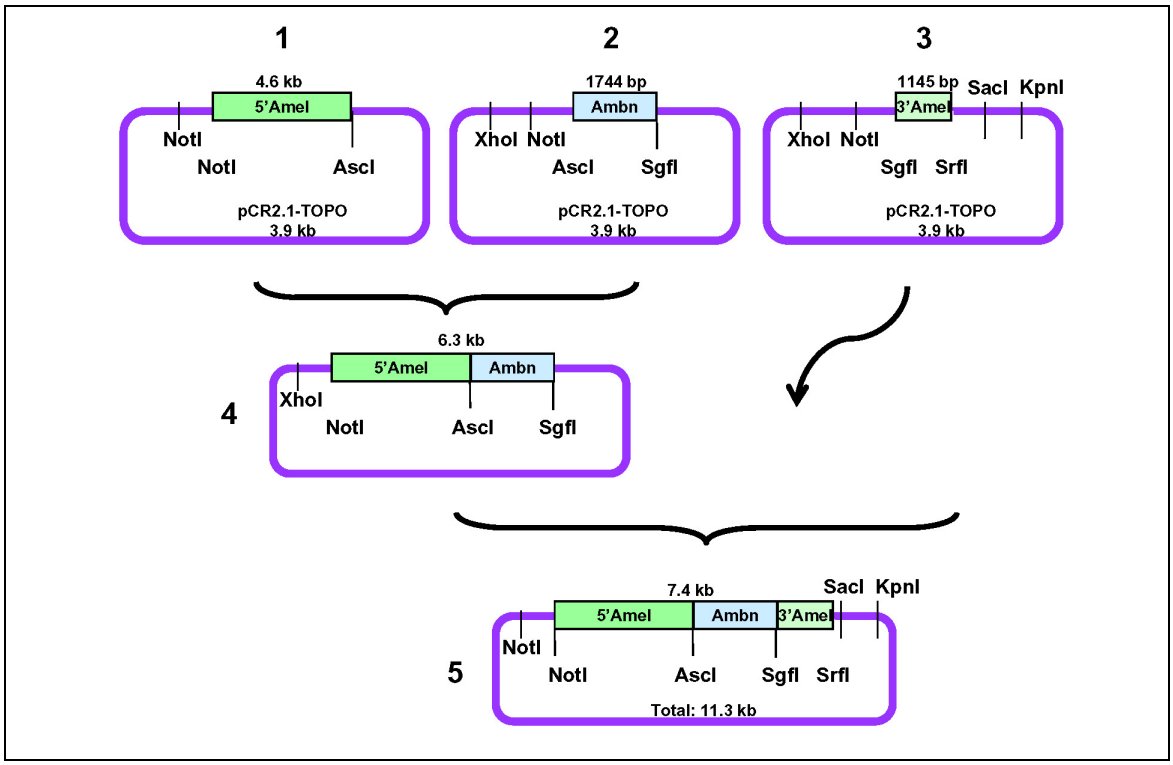

Figure 5.2: Strategy to generate transgene construct.
The three cassettes generated by PCR and cloning are:
1) *AmelX* promoter, 2) *Ambn* coding region, 3) *AmelX3'* end with transcription termination signals. 4) The constructs 1-3 were assembled into one transgene construct (#4). Construct 1 was cut with NotI and AscI and purified for 4.6 kb containing the *AmelX* promoter. Construct 2 was digested with NotI and AscI and purified for 5.1 kb containing the *Ambn* coding region and the vector. Construct 3 was cut with NotI and SgfI and purified for a 5.0 kb segment containing the *AmelX3'* and vector. Construct 4 was assembled by ligating the *AmelX* promoter with *Ambn*-Vector piece from vector 2 together. Construct 4 was cut with NotI and SgfI and a 6.3 kb piece was purified containing the *AmelX5'-Ambn* coding region, which was ligated into construct 3 at NotI and SgfI sites to obtain construct 5. 5) Construct 5 was digested with NotI and SrfI to obtain the 7.4 kb *AmelX5'-Ambn-AmelX3'*construct.

Generation of the ameloblastin transgenic mice

The amelogenin5'-ameloblastin-amelogenin3' construct was released by digestion with NotI and SrfI, and purified from a gel by using QIAquick (Qiagen) (Fig. 5.3). To generate transgenic mice, the transgene construct was microinjected into fertilized C57BL/6 X SJL F2 oocytes and surgically transferred to recipients at the Transgenic Animal Model Core at the University of Michigan. From two microinjections, 34 and 85 independent founders were generated. Tail biopsies were obtained 5 weeks after injecting eggs (3 weeks gestation time and 2 weeks of post-natal growth). The Transgenic Core performed the extraction of genomic DNA from the biopsies using an AutoGen 740 robotic workstation. The DNA was tested by PCR for the transgene. Primers used were unique for detecting the transgene with the forward primer complementary to the sequence of *AmelX* promoter and the reverse primer complementary to the *Ambn 5'* coding region (Fig. 5.3, Tab. 5.2). Primers were designed using the web-based program 'Primer3' (htpp://primer3.sourceforge.net/). The amplification product was a 257 bp band at the border of the *AmelX* promoter and the *Ambn 5'* end. The plasmid construct served as a positive amplification reaction control. Amplification was performed at 94 ˚C for 30 sec, 58 ˚C for 30 sec, and 72 ˚C for 1 min, which was repeated for 30 cycles and followed by incubation for 10 min at 72 ˚C. PCR products were run on a 1.0 % agarose gel and visualized after staining with ethidium bromide.

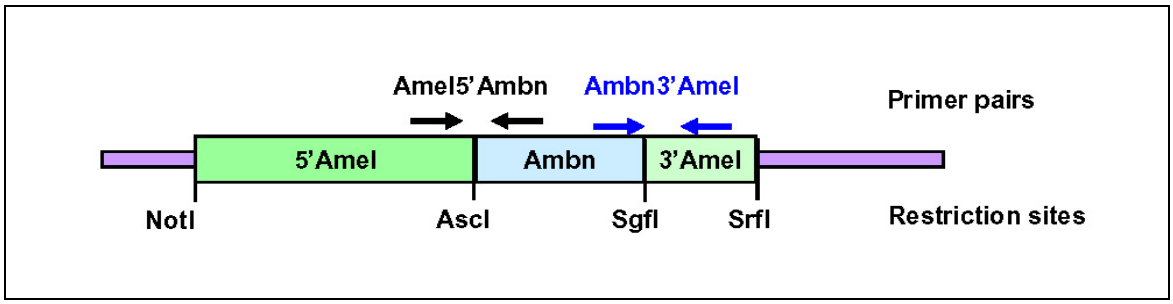

Figure 5.3: Design of primer sets to identify *Ambn* transgene incorporation.
Primers were designed to amplify $Ambn^{Tg}$ specific products. Two primer sets at the borders of Amel5'-Ambn and Ambn3'-Amel were selected.

The Ambn transgenic mice were first mated with C57BL/6 wild-type mice (Jackson Laboratory, Bar Harbor, ME, USA) to determine if the Ambn transgene was transmitted through germline cells and to segregate the transgene copies with integration sites on different chromosomes. Genotyping was performed between postnatal days 10-14. Tail DNA was isolated (DNeasy, Qiagen) from offspring and PCR was performed by using transgene unique primer sets annealing to the 5' and 3' borders of the *Ambn* coding region (Tab.5.2, 5.3, Fig. 5.3).

	Length	**Tm**	**GC %**	**Primer sequence 5' ->3'**
Left primer	19	59.51	45.00	GCCGCACCTTCTTTTTGAT
Right primer	20	57.74	50.00	AAGGCTCAAACTAGCCATGC
Sense				GCATGGCTAGTTTGAGCCTT
Product size	257			

Table 5.2: Primers to amplify a product from the *AmelX-5'Ambn* border.

	Length	**Tm**	**GC %**	**Primer sequence 5' ->3'**
Left primer	20	59.51	45.00	ATGGTGATTGGTGGAAAACC
Right primer	20	57.74	50.00	GAGCAAATGACCAGTCCCTA
Sense				TAGGGACTGGTCATTTGCTC
Product size	347			

Table 5.3: Primers to amplify a product from the *Ambn3'-AmelX* border.

The amplification product was a 347 bp band at the border of the Ambn coding region and the amelogenin 3' end. The positive amplification reaction control was the plasmid construct. Amplification was performed at 94 ˚C for 30", 58 ˚C for 30", and 72 ˚C for 1', followed by incubation for 10 min at 72 ˚C. The reaction was amplified for 30 cycles and the PCR products were run on a 1.0 % agarose gel and visualized after staining with ethidium bromide.

Enamel phenotype

Starting with eruption of the incisors at day 10 in mice, the teeth were evaluated for abnormalities in color and shape. Photographic documentation was obtained of the incisors from adult mice. The tooth phenotype was rated as one of the five categories mild, mild-moderate, moderate, severe, very severe.

Ameloblastin transgene expression

To quantify the level of gene expression from the transgene, the transgene expression level in the enamel organ epithelium (EOE) was determined by real-time PCR. First and second molars of the mandible and maxilla from 5-day old mice were harvested on dry ice under the dissecting microscope. Teeth were stored at -80 ºC. The molars from one pup were pooled, homogenized using a mortar and pestle and RNA was extracted using the RNeasy kit (Qiagen) with removal of DNase (RNase-free DNase, Qiagen). For cDNA synthesis, mRNA was primed using OligoDT (Invitrogen), and the second strand was synthesized using SuperScript II reverse transcriptase (Invitrogen).

RNA was removed by RNase H (Invitrogen) and the cDNA was amplified using primers for *Ambn*^{Tg}, *Ambn*^{WT} and *AmelX*^{WT} (Tab. 5.4).

	Length	Tm	Primer sequence 5' ->3'
Ambn^{Tg}			
Probe	17	60	AAAGAACCATCAAGGGC
Left primer	26	60	CAGACAGAAACTCACTGAGCATACAC
Right primer	21	60	AACAGGATCAGGCCCTTCATT
Sense			AATGAAGGGCCTGATCCTGTT
Product size	76		
Ambn^{WT}			
Probe	17	60	TGTCAGCATCTAAGATT
Left primer	18	60	GGCCTGGGAGCACAGTGA
Right primer	19	60	AACAGGATCAGGCCCTTCATT
Sense			AATGAAGGGCCTGATCCTGTT
Product size	68		
AmelX^{WT}			
Probe	18	60	CAAAGAACCATCAAGAAA
Left primer	26	60	CAGACAGAAACTCACTGAGCATACAC
Right primer	19	60	GGCAGGCAAACAAAATCCA
Sense			TGGATTTTGTTTGCCTGCC
Product size	72		
GAPDH			
Probe			GAACGGATTTGGCCGTATTGGGCGC

Table 5.4: Primer and probe sequences for real-time PCR for Ambn^{Tg}, Ambn^{WT}, AmelX^{WT} and GAPDH.

Real-time PCR (7500 Real-time System, Applied Biosystems, Foster City, CA, USA) was performed using cDNA from *Ambn*^{Tg} positive and negative pups. Primers and probes for *Ambn*^{Tg}, *Ambn*^{WT} and *AmelX*^{WT} were manually designed (Tab. 5.4). The primer set for *Ambn*^{Tg} was designed at the *Amel-Ambn5'* border with the probe recognizing the introduced AscI site. The *Ambn*^{Tg} forward primer was used for the *AmelX*^{WT} primer set,

and the $Ambn^{Tg}$ reverse primer was used for $Ambn^{WT}$. For normalization of expression, mouse *GAPDH* was used (Mm99999915_g1, Taqman Gene Expression Assays, Applied Biosystems). The reactions were optimized for primer and probe concentrations used with PCR mix (TaqMan, Applied Biosystems). Each sample was applied in triplicates. Amplifications were performed at 95 ºC for 15 seconds and 60 ºC for 1 minute for 45 cycles. Relative quantities of $Ambn^{Tg}$, $Ambn^{WT}$ and $AmelX^{WT}$ were determined using the standard curve method (Livak, 1997).

Combining the data from the clinical inspection, the real-time PCR and ability to breed, four F1 animals from different founders were selected to establish stable lines to the rescue experiment.

Rescue of the enamel phenotype in the *Ambn* null mouse by introducing the ameloblastin transgene

Rescue of the enamel phenotype was accomplished by introducing the ameloblastin transgene into *Ambn* null mice by mating. The ameloblastin null-mouse was obtained from Dr. Yoshihiko Yamada at National Institutes of Health, NIDCR, transferred, and housed for breeding at the Dental ULAM facility, University of Michigan. The *Ambn* null mouse was generated by replacing exon 5 and 6 by the PGK promoter-neomycin resistance –polyA cassette (Fig. 5.4). The targeting vector was electroporated into R1 mouse embryonic stem cells with a 129/Sv background and then backcrossed with C57BL/6 mice for 10 generations (Fukumoto *et al.*, 2004).

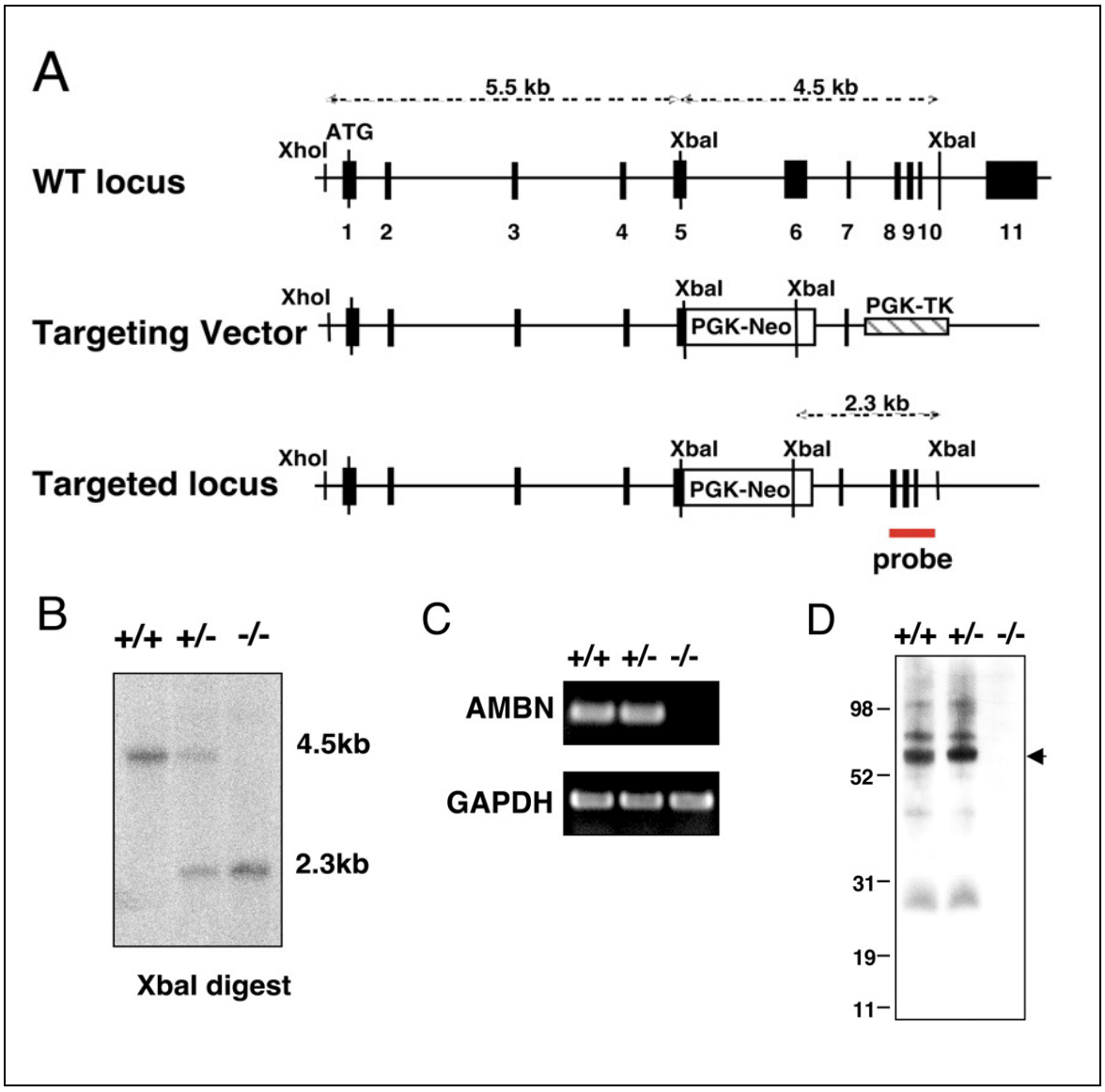

Figure 5.4: Generation of ameloblastin-null mice.
A) Structure of the *Ambn* gene, targeting vector, and targeted allele after homologous recombination. The location of the fragment used as a probe in Southern blotting and the sizes of the XbaI fragment detected for wild-type and targeted alleles. Exons are depicted as closed boxes. The PGK-neo and PGK-TK cassettes are depicted as open and oblique boxes.
B) Southern blot analysis of 6-wk-old mouse genomic DNA. Genomic DNA was isolated from tails, digested with XbaI and hybridized with the probe containing exons 8–10. The wild-type and mutant alleles were detected as 4.5- and 2.3-kb fragments, respectively.
C) RT-PCR analysis of *Ambn* mRNA expression in wild-type, heterozygous, and homozygous mice. 2 µg of total RNA isolated from P3 mouse molars were reverse transcribed and amplified with primers for *Ambn* and *GAPDH*.
D) Western blot analysis of ameloblastin in wild-type, heterozygous, and homozygous mice. Two P3 maxillary first molars were dissected and lysed with 100 µl of lysis buffer, and 20 µl were separated by SDS-PAGE and immunoblotted with polyclonal anti-ameloblastin antibodies. (Fukumoto *et al.*, 2004)

The *Ambn*$^{-/-}$ breeding colony was expanded for matings for the rescue experiment and genotyping was determined by PCR analysis of genomic DNA from tail biopsy (DNeasy Blood and Tissue Kit, Qiagen). Primer sets were designed recognizing intron 5 and the neomycin cassette introduced by the targeting vector (Tab. 5.5, Tab. 5.6).

	Length	**Tm**	**GC %**	**Primer sequence 5' ->3'**
Left primer	20	59.98	50.00	AGACAATCGGCTGCTCTGAT
Right primer	20	57.98	50.00	ATACTTTCTCGGCAGGAGCA
Sense				TGCTCCTGCCGAGAAAGTAT
Product size	261			

Table 5.5: Primers to amplify a product from the neomycin phosphotransferase cassette.

	Length	**Tm**	**GC %**	**Primer sequence 5' ->3'**
Left primer	20	59.94	50.00	GGAACCCTTTTAAGCCCAAG
Right primer	20	59.80	45.00	GAGGTTTGGAATTGGCACAT
Sense				ATGTGCCAATTCCAAACCTC
Product size	278			

Table 5.6: Primers to amplify a product from the *Ambn* intron 5.

The conditions for the PCR reaction of both primer sets was 94 ˚C 30 sec, 58 ˚C 30 sec, 72 ˚C 1 min for 30 cycles. The two primer sets were designed to distinguish heterozygous and homozygous *Ambn* mice. The primer set complementary to neomycin cassette served to detect *Ambn* null alleles. The second primer set indicated the absence of intron 5 in the homozygous *Ambn* animal.

The *Ambn*^{Tg} was introduced into *Ambn* null mice by mating (Fig. 5.5). Four *Ambn*^{Tg} animals were selected for breeding with *Ambn* null mice. Within 2 generations, *Ambn*^{Tg} should be bred into *Ambn* null mice in 25 % of offspring (Fig. 5.5).

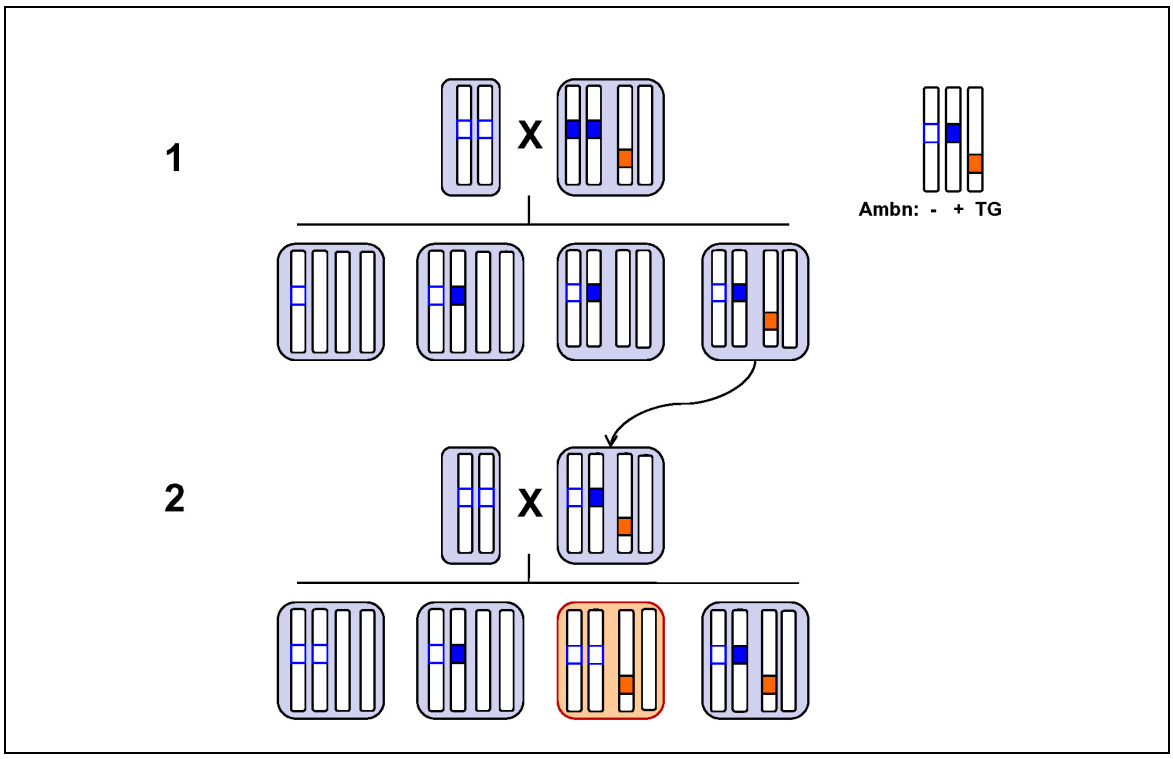

Figure 5.5: Mating of *Ambn* null with hemizygous transgenic *Ambn* mouse.
In mating 1 an $Ambn^{-/-}$ animal is crossed with an $Ambn^{Tg}$ animal. Offspring with the genotype $Ambn^{+/-Tg}$ are identified and crossed with $Ambn^{-/-}$ (mating 2). Statistically 25 % of the litter is $Ambn^{-/-Tg}$. Controls are littermate *Ambn* null mouse and wild-type mice from a different litter.

General characterization of mice

Genotype of offspring was identified by PCR using tail DNA. Littermates were evaluated for their appearance, physical activity, body size, rate of growth, food intake and reproducibility. Age-matched, non-transgenic animals from the same breeding stock were taken as controls. The tooth phenotype of adult mice was documented by photographs.

Scanning electron microscopy evaluation of enamel

Teeth from two- week old *Ambn*$^{-/-}$, *Ambn*$^{+/-Tg}$, *Ambn*$^{-/-}$, *Ambn*$^{+/-}$ and wild-type mice were characterized by scanning electron microscopy (SEM) to evaluate overall tooth morphology, enamel thickness, enamel surface characteristics such as enamel pitting or chipping, prism structures to look for structural abnormalities, and crystal organization into rods and interrods. Erupted incisor and unerupted molar teeth were ethanol dehydrated and dried overnight. Samples were mounted on stubs using conductive carbon cement before examined in whole or transversely fractured. Samples were sputter coated with an Au-Pd film and examined in an Amray EF 1910 scanning electron microscope at 5 kV.

Future characterization of enamel

The developing teeth (day 4) of mice will be histologically evaluated in sections stained with von Kossa staining for calcium phosphate in mineral deposits. Paraffin sections will be deparaffinized and hydrated to water. Sections will be incubated in 1 % silver nitrate solution and exposed to UV light. Unreacted silver will be removed with 5 % sodium thiosulfate. After rinsing in water the sections will be dehydrated in alcohol and xylene.

For high-resolution cross-sectional images and 3-D reconstruction, unsectioned teeth (day 16-18) will be analyzed by micro-computer tomography (microCT, GE Healthcare Biosciences, London, Ontario) for detection of enamel mineral content. Hemimandibles will be exposed to polychromatic x-rays while rotating. X-rays passing through the sample will be intensified and captured by a camera. Individual 2-D slices of

18 μm thickness will be generated for 3-D reconstruction. The equipment will be calibrated with materials of known densities prior to use.

RESULTS

An *in vivo* system was developed to study Ambn function in the context of the enamel organ and its environment. This system consisted of an *AmelX* promoter of 4.6 kb, the *Ambn* coding region and the *AmelX3'UTR* (1.1 kb). Previously, the *AmelX* 2.3 kb promoter was shown to target secretory stage ameloblasts (Snead *et al.*, 1996; Snead *et al.*, 1998). This system was tested by using the full-length *Ambn* coding region to be expressed in the *Ambn* null background. First, $Ambn^{Tg}$ mice were generated, screened for expression levels in the EOE and then bred with *Ambn* null mice. To evaluate the rescue of the enamel phenotype, SEM analysis was performed.

Generation of Ameloblastin transgenic mice

Mice overexpressing Ambn were generated by random integration into the host genome. The ameloblastin gene was expressed from a 5' amelogenin promoter (4.6 kb) and expression was terminated from an amelogenin 3'UTR. To demonstrate germline transmission of the transgene, $Ambn^{Tg}$ transmission was evaluated in offspring from crossings with wild-type C57BL/6 mice. Of the 119 independent lines, 17 mice (10 female, 7 male) were identified by PCR as transgene positive founders harboring the construct. At the age of 3 weeks, the pups were weaned and transferred to the animal room of the School of Dentistry. Of the 17 founder mice, 13 transmitted the transgene

within 2 - 4 litters (Tab. 5.7). The transgene was identified in the offspring by genotyping using unique primer sets at the *Amel-5'Ambn* and *Ambn-3'Amel* borders (Fig. 5.3, Fig. 5.6). Results from both primer sets displayed consistency.

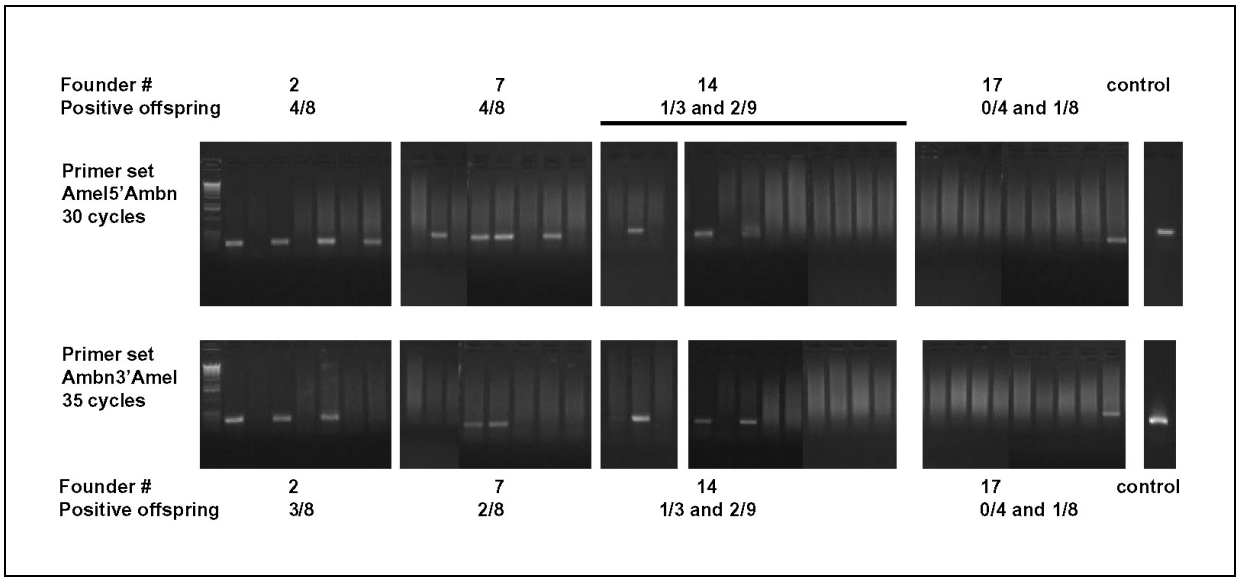

Figure 5.6: PCR genotyping using primer sets at the *AmelX-5'Ambn* and *Ambn3'-AmelX* borders.
Genotyping was performed on tail DNA from litters of founder #2, 7, 14 and 17. Founders differ in transmission of the $Ambn^{Tg}$ allele.

Gross tooth morphology and appearance

Photographic evaluation of adult founder mice revealed differences in tooth color. The majority of founder mice display loss of translucency in incisor enamel with varying degrees of intensity. The loss of translucency was most severe at the incisal edge and expanded towards the cervical region depending on the severity. In 2 founders in addition to the mandibular incisor, the maxillary incisors were affected (founders #13, 15).

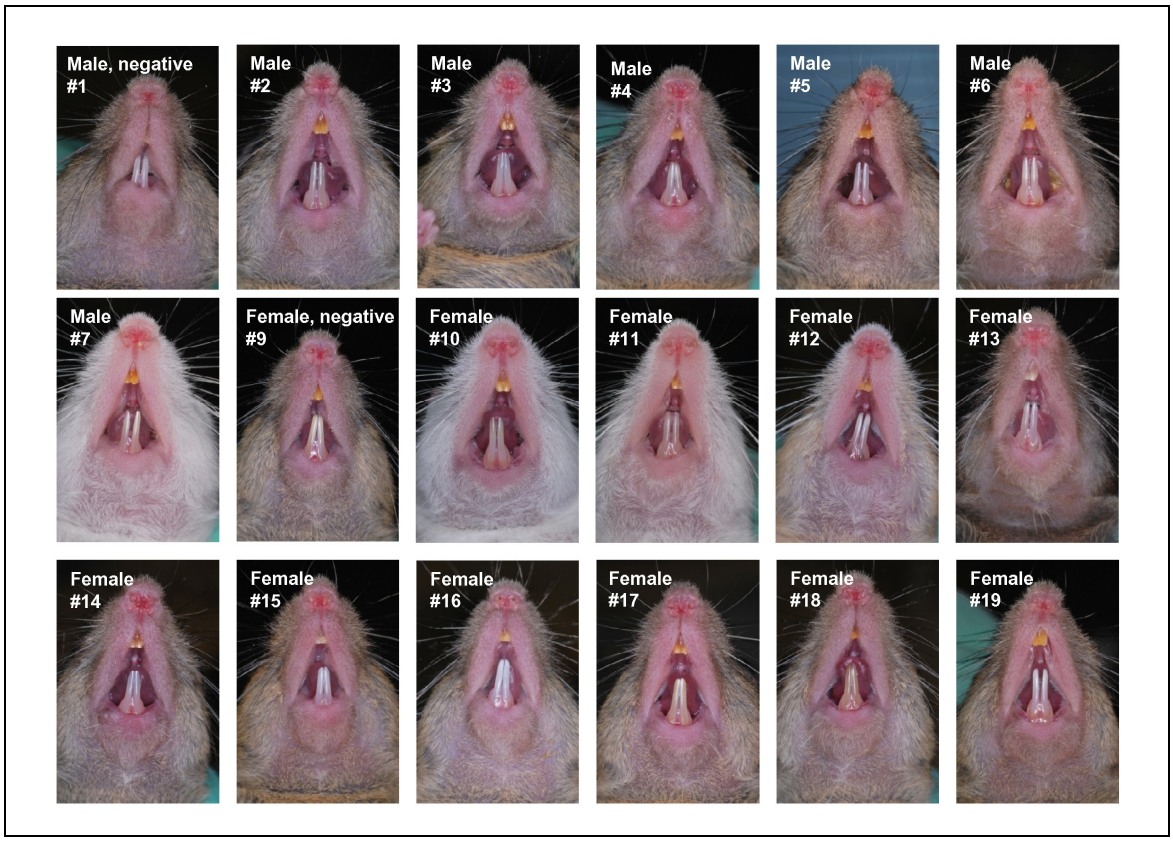

Figure 5.7: Overview of the tooth phenotype in adult *Ambn*^{Tg} founder mice.
The founders were composed of 7 males and 10 females. One of the males had to be sacrificed due to severe dermatitis (#8). Male #1 and female #10 served as *Ambn*^{Tg} negative controls. Founder mice differed in the severity of enamel phenotype.

Transmission of ameloblastin transgene

All 17 ameloblastin Tg founders were mated with wild-type C57BL/6 mice. 13 founders transmitted the transgene to offspring. Litters were either collected for real-time PCR or saved for matings for rescuing the *Ambn* null phenotype. Offspring of founders #2, 3, 4, 7, 10, 11, 12, 13, 14, 15, 16, 17, and 18 were positive for the *Ambn* transgene (Tab. 5.7). As the degree of positive germline cells varied, the number of positive pups per litter varied and the overall percentage of transmission ranged from 8.0 to 45.4 % in founder 18 and 3 (Tab. 5.7, Fig. 5.7). Founders #5, 6, 8, and 19 did not produce transgene

positive pups from at least 3 litters. Founder #8 developed severe dermatitis and had to be terminated. Founders #1 and 9 were negative for the *Ambn* transgene.

Founder	Gender	Litters	Total pups	Tg Day-5 Teeth	Tg Founder Offspring	Tg Transmission %
1	Male					Neg. control
2	Male	4	8+6+6+10	5	3 F, 3 M	36.6
3	Male	4	0+9+8+5	6	2 F, 2 M	45.4
4	Male	4	4+8+12+11	0	2 F, 1 M	8.6
5	Male	4	7+9+10+8	0	0	0
6	Male	5	1+3+11+11+7	0	0	0
7	Male	3	8+8+9	6	2 F	32.0
8	Male	4	8+5+10+10	0	0	0
9	Female					Neg. control
10	Female	2	1+10	0	2 F, 2 M	36.4
11	Female	4	3+11+5+11	8	2 F, 1 M	36.6
12	Female	3	9+12+11	2	2 F, 2 M	18.7
13	Female	3	10+9+7	4	2 F	23.0
14	Female	4	9+9+10+10	6	2 F, 6 M	36.8
15	Female	2	4+1	0	1 F	20.0
16	Female	4	7+4+3+10	5	1 F	25.0
17	Female	3	5+9+10	3	3 M	25.0
18	Female	3	7+10+8	0	1 F, 1 M	8.0
19	Female	3	7+6+4	0	0	0

Table 5.7: Overview of *Ambn*^{Tg} founders and transmission rate of the *Ambn* transgene.
The ability to produce litter varies in founder from 2-5 litter. The transmission of *Ambn*^{Tg} ranged from 8.6 % (founder #18) to 45.4 % (founder #3).

Expression level of *Ambn^{Tg}*

The expression level of the transgene depends on the promoter, integration site and copy number. The ameloblastin transgene expression was quantitated by real-time PCR using mRNA from secretory stage EOE littermates (day 5). The goal was to determine the range of Ambn expression levels in the *Ambn^{Tg}* founder offspring and to select an expression range that would be similar to physiological Ambn as being most appropriate for recovering the enamel phenotype in Ambn null mice. Expressions of Ambn^{Tg}, Ambn^{WT} and AmelX^{WT} were determined in EOE. Teeth from founder offspring #2, 3, 7, 14, 16, and 17 were selected for real-time PCR based on the availability of day 5 EOE. Gene expression was normalized to GAPDH and compared among littermates to wild-type genotype. The Ambn transgene expression was related to Ambn^{WT} expression and showed a wide range of expression between different founders and within littermates (Fig. 5.9 A). Transgene positive offspring of founder #7 had the highest Ambn^{Tg}/Ambn^{WT} expression with 4.97 and a standard deviation of 2.34. Offspring of founder #17 had the second highest expression with 4.56 and a standard deviation of 1.93. Offspring of founder 2 had Ambn^{Tg}/Ambn^{WT} expression of 2.84. Offspring from founders #14, 16 and 3 had Ambn^{Tg}/Ambn^{WT} expression below 1.

In *Ambn^{Tg}* animals, the Ambn^{WT} gene expression reflects the combined expression from Ambn^{Tg} and Ambn^{WT}. Ambn^{WT} expression was slightly increased in founder offspring #2, 14, 15 with a maximal expression of 1.4 compared to a wild-type littermate (Fig. 5.9 B). Amelogenin is found in enamel matrix with the highest abundance and served as a control. In *Ambn^{Tg}* animals AmelX expression was slightly decreased with up to 0.4 relative to wild-type animals.

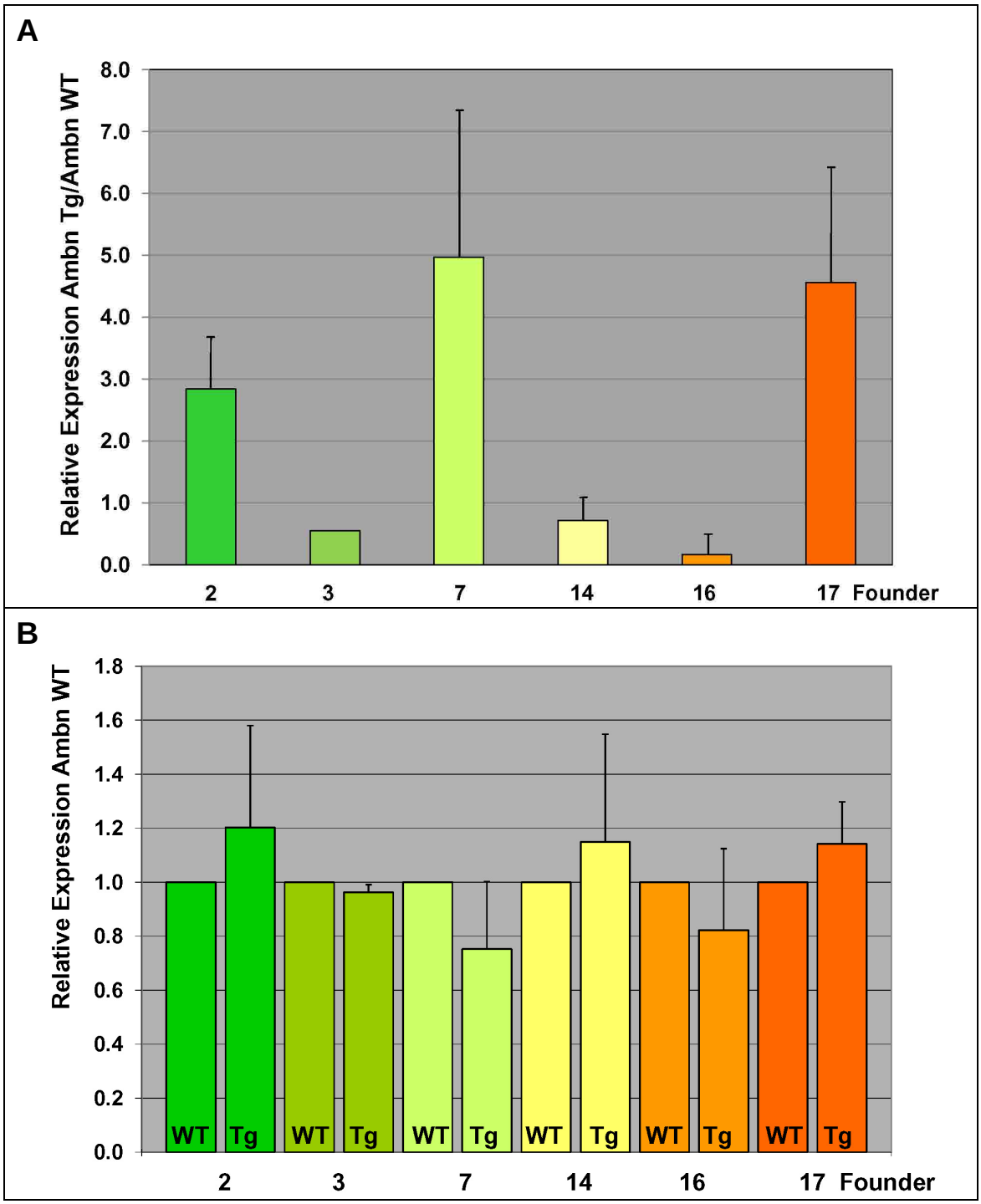

Figure 5.8: Gene expression of Ambn^{TG}, Ambn^{WT} and Amel^{WT} in dental tissues of founder offspring determined by real-time PCR.
Relative expression in Ambn transgenic (Tg) and Ambn wild-type (WT) litter mates from founders #2, 3, 7, 14, 16, 17. Each bars represent wild-type (n=1) or Ambn transgenic (n=2) animals.
A) The *Ambn*^{Tg} expression was related to the *Ambn*^{WT} expression in *Ambn*^{Tg} animals. Offspring of founders #2, 7, 17 had higher expression of *Ambn*^{Tg} relative to *Ambn*^{WT}.
B) *Ambn*^{WT} expression is composed of endogenous and transgene expression.

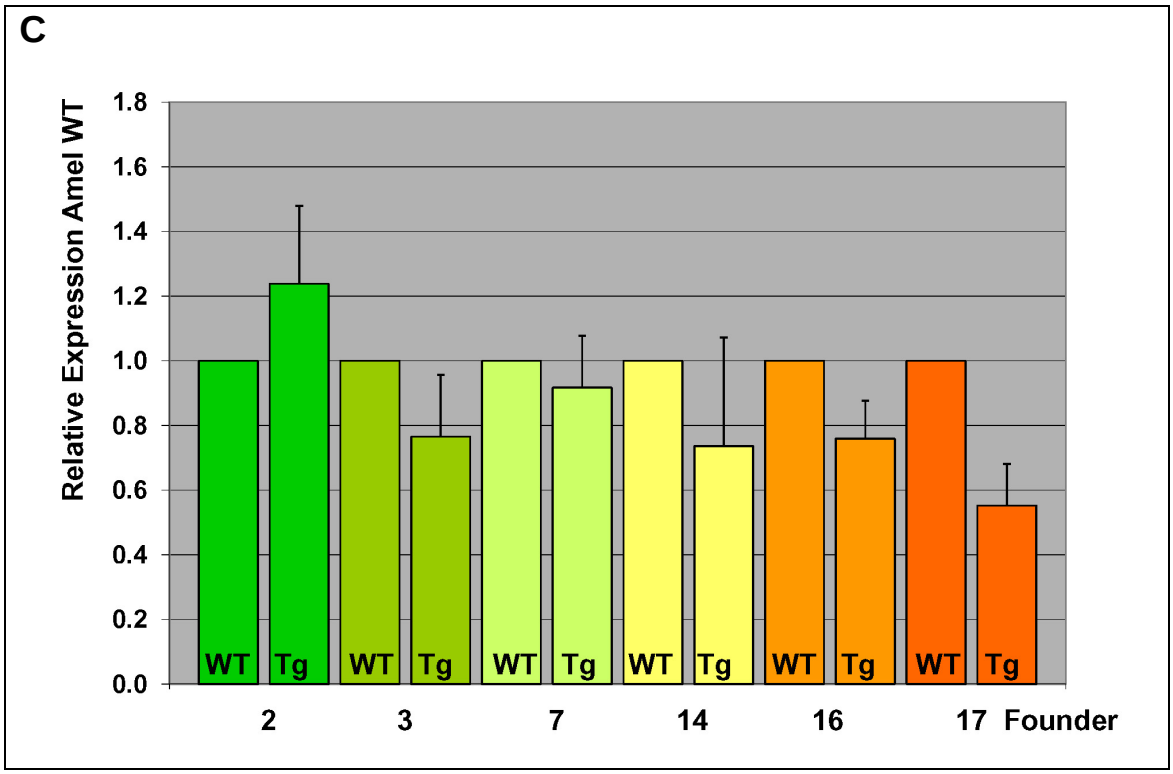

Figure 5.8: Gene expression of Ambn^{TG}, Ambn^{WT} and Amel^{WT} in dental tissues of founder offspring determined by real-time PCR.
Relative expression in Ambn transgenic (Tg) and Ambn wild-type (WT) litter mates from founders #2, 3, 7, 14, 16, 17. Each bars represent wild-type (n=1) or Ambn transgenic (n=2) animals.
C) *Amel*^{WT} endogenous expression. In *Ambn*^{Tg} mice the *Amel*^{WT} expression is lower compared to WT animals.

Selection of founder lines for rescue experiment

Data from real-time PCR, incisor phenotype was used to select founder lines for crossings with *Ambn* null mice (Tab. 5.8). Variation in gene expression and tooth phenotype were observed among offspring from the same founder (Fig. 5.11, Ambn^{Tg} 2-81, 2-115, 2-119, 2-118). Multiple chromosomal integration sites could account for these differences. Gene expression data was available for founder lines 2, 3, 14, 7, 14, 16, and 17. Transgenic offspring 3-40, 14-83, 17-113 demonstrated most severe loss of

translucency. From the combination of gene expression, tooth phenotype evaluation and breeding ability, transgenic offspring #2-118, 3-40, 14-83, and 17-113 (Tab. 5.8, Fig. 5.9) were selected for matings with Ambn null animals aiming for rescue of the Ambn null tooth phenotype.

F1	Gender	DOB	Real time PCR -founder	Loss of translucency of Teeth
2-116	Male	9-19-08	2.85 times $Ambn^{TG}/Ambn^{WT}$	Moderate
2-118	Male	9-19-08	2.85 times $Ambn^{TG}/Ambn^{WT}$	Moderate
2-121	Male	9-19-08	2.85 times $Ambn^{TG}/Ambn^{WT}$	Mild-moderate
3-40	Male	8-18-08	0.55 times $Ambn^{TG}/Ambn^{WT}$	Severe
4-67	Female	9-10-08		Moderate
4-89	Female	9-10-08		Moderate
7-97	Female	9-10-08	4.97 times $Ambn^{TG}/Ambn^{WT}$	Mild
8-186	Male	10-11-08		Mild-moderate
11-133	Female	10-7-08		Moderate
11-210	Female	11-28-08		Moderate
14-83	Female	9-7-08	0.71 times $Ambn^{TG}/Ambn^{WT}$	Very severe, upper + lower teeth
14-85	Male	9-7-08	0.71 times $Ambn^{TG}/Ambn^{WT}$	Mild
15-123	Female	9-27-08		Moderate
16-62	Female	8-20-08	0.16 times $Ambn^{TG}/Ambn^{WT}$	Moderate
17-113	Male	9-15-08	4.56 times $Ambn^{TG}/Ambn^{WT}$	Severe
18-172	Male	10-11-08		Moderate

Table 5.8: Summary of gene expression and tooth phenotype of transgene positive offspring.
The mice highlighted in red were selected for establishing stable *$Ambn^{-/-}Tg$* lines.

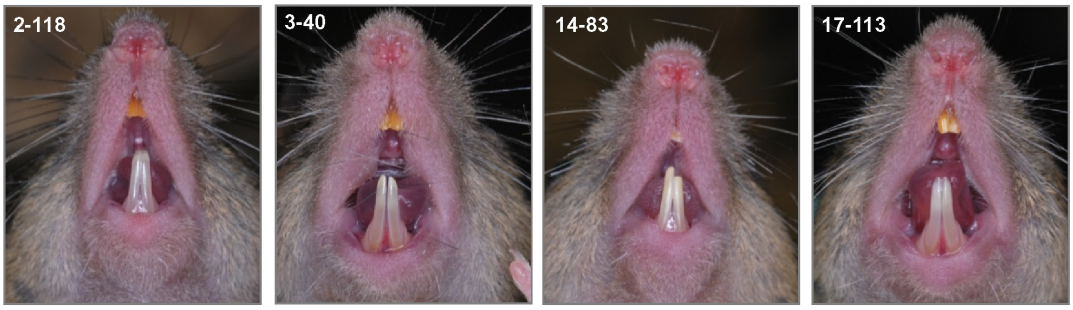

Figure 5.9: *Ambn* transgenic founder offspring selected for rescue experiment.
Founder offspring #2-118, 3-40, 14-83 and 17-113 were selected for generation of stable mouse lines *Ambn*$^{-/-Tg}$. All differed in the appearance of the enamel phenotype.

Breeding of stable mouse lines

To create stable *Ambn*$^{-/-Tg}$ mice mouse lines #2-118, 3-40, 14-83, and 17-113 were mated with *Ambn* null mice (Fig. 5.10). Line #2-118 had advanced furthest in matings with *Ambn* null mice. After two matings with *Ambn* null mice, 2 litters with the genotypes *Ambn*$^{+/-Tg}$, *Ambn*$^{+/-}$, and *Ambn*$^{-/}$ were produced.

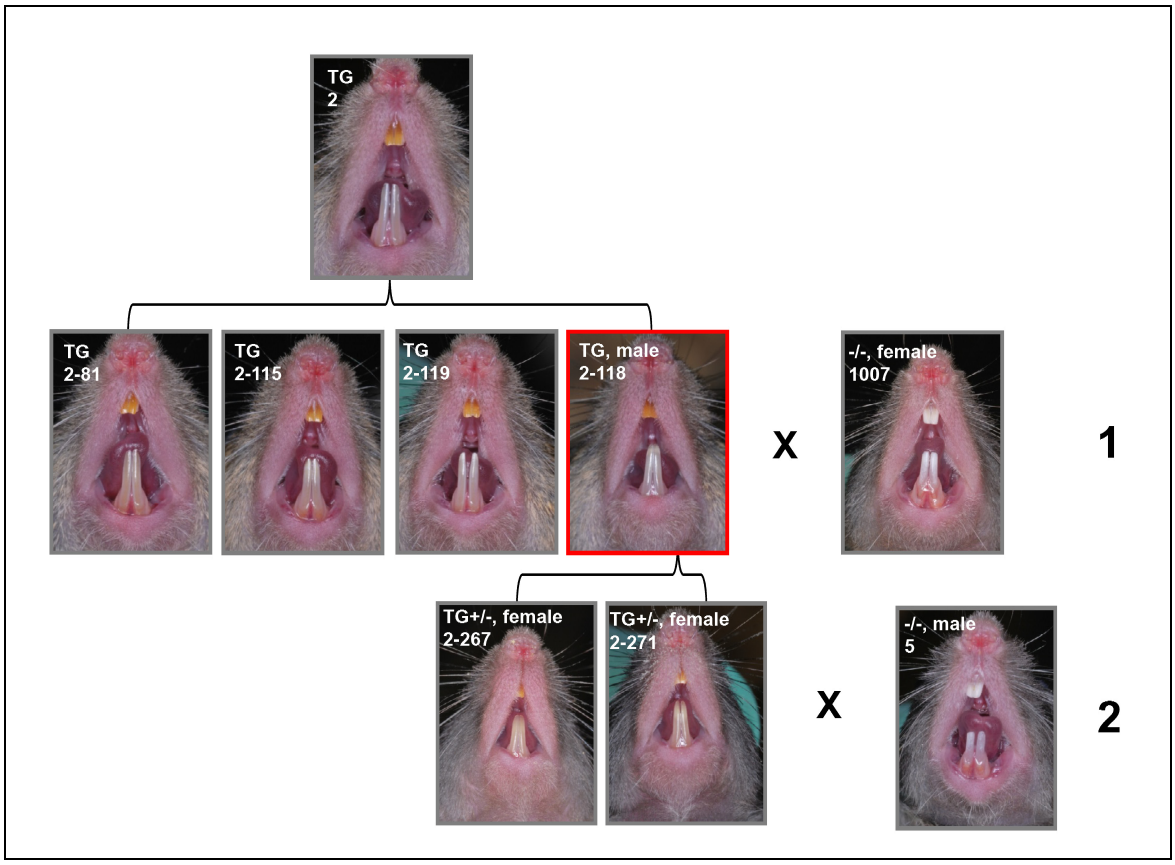

Figure 5.10: *Ambn* transgenic line derived from founder #2 crossed with *Ambn* null mouse. *Ambn* transgene positive offspring from founder 2 from matings with wild-type mice. *Ambn* transgenic mouse 2-118 was selected for matings with *Ambn* null mouse (1). $Ambn^{+/-Tg}$ were mated with $Ambn^{-/-}$ animals (2).

Enamel characterization by SEM

Preliminary SEM analysis in one litter was performed at 2 weeks postnatally to characterize early enamel mineralization. Erupted incisors were analyzed at magnifications ranging from 250 to 10,000 x. Enamel of $Ambn^{+/+}$ animals exhibited normal thickness and regular prism organization (Fig. 5.11 A: a, e, i, m). The crystallites in the rod were fused and fractured evenly (Fig. 5.11 A: m). In $Ambn^{-/-}$ animals the enamel thickness was greatly reduced and the dentin was covered by a thin layer of prismless material creating a rough outer surface (Fig. 5.11 A: d, h). This layer did not

exhibit recognizable crystallites or organization of prisms. Deeper layers displayed inclusion of voids with possibly initial crystal formation (Fig. 5.11 A: l, p; B: d, h). *Ambn*$^{+/-}$ animals had an enamel layer that easily fractured off during sample processing (Fig. 5.11 A: c). Rod-interrod organization was present, but was progressively ill defined in the outer enamel (Fig. 5.11 A: g; B: c, g). The rod crystallites seemed to lack fusion with each other and sheared off diagonally during fracture (Fig. 5.11 A: k, o). The enamel appeared to separate from the underlying dentin at the DEJ (Fig. 5.11 B: k) most likely due to sample manipulation. The *Ambn*$^{+/-Tg}$ animals demonstrated rescue of enamel thickness and organization compared to *Ambn*$^{-/-}$ animals (Fig. 5.11 A: b, f, j, m). At higher magnification, the prism pattern seemed to be similar to the wild-type enamel. The spacing between parallel rods may be greater than in the wild-type (Fig. 5.11 A: i, j, m, n). The crystallites within one rod seem to be less fused, and fractured in a tapered pattern. Outer crystallites fractured earlier than center crystallites leaving rods with a tapered appearance (Fig. 5.11A: i, m).

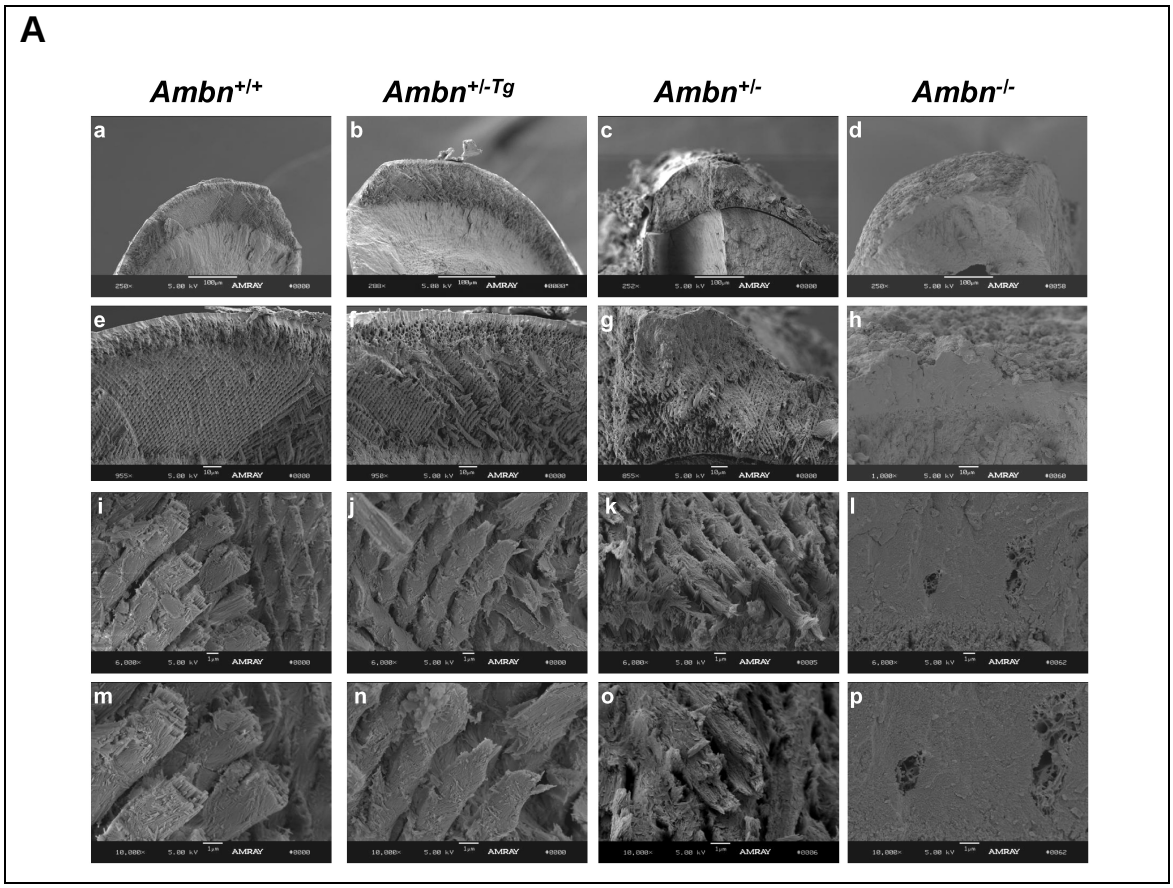

Figure 5.11: SEM images of enamel cross-sections of incisors from *Ambn*$^{+/+}$, *Ambn*$^{+/-Tg}$, *Ambn*$^{+/-}$, *Ambn*$^{-/-}$ animals on day 5.

A) Overview of enamel thickness and rod organization. Images a, e, i, m are from *Ambn*$^{+/+}$ animals; b, f, j, n from *Ambn*$^{+/-Tg}$ animals; c, g, k, o from *Ambn*$^{+/-}$ and d, h, l, p from *Ambn*$^{-/-}$ animals. Cross-sections in images a, b, c, d provide overview of the enamel and dentin layers at 250 x. Images e, f, g, h show the thickness of the enamel layer at 950 x. Images i, j, k, l demonstrate the rod-interrod pattern at 6000 x. Images m, n, o, p at 10,000 x display the crystallites within the rod.

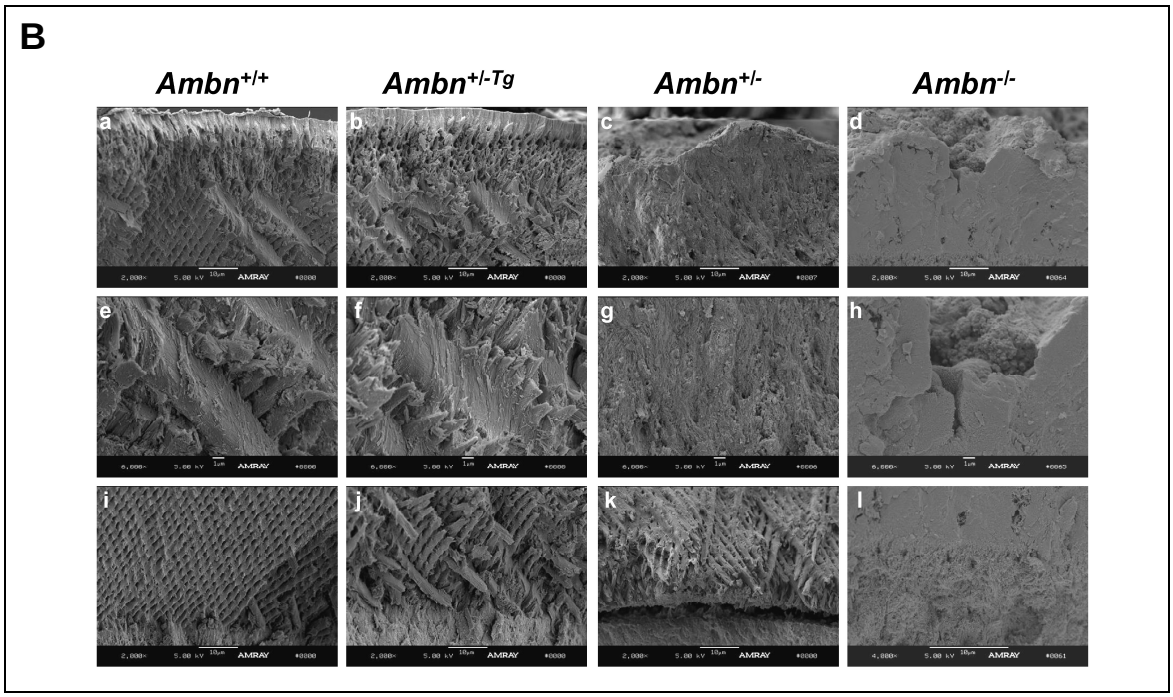

Figure 5.11: SEM images of enamel cross-sections of incisors from *Ambn*$^{+/+}$, *Ambn*$^{+-/Tg}$, *Ambn*$^{+/-}$, *Ambn*$^{-/-}$ animals on day 5.
B) Outer enamel organization and dentino-enamel junction. Images a, e, i are from *Ambn*$^{+/+}$ animals; b, f, j from *Ambn*$^{+/-Tg}$ animals; c, g, k from *Ambn*$^{+/-}$ and d, h, l from *Ambn*$^{-/-}$ animals. In images a, b, c, d the outer enamel layer is displayed at 2000 x and in e, f, g, h at 6000 x. In images I, j, k, l the DEJ is displayed at 2000 x.

DISCUSSION

Ameloblastin expression is restricted to dental tissues, where its onset in ameloblasts is slightly earlier than amelogenin (Torres-Quintana et al., 2005). *Ambn* is also transiently expressed in pre-odontoblasts prior to the differentiation of ameloblasts (Begue-Kirn et al., 1998; Fong et al., 1998). Outside of enamel, Ambn has been located at the cemento-enamel junction (Bosshardt and Nanci, 1998) along the root in Hertwig's epithelial root sheath (Fong *et al.*, 1996; Fong and Hammarstrom, 2000).

The *Ambn* null-mouse shows that Ambn is critical for enamel formation (Fukumoto *et al.*, 2004). Since *in vitro* experiments are not appropriate to recreate the

physiological situation during enamel formation, an established *in vivo* model was required to study Ambn function. For this purpose, mice overexpressing Ambn from the mouse 4.6 kb AmelX promoter were generated and crossed with Ambn null mice.

The mouse amelogenin promoter (2.3 kb) has the capacity to target gene expression specifically in ameloblasts during the secretory stage (Snead *et al.*, 1996; Snead *et al.*, 1998). Analysis of the mouse *AmelX* promoter region identified binding sites for transactivators: at -70/+52 a binding site for CCAAT/enhancer-binding protein (C/EBP), and at -58/-54 a reversed CCAAT box for binding of nuclear factor Y (NF-Y) (Xu *et al.*, 2006; Zhou and Snead, 2000). In contrast, *AmelX* promoter activity is repressed by Msx2 through protein-protein interactions with C/EBP alpha (Xu *et al.*, 2007; Zhou *et al.*, 2000). Other consensus sequences for transcription factor binding in the *AmelX* promoter were reported between 1 kb and 3.5 kb upstream for AP1, RXRβ, and glucocorticoid receptor binding (Gibson *et al.*, 1997).

The mouse *AmelX* 2.3 kb promoter has been used to overexpress enamel genes in secretory stage ameloblasts in mice (Snead *et al.*, 1996; Snead *et al.*, 1998). When Ambn, tyrosine-rich amelogenin peptide (TRAP), or biglycan were overexpressed from this promoter, the overall phenotype in enamel has been rather subtle with abnormalities in prism structure evident at SEM level only in the Ambn overexpressing mouse (Paine *et al.*, 2003; Paine *et al.*, 2004; Wen *et al.*, 2008).

When a larger bovine *AmelX* promoter region of 5.5 kb was used to overexpress bovine leucine-rich amelogenin peptide (LRAP) or the most abundant mouse amelogenin (M180), the enamel had normal prism-interrod structure (Chen *et al.*, 2003; Gibson *et al.*, 2007). The bovine LRAP overexpressing mouse displayed opaque and pitted enamel

(Chen *et al.*, 2003). The 5.5 kb promoter region contains the bovine signal peptide and intron 1. The 3' untranslated region of *AmelX* was used to terminate transcription (Chen *et al.*, 2003). Although the *AmelX* promoter and coding sequences are highly homologous to about 90 %, it is not clear if these differences could affect the outcome.

To overexpress mouse Ambn in our study, a 4.6 kb upstream genomic *AmelX* sequence from mouse was used. By using a promoter region twice the size as previously used (Snead *et al.*, 1996), we intended to include potential far upstream regulatory elements. For the expression of Ambn in our study, elements from the amelogenin genomic sequence were used. The 5' region contained the *AmelX* promoter, signal peptide and intron 1. The 3' untranslated region of *AmelX* was used to terminate transcription. The 5' region of the 4.6 kb promoter used in our study might contain important DNA regulatory elements that are possibly missing in the 2.3 kb promoter and that are recognized by co-activators to initiate expression. However, *AmelX* is the most highly expressed enamel protein, with 85-90 %. Using its promoter to overexpress Ambn, we expected to find comparably high gene expression. Instead real-time RT-PCR of mRNA from the EOE from 6 founder offspring showed that gene expression of the Ambn Tg was very low. This low expression can be explained by enhancers beyond 4.6 kb on translation initiation. Further, the *AmelX* gene could contain enhancer elements that are located at intronic sites that are absent from the Ambn cDNA (although intron 1 of the amelogenin gene was included). The post-transcriptional control regulating mRNA stability and rate of translation could be altered during Ambn transgene expression.

Real-time PCR confirmed that $Ambn^{Tg}$ was expressed. The variation of the $Ambn^{Tg}$ expression level between animals can be explained by the segregation of

different, multiple chromosomal integration sites. Once the Ambn Tg is germline, its expression level is expected to be stable, if there is a single integration site. The Ambn WT expression in transgenic animals reflects the WT and Tg expression of Ambn. Compared to wild-type littermates, Ambn WT expression in transgenic animals was not very different. Overall, the Ambn Tg expression was low, but comparable to wild-type levels (Ambn accounts for 3-5 % of amelogenin expression), and sufficient to at least partially recover the normal enamel phenotype. The slight down regulation of Amel wild-type expression might relate to feedback control mechanisms regulating total Amel output. The integration of the *AmelX* promoter may be recognized by internal control mechanisms.

Besides different purposes in creating an Ambn overexpressing/transgenic mouse, our Ambn transgene expression construct was designed very differently from previous studies (Paine *et al.*, 2003). These differences may explain differences in phenotype. The Ambn overexpressing mouse was designed to study the effect of a high dose of Ambn on enamel formation. For this particular construct, the selection of the mouse DSPP signal peptide, the DSPP 3' untranslated region, and the inclusion of multiple VSV-G and c-Myc epitopes were primarily based on ease of construction from available plasmids and relevance to other ongoing transgenic studies (Paine *et al.*, 2003). At the SEM level, the enamel was porous and the rod – interrod organization was disrupted. Some crystallites were thicker in diameter and much shorter in length. As rat Ambn is highly homologous to mouse Ambn (96.7 %) (Simmons *et al.*, 1998), differences could be due to construct design.

Physiological enamel formation relies on appropriate doses of enamel proteins. Ameloblastin and enamelin are much less abundant than amelogenin, but each is essential for enamel formation as null mice exhibit severe hypoplastic amelogenesis imperfecta (Fukumoto *et al.*, 2004; Hu *et al.*, 2008). For Ambn no human AI-causing mutations are reported so far. But enamel phenotypes in enamelin human mutations are very heterogenous in terms of severity and extent of amelogenesis imperfecta, and the mode of inheritance (Hu and Yamakoshi, 2003). Generalized hypoplastic AI correlates to dominant inheritance and splice donor or acceptor mutations introducing a stop codon and elimination through nonsense-mediated decay (Kida *et al.*, 2002; Kim *et al.*, 2005; Rajpar *et al.*, 2001). Local hypoplastic AI is inherited as a dominant trait and is caused by haploinsufficiency, dominant-negative effects, or lack of C-terminal cleavage products (Hart *et al.*, 2003; Mardh *et al.*, 2002; Ozdemir *et al.*, 2005). Similarly, the appropriate dose of Ambn could be critical. Excess or deficiency of Ambn could result in disruption of regular enamel.

The evaluation of Ambn gene expression was important for finding the correct dose of Ambn for rescuing the Ambn null phenotype. Real-time PCR of 6 founder offspring displayed variation between littermates possibly due to multiple chromosomal integration sites or mosaic founders. Tg transmission to 30 % or less is a hint for mosaic germ cells due to late Tg integration during embryogenesis. The gene expression was combined with the enamel phenotype to determine transgenic lines for subsequent crossings. Instead of founders, their offspring with the transgene in germline was used to provide stable transmission of transgene quantity. Overall, the expression level of Ambn from the introduced *AmelX* promoter is significantly less than expression of amelogenin

from the endogenous *AmelX* promoter, which produces Amel at a level equaling 90 % of all enamel proteins. However, the quantity of the Ambn transgene may be sufficient to substitute Ambn expression, which accounts for only about 5 % of enamel proteins. The mechanism of this regulation is unknown but indicates that the *AmelX* promoter is very responsive for controlling the absolute amount of Amel. Similarly, in the Ambn null mouse *AmelX* gene and protein expression were significantly decreased (Fukumoto *et al.*, 2004; Fukumoto *et al.*, 2005). As other enamel proteins were not affected, it has been speculated that Amel is specifically regulated by Ambn through cell adhesion, inhibition of cell cycle and inhibition of Msx2 (Fukumoto *et al.*, 2004; Fukumoto *et al.*, 2005). However, this hypothesis is challenged as cell-binding motifs for integrin and thrombospondin DGEA and VYKG are only present in rodent Ambn and are not conserved throughout mammals. Therefore, mechanisms of Amel regulation are presently unknown and require more in depth investigations of the promoter and its regulation.

The Ambn null mouse was generated by targeting the XbaI site in exon 5 and EcoRI in intron 6 of the *Ambn* gene and replacing with region with a PGK-neo cassette (Fukumoto *et al.*, 2004). In Ambn all exon-intron borders are in 0 phase, thus by targeting exon 5 and 6, Tyr^{57} through Glu^{158} are spliced from the 381 amino acid protein, leaving a protein from Met^{1} to Gln^{56} and Val^{159} to Pro^{397}. The mutant protein has 295 residues, including the signal peptide and could be secreted as a 279-residue protein with a calculated molecular weight of 29.7 kDa. cDNA analysis of Ambn from $Ambn^{-/-}$ enamel organ mRNA demonstrated that *Ambn* mRNA is produced in these animals missing exon 5 and 6 (Wazen *et al.*, 2009). $Ambn^{-/-}$ animals could be secreting a truncated protein and

might not be completely null for Ambn. However, they are functionally null since the enamel layer is completely disrupted.

In vivo function of enamel proteins has been studied by supplying protein from transgenes in null mice. For *AmelX* the null phenotype was partially recovered with the most abundant amelogenin isoform (M180) in mice (Li *et al.*, 2008). The enamel layer gained in thickness and volume but not to the full thickness of wild-type enamel. Since the TG M180 expression level or the number of TG lines bred with *Amel* null mice have not been mentioned, the TG M180 expression level of the mouse line used for the rescue experiment could have been low. Alternatively spliced isoforms of *Amel* could also contribute to the final thickness of enamel. In contrast, LRAP was not able to substitute the enamel of Amel KO/TG LRAP and remained similar to Amel KO enamel (Chen *et al.*, 2003; Gibson *et al.*, 2009). Therefore, for full recovery of Amel null phenotype different Amel isoforms may be required.

Preliminary results from our study of Ambn function indicate recovery of enamel thickness in $Ambn^{+/-Tg}$ animals. The enamel rod organization has wider spaces between rods compared to wild-type and crystallites are less fused. As the $Ambn^{+/-}$ animals display an enamel phenotype at 2 weeks, Ambn dose is critical. The reduced dose of Ambn in outer enamel results in failure of formation of prisms. To investigate further the effect of the Ambn dose, $Ambn^{-/-Tg}$ animals need to be generated and analyzed during early and late maturation of enamel.

If the enamel phenotype in $Ambn^{-/-}$ is recovered in $Ambn^{-/-Tg}$ animals, this approach will allow asking questions about the function of specific Ambn cleavage products or point mutations at cleavage sites on enamel mineralization at the level of an animal model.

REFERENCES

Begue-Kirn C, Krebsbach PH, Bartlett JD, Butler WT (1998). Dentin sialoprotein, dentin phosphoprotein, enamelysin and ameloblastin: tooth-specific molecules that are distinctively expressed during murine dental differentiation. *Eur J Oral Sci* 106:963-970.

Bosshardt DD, Nanci A (1998). Immunolocalization of epithelial and mesenchymal matrix constituents in association with inner enamel epithelial cells. *J Histochem Cytochem* 46:135-142.

Chen E, Yuan ZA, Wright JT, Hong SP, Li Y, Collier PM, Hall B, D'Angelo M, Decker S, Piddington R, Abrams WR, Kulkarni AB, Gibson CW (2003). The small bovine amelogenin LRAP fails to rescue the amelogenin null phenotype. *Calcif Tissue Int* 73:487-495.

Fong CD, Slaby I, Hammarstrom L (1996). Amelin: an enamel-related protein, transcribed in the cells of epithelial root sheath. *J Bone Miner Res* 11:892-898.

Fong CD, Cerny R, Hammarstrom L, Slaby I (1998). Sequential expression of an amelin gene in mesenchymal and epithelial cells during odontogenesis in rats. *Eur J Oral Sci* 106 (Suppl 1) 324-330.

Fong CD, Hammarstrom L (2000). Expression of amelin and amelogenin in epithelial root sheath remnants of fully formed rat molars. *Oral Surg Oral Med Oral Pathol Oral Radiol Endod* 90:218-223.

Fukumoto S, Kiba T, Hall B, Iehara N, Nakamura T, Longenecker G, Krebsbach PH, Nanci A, Kulkarni AB, Yamada Y (2004). Ameloblastin is a cell adhesion molecule required for maintaining the differentiation state of ameloblasts. *J Cell Biol* 167:973-983.

Fukumoto S, Yamada A, Nonaka K, Yamada Y (2005). Essential roles of ameloblastin in maintaining ameloblast differentiation and enamel formation. *Cells Tissues Organs* 181:189-195.

Gibson CW, Collier PM, Yuan ZA, Chen E, Adeleke-Stainback P, Lim J, Rosenbloom J (1997). Regulation of amelogenin gene expression. *Ciba Found Symp* 205:187-199.

Gibson CW, Yuan ZA, Hall B, Longenecker G, Chen E, Thyagarajan T, Sreenath T, Wright JT, Decker S, Piddington R, Harrison G, Kulkarni AB (2001). Amelogenin-deficient mice display an amelogenesis imperfecta phenotype. *J Biol Chem* 276:31871-31875.

Gibson CW, Yuan ZA, Li Y, Daly B, Suggs C, Aragon MA, Alawi F, Kulkarni AB, Wright JT (2007). Transgenic mice that express normal and mutated amelogenins. *J Dent Res* 86:331-335.

Gibson CW, Li Y, Daly B, Suggs C, Yuan ZA, Fong H, Simmons D, Aragon M, Kulkarni AB, Wright JT (2009). The leucine-rich amelogenin peptide alters the amelogenin null enamel phenotype. *Cells Tissues Organs* 189:169-174.

Hart TC, Hart PS, Gorry MC, Michalec MD, Ryu OH, Uygur U, Ozdemir D, Firatli S, Aren G, Firatli E (2003). Novel ENAM mutation responsible for autosomal recessive amelogenesis imperfecta and localised enamel defects. *J Med Genet* 40:900-906.

Hu JC, Yamakoshi Y (2003). Enamelin and autosomal-dominant amelogenesis imperfecta. *Crit Rev Oral Biol Med* 14:387-398.

Hu JC, Chun Y-HP, Al-Hazzazzi T, Simmer JP (2007). Enamel formation and amelogenesis imperfecta. *Cells Tissues Organs* 186:78-85.

Hu JC, Hu Y, Smith CE, McKee MD, Wright JT, Yamakoshi Y, Papagerakis P, Hunter GK, Feng JQ, Yamakoshi F, Simmer JP (2008). Enamel defects and ameloblast-specific expression in Enam knock-out/lacz knock-in mice. *J Biol Chem* 283(16)*:*10858-10871.

Kida M, Ariga T, Shirakawa T, Oguchi H, Sakiyama Y (2002). Autosomal-dominant hypoplastic form of amelogenesis imperfecta caused by an enamelin gene mutation at the exon-intron boundary. *J Dent Res* 81:738-742.

Kim JW, Simmer JP, Hu YY, Lin BP, Boyd C, Wright JT, Yamada CJ, Rayes SK, Feigal RJ, Hu JC (2004). Amelogenin p.M1T and p.W4S mutations underlying hypoplastic X-linked amelogenesis imperfecta. *J Dent Res* 83:378-383.

Kim JW, Seymen F, Lin BP, Kiziltan B, Gencay K, Simmer JP, Hu JC (2005). ENAM mutations in autosomal-dominant amelogenesis imperfecta. *J Dent Res* 84:278-282.

Li Y, Suggs C, Wright JT, Yuan ZA, Aragon M, Fong H, Simmons D, Daly B, Golub EE, Harrison G, Kulkarni AB, Gibson CW (2008). Partial rescue of the amelogenin null dental enamel phenotype. *J Biol Chem* 283:15056-15062.

Livak KJ (1997). ABI prism 7700 Sequence Detection System, Use Bulletin 2. Foster City, CA: Applied Biosystems.

Mardh CK, Backman B, Holmgren G, Hu JC, Simmer JP, Forsman-Semb K (2002). A nonsense mutation in the enamelin gene causes local hypoplastic autosomal dominant amelogenesis imperfecta (AIH2). *Hum Mol Genet* 11:1069-1074.

Ozdemir D, Hart PS, Firatli E, Aren G, Ryu OH, Hart TC (2005). Phenotype of ENAM mutations is dosage-dependent. *J Dent Res* 84:1036-1041.

Paine ML, Wang HJ, Luo W, Krebsbach PH, Snead ML (2003). A transgenic animal model resembling amelogenesis imperfecta related to ameloblastin overexpression. *J Biol Chem* 278:19447-19452.

Paine ML, Zhu DH, Luo W, Snead ML (2004). Overexpression of TRAP in the enamel matrix does not alter the enamel structural hierarchy. *Cells Tissues Organs* 176:7-16.

Rajpar MH, Harley K, Laing C, Davies RM, Dixon MJ (2001). Mutation of the gene encoding the enamel-specific protein, enamelin, causes autosomal-dominant amelogenesis imperfecta. *Hum Mol Genet* 10:1673-1677.

Simmons D, Gu TT, Krebsbach PH, Yamada Y, MacDougall M (1998). Identification and characterization of a cDNA for mouse ameloblastin. *Connect Tissue Res* 39:3-12; discussion 63-67.

Snead ML, Paine ML, Chen LS, Luo BY, Zhou DH, Lei YP, Liu YH, Maxson RE, Jr. (1996). The murine amelogenin promoter: developmentally regulated expression in transgenic animals. *Connect Tissue Res* 35:41-47.

Snead ML, Paine ML, Luo W, Zhu DH, Yoshida B, Lei YP, Paine CT, Chen LS, Burstein JM, Jitpukdeebudintra S, White SN, Bringas P, Jr. (1998). Transgene animal model for protein expression and accumulation into forming enamel. *Connect Tissue Res* 38:279-286; discussion 295-303.

Torres-Quintana MA, Gaete M, Hernandez M, Farias M, Lobos N (2005). Ameloblastin and amelogenin expression in postnatal developing mouse molars. *J Oral Sci* 47:27-34.

Wazen RM, Moffatt P, Zalzal SF, Yamada Y, Nanci A (2009). A mouse expressing a truncated form of ameloblastin exhibits dental and junctional epithelium defects. *Matrix Biol* doi:10.1016/j.matbio.2009.04.004.

Wen X, Zou Y, Luo W, Goldberg M, Moats R, Conti PS, Snead ML, Paine ML (2008). Biglycan overexpression on tooth enamel formation in transgenic mice. *Anat Rec (Hoboken)* 291:1246-1253.

Wright JT, Robinson C, Kirkham J (1992). Enamel protein in the different types of amelogenesis imperfecta. In: Chemistry and Biology of Mineralized Tissues. H Slavkin and P Price editors. Amsterdam: Elsevier, pp. 441-450.

Wright JT (2006). The molecular etiologies and associated phenotypes of amelogenesis imperfecta. *Am J Med Genet A* 140:2547-2555.

Wright JT, Hart TC, Hart PS, Simmons D, Suggs C, Daley B, Simmer J, Hu J, Bartlett JD, Li Y, Yuan ZA, Seow WK, Gibson CW (2009). Human and mouse enamel phenotypes resulting from mutation or altered expression of AMEL, ENAM, MMP20 and KLK4. *Cells Tissues Organs* 189:224-229.

Xu Y, Zhou YL, Luo W, Zhu QS, Levy D, MacDougald OA, Snead ML (2006). NF-Y and CCAAT/enhancer-binding protein alpha synergistically activate the mouse amelogenin gene. *J Biol Chem* 281:16090-16098.

Xu Y, Zhou YL, Erickson RL, Macdougald OA, Snead ML (2007). Physical dissection of the CCAAT/enhancer-binding protein alpha in regulating the mouse amelogenin gene. *Biochem Biophys Res Commun* 354:56-61.

Zhou YL, Lei Y, Snead ML (2000). Functional antagonism between Msx2 and CCAAT/enhancer-binding protein alpha in regulating the mouse amelogenin gene expression is mediated by protein-protein interaction. *J Biol Chem* 275:29066-29075.

Zhou YL, Snead ML (2000). Identification of CCAAT/enhancer-binding protein alpha as a transactivator of the mouse amelogenin gene. *J Biol Chem* 275:12273-12280.

CHAPTER 6

CONCLUSION

SUMMARY

Enamel formation results in a highly mineralized, highly organized, acellular tissue. The development of enamel relies on a delineated extracellular space, the secretion of enamel proteins from the Tomes' process, processing and digestion of proteins by proteinases, reabsorption of enamel proteins and supply of calcium and phosphate. Disruption in any of these tasks can result in amelogenesis imperfecta. To patients, amelogenesis imperfecta is a very debilitating condition affecting their intake of nutrients, susceptibility to caries and malocclusion, esthetics, and self-esteem.

Ameloblastin, the focus of this dissertation work, is critical for dental enamel formation. Disruption of *Ambn* in mice results in an amelogenesis imperfecta. Information about Ambn's function has been gained through a better appreciation of its evolution, structure, and processing by proteases. It is one of the three "structural" enamel proteins that are the specialized secreted proteins required for the formation of enamel mineral ribbons. An important part of the mechanism of enamel formation is the proteolytic processing of these proteins.

Our goal was to characterize Ambn in terms of its evolutionary origin and structure. In order to obtain the full-length protein, Ambn was expressed as a

recombinant protein in mammalian cells. The size and post-translational modifications were evaluated, which showed the recombinant protein to be like the native protein in every way, except for the presence of a small C-terminal domain to facilitate purification. The recombinant protein opened new opportunities to study the structure and function of full-length Ambn. How Mmp-20 and Klk4 cleavage the recombinant protein was investigated. The function of Ambn was studied *in vivo* by introducing Ambn as a transgene into *Ambn* null mice. The major contributions of this dissertation to the understanding of Ambn in enamel formation are summarized below.

The evolution of genes in enamel formation was addressed in Chapter 2. The diversity of biomineralization in modern vertebrates is extraordinary. Numerous mineralized tissues have been selected throughout evolution; many of them are related to feeding. Mammalian teeth are composed of three different mineralized tissues that rely on the expression of different secreted proteins. SPARC was identified as the primordial gene of biomineralization and is associated with the onset of the dermal skeleton. As the result of a genome wide duplication SPARC spawned SPARC-L1, which generated the SCPP family of proteins regulating mineralization. A universal feature of all SCPPs is a conserved signal peptide (Kawasaki and Weiss, 2003; Kawasaki *et al.*, 2007). Targeting of the extracellular space offered opportunities to radiate into novel functions in the context of biomineralization. All of the structural enamel proteins (amelogenin, ameloblastin and enamelin) belong to the proline/glutamine rich part of the SCPP family.

To gain insight into a protein ancestral to Ambn, porcine SPARC was purified from dentin, its cDNA was cloned from a porcine, tooth-specific cDNA library, and its 3D structure was modeled based upon the published crystal structures of SPARC from

other organisms. Our computer model of porcine SPARC revealed a very tight conformation that included 7 disulfide bridges and 2 EF hands. The SPARC sequence is extremely conserved in evolution. While SPARC has not changed significantly, Ambn has diverged. Apart from its signal peptide and phosphorylated N-terminal segment (which were not included in the crystal structure), Ambn is distinct from SPARC. It is deduced to be a two-domain, intrinsically unstructured protein exhibiting many loops that are accessible to enzymatic cleavage. SPARC and ameloblastin exemplify how genes can radiate into novel structures and functions.

To study the complete structure of ameloblastin, the protein had to be produced as a recombinant protein. *In vivo* ameloblastin is rapidly cleaved. Chapter 3 describes the expression and isolation of recombinant ameloblastin in mammalian cells. RpAmbn was expressed from the pEF6/V5-his-TOPO vector that was stably integrated in HEK293 cells. In monolayer culture, secreted ameloblastin was stable and purified by ammonium sulfate precipitation, immobilized metal affinity chromatography and RP-HPLC. Post-translational modifications of recombinant Ambn were characterized by the removal of glycoslylations. RpAmbn has an apparent weight of 64 kDa and is O-glycosylated.

Cleavage of enamel proteins is necessary for mineralization. If one of the enamel proteinases, Mmp-20 or Klk4, is missing, the enamel is hypomineralized (Hart *et al.*, 2004; Kim *et al.*, 2005; Papagerakis *et al.*, 2008). Ameloblastin is processed during the secretory stage and degraded during maturation stage (Lu *et al.*, 2008). For the characterization of the specific cleavage sites, rpAmbn and synthetic Ambn peptides were used. The synthetic peptides contained sequences from the N- and C-terminus of known Ambn sites that have been difficult to reproduce and to detect *in vitro*. The substrates

were incubated with rpMmp-20 or Klk4. The *in vitro* cleavage pattern of rpAmbn generated by rpMmp-20 resembled the cleavage pattern from *in vivo* immature enamel. Cleavages sites after Pro^{2}, Asn^{31}, Gln^{130}, Arg^{170}, Ala^{222}, Gly^{300}, and Ala^{342} were made by Mmp-20 and correspond to secretory stage enamel. In contrast, Klk4 digested rpAmbn into lower molecular weight products and at different sites after Gln^{28}, Lys^{43}, Arg^{170}, Tyr^{191}, Tyr^{346} and Arg^{391}. Processing of Ambn occurs concurrently at different sites leading to rapid generation of cleavage products. These products are then digested further by Klk4.

There is no *in vitro* system for the synthesis of enamel crystals. Such a system would require intact amelogenin, ameloblastin, and enamelin, which are not available. To study the function of ameloblastin, we developed an *in vivo* mouse model system to investigate ameloblastin structure and function. Ambn is critical for enamel formation and requires the tissue context for functional studies. In the absence of *Ambn,* mice display hypoplastic amelogenesis imperfecta (Fukumoto *et al.*, 2004). To test the requirement of Ambn for enamel formation, a construct was fabricated to specifically target ameloblastin transgene expression by secretory stage ameloblasts. The Ambn transgene ($Ambn^{TG}$) was expressed from the mouse amelogenin promoter. A stable $Ambn^{-/-}$ TG line was bred and analyzed for transgene expression by real-time PCR using cDNA generated from RNA isolated from the enamel organ epithelia of day 5 first molars. The enamel of the Ambn null mouse was reconstituted with a full-length *Ambn* transgene by mating. The enamel thickness and prism pattern were analyzed by SEM. Rescue of the enamel phenotype using wild-type ameloblastin establishes a system that

will allow us to assess the ability of modified ameloblastin proteins to function properly and to rescue the enamel phenotype in the *Ambn* null background.

In summary, ameloblastin is an enamel protein of the secretory stage and is critical for enamel formation. Our findings link Ambn to SPARC and the evolution of biomineralization. Derived from our SPARC characterization, the signal peptide contains the essential role of targeting the extracellular space as a prerequisite for biomineralization. The structure of Ambn contains multiple cleavage sites that are specific for Mmp-20 and Klk4. This suggests that during secretory stage when crystallites grow in length, Ambn is cleaved by Mmp-20. During the maturation stage, Ambn cleavage products are further digested by Klk4 and crystallites grow in width and thickness. The Ambn null amelogenesis imperfecta was recovered when Ambn was supplied as a full-length transgene. The *Amel* promoter drives gene expression specifically in ameloblasts, thereby serving as a study model for secretory stage enamel proteins.

PROSPECTS

Stemming from our fundamental characterization of ameloblastin, new questions can be posed. The characterization of the cleavage site of Ambn revealed that multiple cleavages are made at the N- and C-terminus during secretory and maturation stage. Since these cleavage products have different localizations and different fates (Hu *et al.*, 1997; Uchida *et al.*, 1997; Uchida *et al.*, 1998), their specific functions seem to be very

different. N-terminal cleavage products of 17 kDa were generated by Mmp-20 and Klk4 that remained stable even after long incubations.

In vivo amelogenin accounts for 85-90 % of the enamel proteins, while Ambn for only 3-5 %. Both proteins tend to form homodimers and aggregates, even under the denaturing conditions of SDS-PAGE. At the mineralization front Amel and Ambn are secreted at the same time and are processed by Mmp-20. It is likely that they are interacting as full-length proteins or as cleavage products. It is unknown, how heterodimers form or behave as mineralization progresses.

The studies on functions of Ambn can be continued based on our *in vivo* study model. The construct successfully targets secretory stage ameloblasts, however the expression level of the transgene is low. Site-directed mutagenesis can be applied to produce specifically N- or C-terminal cleavage products. It would be interesting to learn, if N- or C-terminal cleavage products would be sufficient to recover the Ambn null phenotype. Further, the role of the conserved O-linked glycosylations at Ser^{91} or Thr^{358} in mouse could be studied by mutating these. As no human *AMBN* mutations have been found at this point, it is not possible to recreate a clinically relevant amelogenesis imperfecta.

Eventually, the identification of an *AMBN* mutation in humans causing amelogenesis imperfecta would be highly relevant to learn more about Ambn. So far, several non-synonymous single nucleotide polymorphisms have been identified, but the null mouse suggests that *Ambn* deficiency causes amelogenesis imperfecta.

REFERENCES

Fukumoto S, Kiba T, Hall B, Iehara N, Nakamura T, Longenecker G, Krebsbach PH, Nanci A, Kulkarni AB, Yamada Y (2004). Ameloblastin is a cell adhesion molecule required for maintaining the differentiation state of ameloblasts. *J Cell Biol* 167:973-983.

Hart PS, Hart TC, Michalec MD, Ryu OH, Simmons D, Hong S, Wright JT (2004). Mutation in kallikrein 4 causes autosomal recessive hypomaturation amelogenesis imperfecta. *J Med Genet* 41:545-549.

Hu CC, Fukae M, Uchida T, Qian Q, Zhang CH, Ryu OH, Tanabe T, Yamakoshi Y, Murakami C, Dohi N, Shimizu M, Simmer JP (1997). Sheathlin: cloning, cDNA/polypeptide sequences, and immunolocalization of porcine enamel sheath proteins. *J Dent Res* 76:648-657.

Kawasaki K, Weiss KM (2003). Mineralized tissue and vertebrate evolution: the secretory calcium-binding phosphoprotein gene cluster. *Proc Natl Acad Sci U S A* 100:4060-4065.

Kawasaki K, Buchanan AV, Weiss KM (2007). Gene duplication and the evolution of vertebrate skeletal mineralization. *Cells Tissues Organs* 186:7-24.

Kim JW, Simmer JP, Hart TC, Hart PS, Ramaswami MD, Bartlett JD, Hu JC (2005). MMP-20 mutation in autosomal recessive pigmented hypomaturation amelogenesis imperfecta. *J Med Genet* 42:271-275.

Lu Y, Papagerakis P, Yamakoshi Y, Hu JC, Bartlett JD, Simmer JP (2008). Functions of KLK4 and MMP-20 in dental enamel formation. *Biol Chem* 389:695-700.

Papagerakis P, Lin HK, Lee KY, Hu Y, Simmer JP, Bartlett JD, Hu JC (2008). Premature stop codon in MMP20 causing amelogenesis imperfecta. *J Dent Res* 87:56-59.

Uchida T, Murakami C, Dohi N, Wakida K, Satoda T, Takahashi O (1997). Synthesis, secretion, degradation, and fate of ameloblastin during the matrix formation stage of the rat incisor as shown by immunocytochemistry and immunochemistry using region-specific antibodies. *J Histochem Cytochem* 45:1329-1340.

Uchida T, Murakami C, Wakida K, Dohi N, Iwai Y, Simmer JP, Fukae M, Satoda T, Takahashi O (1998). Sheath proteins: synthesis, secretion, degradation and fate in forming enamel. *Eur J Oral Sci* 106 (Suppl 1) 308-314.